nagra National Cooperative for the Disposal of Radioactive Waste

TECHNICAL REPORT 93-45

Modelling Bentonite Pore Waters for the Swiss High-level Radioactive Waste Repository

November 1993

E. Curti

PSI, Würenlingen and Villigen

Hardstrasse 73, CH-5430 Wettingen/Switzerland, Telephone + 42-56-37 11 11

nagra National Cooperative for the Disposal of Radioactive Waste

TECHNICAL REPORT 93-45

Modelling Bentonite Pore Waters for the Swiss High-level Radioactive Waste Repository

November 1993

E. Curti

PSI, Würenlingen and Villigen

Hardstrasse 73, CH-5430 Wettingen/Switzerland, Telephone + 42-56-37 11 11

This report was prepared as an account of work sponsored by Nagra. The viewpoints presented and conclusions reached are those of the author and do not necessarily represent those of Nagra.

"Copyright (c) 1993 by Nagra, Wettingen (Switzerland). / All rights reserved.
All parts of this work are protected by copyright. Any utilisation outwith the remit of the copyright law is unlawful and liable to prosecution. This applies in particular to translations, storage and processing in electronic systems and programs, microfilms, reproductions, etc."

Contents

Abstract 1

Zusammenfassung 3

Riassunto 5

1. Introduction 7

2. The BGS experiments 9

3. Survey of preliminary results 12

4. Structural formula for montmorillonite 16

5. Cation exchange equilibria 18

5.1 Formal treatment of exchange equilibria 18

5.2 Extrapolation of exchange and surface complexation constants from the BGS experiments 20

6. Analysis of BGS solution data: are fluid compositions controlled by saturated solids ? 24

6.1 Mineral composition of bentonites: implications for the solution chemistry 24

6.2 Procedure for the definition of bentonite pore waters 25

6.3 Incongruent dissolution of montmorillonite 27

6.4 A method for determining solids in equilibrium with a solution 28

6.5 Simple correlations 30

6.6 Al-Si-pH relations 35

6.7 Other activity correlations 40

7. Redox control in bentonite pore waters 45

7.1 Significance of the oxidation potential for repository safety 45

7.2 Modelling the oxidation potential in bentonite pore waters 45

8. Modelling bentonite pore waters 51

8.1 Why a model ? 51

8.2 Definition of input waters 51

8.3 Definition of bentonite 52

8.4 Calculation of bentonite pore waters 57

8.5 Calculations with a reduced set of saturated solids 62

8.6 Non-uniqueness of the model solids 63

8.7 Testing the model against specific BGS waters 63

9. Summary and conclusions 68

Acknowledgements 70

References 71

Appendix A 75

Appendix B 83

Abstract

The main objective of this investigation is to contribute to definition of representative compositions of bentonite pore waters in the near-field of the Swiss repository for high-level radioactive waste. Such compositions are necessary for determining the solubility limits of radionuclides for the safety analysis KRISTALLIN I.

To date, there is no generally accepted thermodynamic model which describes the dissolution behaviour of bentonite satisfactorily. Even the applicability of the concept of *thermodynamic equilibrium* to complex clay minerals (in this case montmorillonite) has been questioned. The model developed here is based on the premise, supported by experimental data, that the composition of bentonite pore waters is largely controlled by the dissolution or precipitation of reactive trace solids in bentonite. Although these solids occur in minor amounts (below 5% volume), they may have a large effect on the pore water chemistry, by virtue of the very low water/rock ratios of the bentonite-water mixtures, and saturation may be easily reached.

Selectivity constants for the exchange equilibria among Na-K , Na-Ca, and Ca-Mg were derived from water-bentonite interaction experiments performed for *NAGRA* by the *British Geological Survey* (BGS). These constants proved to be consistent with known literature values. In a second step, cross activity plots for dissolved chemical species were prepared with the help of speciation calculations. From these plots empirical solubility constants were extrapolated for a set of model solids which served, together with the exchange constants, to model the bentonite pore waters. The stoichiometries of the model solids were determined applying geochemical criteria. However, it could be demonstrated that many different sets of model solids lead to the same final results.

An important parameter for the prediction of radionuclide solubilities is the oxidation potential of the bentonite water. Since the BGS experiments yielded no information on this, the oxidation potential had to be estimated from model assumptions. It was postulated that it is controlled by equilibria among Fe^{+2}/ Fe^{+3} solids occurring either in the bentonite itself or in other components of the repository. Specifically, it was assumed that the mineral magnetite - which should be the major corrosion product of steel - would be in excess, and that it would be in equilibrium either with goethite or with hematite occurring in the bentonite. Considering the large uncertainties of the thermodynamic data, these equilibria define a range of Eh values between -400 and +100 mV. Possible effects on the oxidation potential due to the release of ferric iron present in montmorillonite (which is the major iron reservoir in bentonite) were neglected because of lack of reliable equilibrium constants.

Bentonite pore waters were defined by computer simulation with the geochemical code MINEQL. The reaction between a sodium bentonite (MX-80) and reference waters for the crystalline basement of Northern Switzerland was evaluated applying the extrapolated selectivity and solubility constants. The ionic strength of the resulting bentonite pore waters was, in all cases, similar to that of the starting solutions. This feature can be easily explained by the absence of soluble anions (Cl^-, SO_4^{-2}) in the model solids. Calcite releases bicarbonate in significant amounts when it dissolves, but this has a limited effect on the ionic strength.

The bentonite pore waters have been modelled in a *closed system*, i.e. assuming that the

bentonite, once it has reacted with a fixed volume of groundwater, does not exchange further chemical species with an external reservoir. No attempt was made to model the evolution of the pore water by simulating diffusive exchange processes.

It can be anticipated that uncertainties in the concentrations of some major elements (e.g. Al, Si) will not significantly affect the calculated radionuclide solubilities. The latter will depend primarily on the concentrations of a few major ligands (OH^- , Cl^- and CO_3^{-2}) and, for multivalent elements, also on the oxidation potential of the solution. As the bicarbonate and chloride concentrations can be predicted with a reasonable degree of confidence, it is recommended to focus future investigations on the assessment of pH-Eh conditions in the near-field pore waters.

Zusammenfassung

Das Hauptziel dieser Arbeit ist ein Beitrag zur Festlegung von representativen Bentonitporenwasserzusammensetzungen im Nahfeld des schweizerischen Endlagers für hochaktive Abfälle. Solche Zusammensetzungen sind nötig für die Berechnung von Radionuklidlöslichkeiten in der Sicherheitsanalyse KRISTALLIN I.

Bis heute existiert kein eindeutiges, thermodynamisches Modell, welches das Löslichkeitsverhalten von Bentoniten befriedigend beschreiben kann. Es ist sogar zweifelhaft, ob der Begriff *thermodynamisches Gleichgewicht* an komplexe Tonmineralien (in diesem Falle Montmorillonit) angewandt werden darf. Das im vorliegenden Bericht entwickelte Modell geht davon aus, dass die Porenwasserzusammensetzung im wesentlichen durch die im Bentonit enthaltenen, reaktionsfreudigen Begleitmineralien und durch den Kationenaustausch am Bentonit bestimmt wird. Diese Annahme ist durch experimentelle Daten belegt. Obwohl der Anteil an Begleitmineralien sehr klein ist (weniger als 5 % v/v), können diese aufgrund des sehr niedrigen Wasser / Feststoffverhältnisses einen grossen Einfluss auf das Porenwasser ausüben (die Sättigung kann schnell erreicht werden).

Ionenaustauschkonstanten für Na-K, Na-Ca und Ca-Mg wurden aus Wasser-Bentonit Wechselwirkungsexperimenten, die für *NAGRA* vom *British Geological Survey* (BGS) durchgeführt wurden, abgeleitet. Diese stimmen sehr gut mit bekannten Literaturwerten überein. In einem zweiten Schritt wurden mit Hilfe von Speziationsrechnungen verschiedene Aktivitätskorrelationsdiagramme erstellt, aus denen empirische Löslichkeitskonstante extrahiert werden konnten. Diese Konstante beziehen sich auf Modellfestkörper, deren Stöchiometrien anhand geochemischer Kriterien festgelegt wurden. Es wird aber auch gezeigt, dass verschiedene Sätze von Modellfestkörpern zu identischen Schlussresultaten führen können.

Ein wichtiger Parameter für die spätere Voraussage von Radionuklidlöslichkeiten ist das Oxidationspotential des Bentonitwassers. Da die Experimente keine Auskunft darüber geben, wird das Oxidationspotenzial unter den zu erwartenden Endlagerbedingungen anhand von Modellannahmen abgeschätzt. Es wird postuliert, dass dieses durch Fe^{2+}/ Fe^{3+} Festphasen (aus dem Bentonit oder aus anderen Endlagerkomponenten) im Gleichgewicht fixiert wird. Insbesondere wird angenommen, dass Magnetit als stabiles Korrosionsprodukt des Stahlkanisters im Überschuss vorhanden ist, und dass dieser mit dem im Bentonit enthaltenem Goethit oder Hämatit im Gleichgewicht steht. Daraus, und auch wegen der Unsicherheit der thermodynamischen Daten, ergibt sich eine Spanne im Eh-Wert zwischen -400 und +100 mV. Allfällige Einflüsse auf das Oxidationspotential als Folge der Auflösung von dreiwertigem Eisen aus Montmorillonit (dem grössten Eisenreservoir in Bentonit) mussten mangels vertrauenswürdiger Gleichgewichtskonstanten vernachlässigt werden.

Bentonitporenwässer wurden mit Hilfe des Programms MINEQL definiert. Die Reaktion zwischen einem Na-Bentonit (MX-80) und jeweils einem Referenzwasser für das Kristallin der Nordschweiz wurde simuliert, indem die oben erwähnten Austausch- und Löslichkeitskonstante gleichzeitig angewandt wurden. Die Resultate zeigen, dass die Ionenstärke der resultierenden Porenwässer nicht wesentlich von derjenigen der Anfangslösung abweicht. Diese Beobachtung wird zwanglos durch die Abwesenheit löslicher Anione (Cl^-, SO_4^{-2}) in den Modellfestkörpern erklärt. Der einzige Mineral, der Anionen in bedeutenden Mengen

freisetzt, ist Calcit. Deren Auflösung hat aber einen begrenzten Einfluss auf die Ionenstärke.

Die Bentonitporenwässer wurden im *geschlossenen System* modelliert, d.h. unter der Annahme, dass der Bentonit, nach Reaktion mit einem fixierten Volumen zugeführter Lösung, keine weitere chemische Spezies mit einem externen Reservoir austauschen kann. Es wurde nicht versucht, die Entwicklung des Porenwassers durch Simulation diffusiver Austauschprozesse zu modellieren.

Es wird vorausgesagt, dass Unsicherheiten in den Konzentrationen gewisser Hauptelemente (z.B. Al, Si) keinen nennenswerten Einfluss auf die zu berechnenden Radionuklidlöslichkeiten haben werden. Diese werden vor allem von den Konzentrationen einzelner Hauptliganden abhängen (OH^-, Cl^-, und CO_3^{-2}) und, für multivalente Elemente, auch vom Oxidationspotential der Lösung. Da die Karbonat- und Chloridkonzentrationen mit genügender Sicherheit vorausgesagt werden können, ist es empfehlenswert, allfällige zukünftige Untersuchungen auf die Bestimmung der pH-Eh Verhältnisse in Nahfeldporenwässern zu richten.

Riassunto

L' obiettivo principale di questo studio è di contribuire alla definizione di composizioni rappresentative per acque interstiziali bentonitiche nel deposito finale svizzero per scorie altamente radioattive. Queste composizioni sono necessarie per determinare, nella zona adiacente alle scorie vetrificate, le solubilità degli isotopi radioattivi che verranno usate per l'analisi di sicurezza KRISTALLIN I.

Visto che tuttora non è possibile modellizzare la speciazione di acque bentonitiche utilizzando una costante di solubilità per la montmorillonite universalmente accettata (il concetto stesso di *equilibrio termodinamico* applicato a minerali argillosi complessi è stato messo in dubbio), si è scelto un metodo alternativo. Il modello qui sviluppato parte dalla premessa, corroborata da dati sperimentali, che il chimismo di acque interstiziali bentonitiche viene in gran misura controllato dalla dissoluzione o precipitazione di minerali in tracce nella bentonite. Malgrado il loro basso tenore (meno del 5 % in volume) questi solidi sono presenti in quantità sufficienti a garantire il raggiungimento di condizioni saturate quando vengono disciolti, in virtù del basso rapporto acqua/solidi nei sistemi considerati.

Costanti di selettività per Na-K, Na-Ca e Ca-Mg sono state derivate dai risultati di esperimenti di interazione tra soluzioni acquose e bentonite, condotti espressamente per la *CISRA* al *British Geological Survey* (BGS). I valori ottenuti sono in accordo con dati tratti dalla letteratura. In un secondo tempo, correlazioni logaritmiche tra attività di speci in soluzione sono state analizzate al fine di identificare minerali in equilibrio di saturazione con la fase acquosa. Tali correlazioni hanno permesso di definire costanti di solubilità empiriche che sono state impiegate, con le costanti di selettività, per la modellizzazione di acque interstiziali bentonitiche. Tali costanti di solubilità si riferiscono a minerali modello con stechiometrie definite in base a criteri geochimici. Tuttavia, si è potuto dimostrare che gli stessi risultati possono essere ottenuti postulando stechiometrie differenti.

Un parametro fondamentale per la determinazione delle solubilità di alcuni radionuclidi è il potenziale di ossidazione della soluzione a contatto con la bentonite. Poichè gli esperimenti BGS non forniscono indicazioni su questo argomento, il potenziale di ossidazione è stato stimato tramite un modello termodinamico. Si suppone che esso venga determinato da equilibri tra soluzione e minerali ferroso-ferrici, presenti sia nella bentonite che in altre componenti del deposito finale. In particolare, si presume che la magnetite, il prodotto stabile di corrosione del contenitore in acciaio, sia presente in eccesso e sia in equilibrio con goethite oppure ematite presenti nella bentonite, fissando il potenziale di ossidazione nell' intervallo tra -400 e +100 mV. Eventuali effetti dovuti al ferro trivalente liberato dalla montmorillonite sono stati trascurati per mancanza di dati termodinamici.

Composizioni di acque interstiziali bentonitiche sono state definite con il programma MINEQL. La reazione tra una bentonite sodica (MX-80) e fluidi dello zoccolo cristallino della Svizzera settentrionale è stata simulata applicando contemporaneamente le costanti di selettività e di solubilità estrapolate dagli esperimenti BGS. I risultati indicano che la forza ionica delle acque bentonitiche rimane in ogni caso simile a quella della soluzione di partenza. Ciò è una conseguenza diretta dell' assenza di anioni solubili (Cl^-, SO_4^{-2}) nei solidi-modello. Solo la dissoluzione della calcite ha un effetto, seppur limitato, sulla forza

ionica.

Le acque bentonitiche interstiziali sono state modellizzate in un *sistema chiuso*. Ciò significa che la bentonite, dopo aver reagito con un volume finito di soluzione proveniente dalle rocce circostanti, non può avere un ulteriore scambio di speci chimiche con l' ambiente esterno. Non si è tentato quindi di tener conto della continua interdiffusione di sostanze disciolte tra bentonite saturata e il reservoir di soluzione esterno.

Si può anticipare che eventuali imprecisioni nella concentrazione di certi elementi principali (p. es. Al, Si) non avranno effetti significativi sulle solubilità degli elementi radioattivi, in quanto esse dipendono avantutto dalle concentrazioni di poche speci chiave (OH^- , Cl^- , CO_3^{-2}) e, per gli elementi multivalenti, anche dal potenziale di ossidazione. Dato che le concentrazioni di cloruro e bicarbonato sono determinabili con sufficiente precisione, si raccomanda di concentrare gli studi futuri sulla determinazione dei valori pH ed Eh nelle soluzioni interstiziali del deposito finale.

1. Introduction

When assessing the safety of a repository for nuclear waste, knowledge of the chemistry of waters which may come into contact with the waste matrix is of primary importance, since these water compositions govern the solubility of radionuclides, affect their sorption on mineral surfaces, and influence the corrosion rate of the vitrified waste matrix. Precipitation and sorption of radionuclides are two of several key processes on which the safety of a Swiss repository for high-level radioactive waste will rely (*NAGRA*, 1985). Therefore, the aqueous chemistry of the repository near-field should be determined accurately. It is especially important to understand the interactions between intruding groundwaters and bentonite, as this material will serve as a backfill in the Swiss high-level waste (HLW) repository, providing a ~ 1.5 m thick protective layer around the waste packages.

Previous work on the chemistry of bentonite pore waters in the Swiss HLW repository is documented in three reports (Wanner, 1986; Grauer, 1986 and 1988). Wanner developed a model, based on Finnish experiments carried out at 25 °C (Snellman et al., 1987), which emphasizes the role of cation exchange reactions and the continuous supply of groundwater from an external reservoir. The consideration of heterogeneous equilibria involving dissolution and precipitation of solids within bentonite was limited to the assumption of calcite and quartz saturation, while the dissolution of montmorillonite and of other trace phases occurring in bentonite was neglected. Wanner's model focused on the *evolution* of the pore water chemistry as the groundwater progressively exchanges calcium for sodium ions when it comes in contact with a sodium bentonite. After a sufficient volume of groundwater has reacted with the bentonite, the model predicts exhaustion of the calcite reservoir in bentonite, and a final pore water composition identical to the original groundwater. Thus, Wanner's model yields a wide range of pore water compositions extending from alkaline solutions at the beginning of the interaction (pH ~ 10) to a final composition identical to that of the pristine groundwater (pH = 7-8).

Grauer (1986,1988) excluded that extensive illitisation or chloritisation of montmorillonite could take place under repository conditions, because of the low repository temperature and the low K- and Mg-concentrations in the Swiss crystalline groundwaters. Further, he pointed out that there is still no chemical model which can describe the water-bentonite interactions satisfactorily. In his opinion, smectites and illites cannot be treated on the basis of a classical thermodynamic equilibrium approach, because these minerals are not homogeneous in composition and structure (these may vary even at the atomic scale). One of the major problems is the almost total ignorance of the potential reactions between bentonite and the iron corrosion products, which could produce a variety of possibly non-sorbing and non-swelling Fe-silicates. The precipitation of such phases would, of course, affect the chemical composition of the pore water.

Based on these considerations, the prediction of equilibrium conditions in a complex system like the repository near-field seems very problematic. Particular difficulties exist in coupling chemical reactions with diffusive transport, in defining the thermodynamic properties and even the nature of the solid phases involved, and in quantifying the complex interactions among the various repository components. For instance, it is still strongly debated whether montmorillonite dissolution may be described by a well-defined,

stoichiometric solubility constant (Tardy and Fritz, 1981; May et al., 1986; Grauer, 1986; Kittrick and Peryea, 1989). There is considerable evidence to support incongruent dissolution of this mineral and some authors claim that the stoichiometric equilibrium constants provided by other investigators are based on ambiguous experimental data.

In view of these facts, it seemed more reasonable to develop an empirical model relying on experiments performed recently by the *British Geological Survey* (BGS) for *NAGRA* (Bateman et al., 1991), rather than to use more or less sophisticated equilibrium models based on uncertain thermodynamic constants for montmorillonite. The BGS experiments used materials and were performed under conditions approaching those expected in the Swiss HLW repository, and therefore appeared suitable as a starting point for the extrapolation of *bentonite pore waters* for the near-field environment.

Because the experiments lasted for a very limited time (up to 4 weeks), and the results did not point to the achievement of an *overall* equilibrium between solution and bentonite, the modelled pore waters do not necessarily reflect the conditions at an advanced stage in the evolution of a repository. They rather represent a first estimate of the *short-term* modifications which specific Swiss crystalline groundwaters chemistries would experience on interaction with a particular Na-bentonite (MX-80) at the low water/rock ratios and temperatures that would prevail in a Swiss repository environment. The influence of chemical species released by the corroding glass has not been considered, and the steel corrosion products are assumed to act only as a redox buffer: no formation of iron silicates is modelled, since it is not known precisely which phases would form (Grauer, 1988).

In spite of the limitations of the model, an attempt is made to specify realistic ranges for all the parameters which could critically affect the solubility of radionuclides in bentonite (e.g. Eh, pH, carbonate concentration). Even if the approach used here differs considerably from conventional thermodynamic methods, the extrapolated values of these parameters are similar to those obtained from other models (see e.g. Fritz and Kam, 1985) and can therefore be used with a good degree of confidence. This report, together with a more qualitative evaluation of the near-field system based on literature data, will thus be used to define the reference waters for the KRISTALLIN I performance assessment (*NAGRA*, in prep.).

2. The BGS experiments

A series of bentonite-water interaction experiments at low water/rock ratios has been carried out recently by the British Geological Survey (Bateman et al., 1991), with the aim of providing a database for the definition of bentonite pore waters for the Swiss high-level waste repository. Sodium-activated *Montigel F* bentonite samples were mixed with prepared solutions simulating two groundwater types of the Swiss crystalline basement. The gels were then introduced into a pressurised cell, where they reacted for 2-4 weeks at 50 ^{o}C and about 10 bars. After completion of the experiment, the fluid phase was squeezed out into a syringe through a 0.2 μm filter, and then analysed for pH and various elemental concentrations (Ca, Mg, Na, K, Si, Ba, Sr, total Fe, Al, Li , HCO_3^-, Cl, SO_4^{-2}, NO_3^-, NO_2^-, HPO_4^{-2}, F). The reacted sample was then retrieved and dried for later analyses.

The original bentonite contained about 4.5 weight % Na_2CO_3, to promote exchange of Ca^{+2} and Mg^{+2} with Na^+ during the beneficiation process. The original samples were dispersed in distilled water and separated into two size fractions. The coarser fraction (< 10 μm) was called *Na-bentonite* and the finer one (< 2 μm) *Na-montmorillonite*, since trace mineral impurities had dropped below the detection limit of X-ray diffraction (XRD) methods, which is about 5 weight %. Both unreacted and reacted bentonite samples were analysed for their mineralogy and bulk chemical compositions. XRD analyses revealed the presence of trace amounts of quartz (SiO_2), kaolinite ($Al_2Si_2O_5(OH)_4$), chlorite and micas in the *Na-bentonite* fraction. Evolved Gas Analyses (EGA) indicated the presence of carbonates in all (reacted and unreacted) samples. The results suggest that calcite, which was the prevailing carbonate in the unreacted samples, was partly replaced by a magnesian carbonate in the residual samples (Bateman et al., 1991).

TABLE 1 - Measured compositions of reacting fluids as given in Bateman et al. (1991). Concentrations are given in [mol/l].

	simple LOW	*simple HIGH*
$[Na]_{tot}$	1.21×10^{-2}	1.71×10^{-1}
$[Ca]_{tot}$	2.50×10^{-4}	2.00×10^{-2}
$[Cl]_{tot}$	1.27×10^{-2}	2.01×10^{-1}
pH (measured)	5.4	5.3

TABLE 2 - Compositions of reacting fluids modelled assuming equilibrium with atmospheric CO_2(g). Concentrations are given in [mol/l].

	simple LOW	*simple HIGH*
$[Na]_{tot}$	1.21×10^{-2}	1.71×10^{-1}
$[Ca]_{tot}$	2.50×10^{-4}	2.00×10^{-2}
$[Cl]_{tot}$	1.27×10^{-2}	2.01×10^{-1}
$[C]_{tot}$	1.32×10^{-5}	1.39×10^{-5}
$[Na^+]$	1.21×10^{-2}	1.71×10^{-1}
$[Ca^{+2}]$	2.50×10^{-4}	2.00×10^{-2}
$[Cl^-]$	1.27×10^{-2}	2.01×10^{-1}
$[HCO_3^-]$	2.44×10^{-6}	2.75×10^{-6}
$[H_2CO_3]$	1.08×10^{-5}	1.08×10^{-5}
pH (modelled)	5.66	5.63
Ionic strength	0.01	0.23

The compositions of both synthetic groundwaters as given by Bateman et al. (1991) are reported in Table 1. Both solutions were prepared by dissolving sodium and calcium chloride to obtain two different ionic strengths. The more dilute solution was called *simple LOW*, the more concentrated *simple HIGH*. The low pH values of both fluids strongly suggest equilibration with atmospheric CO_2(g). This hypothesis is consistent with speciation calculations performed assuming that the solutions specified in Table 1 are in equilibrium with atmospheric CO_2 at 25 ^{o}C, as the predicted pHs are close to the measured values (Table 2).

Ten experiments were carried out starting with considerable amounts of fluid-clay mixtures (250-350 g). In all runs, fluid samples of about 7 ml each were drawn at various times: shortly after a temperature of 50 ± 3 ^{o}C was reached in the cell, after 2 weeks and, in some cases, after 4 weeks reaction time. The relatively small amounts of fluid collected prior to completion of the experiment (about 5-10 % of the initial solution volume), and the large amount of starting material, should have ensured that chemical conditions inside the cell were not too much disturbed by the fluid sampling. However, reductions of the water/rock ratios due to the combined effect of swelling and fluid sampling were not insignificant (Table 3). They have been estimated with the help of data provided by the BGS study, which are reported in their original form in Table 4, Appendix B. The estimates are based on the assumptions that the pore fluid has the density of pure water (ρ_L = 1.0 g/cm^3) and that the solid phase in bentonite has the same density as that specified by Müller-Vonmoos and Kahr (1983) for the MX-80 bentonite (ρ_S = 2.76 g/cm^3). The weights of solid and liquid in the unreacted material are given by the columns labeled *oven-dried weight* (*B*) and *initial moisture weight* (*E*), respectively. Thus, the initial water/rock ratio,

expressed as porosity (ε_0) is given by the expression:

$$\epsilon_0 = \frac{(E/\rho_L)}{(E/\rho_L)+(B/\rho_S)}$$

The moisture weights in the reacted samples are given as percentages of the oven-dried weights of the unreacted material, and are labeled *moisture content % post-test* (*D*). To calculate the final weights of solid in the reacted samples, the contribution of water incorporated through swelling in the montmorillonite structure should be added to the initial mass of solid. This contribution may be computed by using *V**, which is an estimation of the water volume adsorbed during swelling (see equation (2), next chapter). With this information, the final water/rock ratios can be calculated by the following formula:

$$\epsilon_f = \frac{(BD/100\rho_L)}{(BD/100\rho_L)+((B+\rho_L V^*)/\rho_S)}$$

Some experiments were carried out under anaerobic conditions. However, since it was not possible to *prepare* fluid-clay mixtures under air exclusion, the distinction between aerobic and anaerobic experiments becomes meaningless. This is confirmed by the absence of any systematic difference between the results of aerobic and anaerobic experiments (Bateman et al., 1991, p. 11).

The cation concentrations were analysed by *Inductively Coupled Plasma Optical Emission Spectrometry* (ICP), while chloride, sulphate and phosphate were measured by *Ion Chromatography* (IC), and fluoride by means of an *ion sensitive electrode* (ISE). All dissolved concentrations are reported as they appear in Bateman et al. (1991) in Appendix A.

TABLE 3 - Water/rock ratios calculated from experimental data (Table 4, Appendix B). Reductions of the water/rock ratios are generally larger for the 4 week experiments, since more fluid was sampled. The water/rock ratio is defined here as porosity (solution volume divided by the total volume of the bentonite gel):

ε_o : water/rock ratio of the unreacted sample
ε_f : water/rock ratio of the reacted sample
% $\Delta\varepsilon$: change of water/rock ratio in %

LABEL	RUN TIME [weeks]	ε_o	ε_f	% $\Delta\varepsilon$
B1	2	0.83	0.76	8.4
B2	2	0.83	0.70	15.7
B3	2	0.73	0.69	5.5
B4	2	0.73	0.64	12.3
B5	2	0.76	0.66	8.6
B6	2	0.76	0.62	13.2
B7	4	0.75	0.65	13.3
B8	4	0.76	0.62	18.4
B9	4	0.78	0.59	24.4
B10	4	0.78	0.55	29.5

3. Survey of preliminary results

In this section, the interpretation given by Bateman et al. (1991) of preliminary results emerging from the analyses of the BGS experiments will be discussed, and alternative explanations will be proposed when required.

An opening remark concerns the accuracy of the dissolved concentrations. Although Bateman et al. (1991) do not give a quantitative appraisal of the uncertainties involved, analytical errors may be estimated from the accuracy of charge balances (Table 5, Appendix B). Typically, imbalances of 5-10 % excess positive charge are found. Extreme values, however, range from -11 % to + 18 %. Therefore, as a conservative average, an uncertainty of ± 10% for each concentration value is assumed.

In all experiments, the pH increased rapidly to values between 8.2 and 9.3. Bateman et al. (1991) noticed that final pHs in *simple LOW* experiments are about 0.5 units higher than those measured in *simple HIGH* tests, but they do not explain this systematic difference. This incongruence can be understood in terms of carbonate equilibria: since the solubility of calcite is lower in the *simple HIGH* solution (because it has an 80 times higher initial Ca^{+2} concentration than *simple LOW)* far less CO_3^{-2} ions need to be dissolved to reach calcite equilibrium, and consequently the pH increase will be smaller than in the *simple LOW* experiments.

The Ca^{+2} dissolved concentration was found to decrease in all but one case (B1), in which fluid contamination occurred. The decrease in calcium fits well with the assumption of calcite equilibrium: with the high pHs and carbonate concentrations measured in the final solutions, Ca^{+2} concentrations in equilibrium with calcite must be much lower than in the starting solutions. The calcium removed from solution is probably incorporated as an exchanged cation in the clay, as suggested by the increased capacity of this cation in almost all reacted samples (Table 8, Appendix B). Table 4 shows mass balance calculations for Ca and the modelled saturation indices for calcite, from which it is evident that most final solutions are saturated or nearly saturated with calcite. The calculated changes in exchanged calcium concentrations (normalised to the solution volume, not to the sorbent mass) do not match the losses of dissolved calcium ($\delta_1 \neq \delta_2$ in Table 4). This suggests, in the cases where the increase in exchanged concentration overcompensates the loss of dissolved calcium, that there has been calcite dissolution during the reaction between starting solution and bentonite. In other cases, the opposite is stated: the increase in exchanged calcium concentration is smaller than the loss of dissolved calcium, which would indicate calcite precipitation. Calcite precipitation, however, cannot be reconciled with the observed consistent increase in total dissolved carbonate, suggesting the existence of experimental errors in the exchange data. The δ_2 values in Table 4 should be, in any case, interpreted with caution, since the cation exchange capacities may have been overestimated due to the possible contribution of carbonates during the measurements (Bateman et al., 1991). This is inferred from unusually high cation exchange capacities (CEC) determined with the ammonium acetate method. The measured values of 130-150 meq/100g (see Table 8, Appendix B) are considerably higher than the expected figures (80-100 meq/100g).

TABLE 4 - Mass balance calculations for calcium and calculated saturation indices for calcite. The differences in dissolved calcium concentrations between the starting solutions and the final solutions indicate a mass transfer from the fluid phase. In some cases, the increase in sorbed concentration overcompensates the loss of dissolved calcium, suggesting calcite dissolution ($\delta_2 \gg \delta_1$); in other cases, the opposite is true. Definitions:

SI : saturation index of calcite (calculated with MINEQL)
$[Ca]_o$: total dissolved calcium concentration in starting fluids [mol/l]
$[Ca]_f$: final dissolved calcium concentration [mol/l]
δ_1 = $[Ca]_f - [Ca]_o$
δ_2 : change in exchanged calcium concentration (reacted sample - original sample) in [mol/l] calculated with data from Table 3 and Table 8, Appendix B

RUN	SI	$[Ca]_o$	$[Ca]_f$	δ_1	δ_2
B1	+1.9	2.5×10^{-4}	1.2×10^{-3}	$+9.5 \times 10^{-4}$	0.0
B2	+0.7	2.5×10^{-4}	7.5×10^{-5}	-1.8×10^{-4}	$+1.4 \times 10^{-2}$
B3	+0.0	2.0×10^{-2}	1.5×10^{-4}	-2.0×10^{-2}	$+1.5 \times 10^{-2}$
B4	-0.1	2.0×10^{-2}	1.3×10^{-4}	-2.0×10^{-2}	$+3.5 \times 10^{-2}$
B5	-0.2	2.0×10^{-2}	6.9×10^{-5}	-2.0×10^{-2}	$+3.5 \times 10^{-3}$
B6	+0.3	2.0×10^{-2}	1.8×10^{-4}	-2.0×10^{-2}	$+2.3 \times 10^{-2}$
B7	+0.0	2.5×10^{-4}	1.4×10^{-5}	-2.4×10^{-4}	-3.7×10^{-3}
B8	+0.2	2.5×10^{-4}	2.0×10^{-5}	-2.3×10^{-4}	-4.2×10^{-3}
B9	+0.4	2.5×10^{-4}	2.6×10^{-5}	-2.2×10^{-4}	$+7.9 \times 10^{-2}$
B10	+0.7	2.0×10^{-2}	4.3×10^{-4}	-2.0×10^{-2}	$+7.2 \times 10^{-2}$

Another general result is the increase in the chloride concentration in all experiments by up to 40-50 %, which Bateman et al. (1991) ascribe to the incorporation of water in the smectites (swelling). Chloride is not expected to be fixed significantly in silicates and carbonates present in the bentonite used for these experiments. Nevertheless, dissolution of trace amounts of soluble chloride salts cannot be excluded, since the observed increase in chloride concentration would require far less than 1 % volume NaCl in the bentonite. Calculations were made to check whether the increase in chloride concentration may be attributed merely to swelling , or if an extra source of chloride must be assumed. The theoretical chloride concentrations obtained assuming swelling alone were calculated and compared with the measured values (Table 5). The volumes of water incorporated in the smectite by swelling were also estimated. The calculations were performed using the BGS concentration data and moisture volumes (Appendix A and Table 4 in Appendix B), on the basis of the following equations:

$$c_f = \frac{c_o V_o - \sum_{i=1}^{n} c_i \Delta V}{V_f} \qquad (1)$$

$$V^* = V_o - V_f - (n+1)\Delta V \qquad (2)$$

where:

c_f	is the final chloride concentration	[mol/l]
c_o	is the initial chloride concentration (Table 1)	[mol/l]
c_i	is the chloride concentration in the *i*th fluid sample (App.A)	[mol/l]
n	is the number of fluid samples collected before the final sampling	[-]
ΔV	is the moisture volume drawn at each sampling (7 ml)	[l]
V_o	is the initial moisture volume (App. B, Table 4)	[l]
V_f	is the final moisture volume (App. B, Table 4)	[l]
V^*	is the calculated volume of water incorporated by swelling	[l]

The predicted chloride concentrations are always somewhat lower than the measured values, with the notable exception of sample B10 (Table 5). However, this discrepancy cannot be interpreted as evidence for an external chloride source. If small amounts of chloride salts were to dissolve, one would expect a comparable increase in the *absolute* concentration in *all* fluids (the changes should be more or less equal in both low and high ionic strength solutions). Instead, the solutions resulting from the interaction with the *simple LOW* fluid show a much smaller increase in chloride concentration than those derived from the *simple HIGH* fluid. The comparable relative differences ($\Delta c\%$) between calculated and predicted concentrations rather suggest that a systematic analytical error might be the reason for the discrepancy. In fact, this seems reasonable considering the uncertainties involved in the measurements, and the interpretation of Bateman et al. (1991) that the increase in chloride concentration is uniquely due to the swelling of bentonite seems acceptable. Moreover, the presence of trace chloride salts in the starting material is unlikely, as they should have been dissolved completely during the beneficiation process (the raw samples were suspended in distilled water).

TABLE 5 - Calculation of the water volume adsorbed by swelling (V^*) and of the chloride concentration expected as a consequence of swelling (*C(calc)*). The calculated chloride concentrations are compared to the effectively measured concentrations (*C(meas)*). See equations (1) and (2) for symbol definition.

	INPUT DATA FOR CALCULATIONS					RESULTS AND VALUES FOR COMPARISON				
RUN	V_0 [ml]	V_f [ml]	$\Sigma (C_i)$	ΔV	n	C_o	C(calc)	C(meas)	ΔC %	V^* [ml]
B1	196	153	1.88×10^{-2}	7.0×10^{-3}	1	1.27×10^{-2}	1.54×10^{-2}	1.98×10^{-2}	+22	29
B2	197	133	2.47×10^{-2}	7.0×10^{-3}	1	1.27×10^{-2}	1.75×10^{-2}	2.39×10^{-2}	+27	50
B3	113	95	3.15×10^{-1}	7.0×10^{-3}	1	2.01×10^{-1}	2.15×10^{-1}	2.55×10^{-2}	+16	4
B4	145	107	3.67×10^{-1}	7.0×10^{-3}	1	2.01×10^{-1}	2.48×10^{-1}	2.58×10^{-1}	+4	24
B5	160	118	2.80×10^{-1}	7.0×10^{-3}	1	2.01×10^{-1}	2.57×10^{-1}	3.13×10^{-1}	+18	29
B6	137	91	2.87×10^{-1}	7.0×10^{-3}	1	2.01×10^{-1}	2.79×10^{-1}	3.01×10^{-1}	+7	32
B7	131	92	5.42×10^{-2}	7.0×10^{-3}	2	1.27×10^{-2}	1.40×10^{-2}	2.01×10^{-2}	+30	18
B8	137	88	5.63×10^{-2}	7.0×10^{-3}	2	1.27×10^{-2}	1.77×10^{-2}	2.49×10^{-2}	+29	28
B9	142	81	4.56×10^{-2}	7.0×10^{-3}	2	1.27×10^{-2}	1.84×10^{-2}	2.03×10^{-2}	+9	40
B10	152	76	5.33×10^{-1}	7.0×10^{-3}	2	2.01×10^{-1}	3.51×10^{-1}	2.29×10^{-1}	-35	55

4. Structural formula for montmorillonite

An approximate structural formula for the unreacted montmorillonite has been derived with the help of X-ray fluorescence (XRF) analysis of the finer bentonite fraction (see Table 9 in Appendix B, *Na-montmorillonite*) and using the cation exchange data (Table 8, Appendix B). The resulting formula (Table 6) is normalised to 22 negative charges. It was obtained assuming that all tetrahedral sites are shared between Si and Al, and postulating the same ratio of ferrous to ferric iron as that reported by Müller-Vonmoos and Kahr (1983) in their Table A2 for the purified Montigel bentonite. The occupancies of octahedral sites for Ca^{+2} and Mg^{+2} were determined by subtracting the exchanged fractions from the total amount determined through XRF analysis.

This formula is an approximation, inasmuch as the XRF data cannot be corrected for impurities (especially carbonates, kaolinite and quartz) and by virtue of the assumptions mentioned above. However, the stoichiometric coefficient for the hydroxyl groups calculated from the ignition loss (LOI in Table 9, Appendix B) is fairly close to the theoretical value of 2, indicating that the approximation is reasonably accurate.

TABLE 6 - Derivation of an approximate structural formula for the unreacted montmorillonite used in the BGS experiments. Symbol definitions are as follows:

W : weight % oxide
M_1 : moles oxide per 100g dry bentonite (total)
M_2 : moles oxide exchanged per 100 g dry bentonite
M_3 : moles oxide per 100 g dry bentonite on a specific site or as corrected total
X : elemental stoichiometric coefficient ($X = f \xi M_3$, where f = 22 / [total positive charge] is a normalisation factor, and ξ is the number of cations in the oxide formula, i.e. 2 for K_2O)

OXIDE FORMULA	W [g/100g]	M_1 [mol/100g]	M_2 [mol/100g]	SITE	M_3 [mol/100g]	X
SiO_2	56.58	0.942	-	tetrahedral	0.942	3.785
Al_2O_3	18.77	0.104	-	total tetrahedral octahedral	0.184	1.478 0.215* 1.263**
MgO	4.77	0.118	0.010	total octahedral interlayer	0.118 0.108 0.010	0.474 0.434 0.040
CaO	2.35	0.042	0.020	total octahedral interlayer	0.042 0.022 0.020	0.168 0.088 0.080
Na_2O	2.89	0.047	0.037	interlayer	0.037	0.297
K_2O	0.79	0.008	0.007	interlayer	0.007	0.056
Fe_2O_3	5.18	0.032	-	octahedral	0.032	0.257
FeO	0.17	0.002	-	octahedral	0.002	0.008
(OH^-)	8.35	0.464	-	-	0.464 LACKING :	1.864 0.136

NOTES: $^*X_{Al\ (tetrahedral)} = 4 - X_{Si} = 4 - 3.785$

$^{**}X_{Al(octahedral)} = X_{Al(total)} - X_{Al(tetrahedral)} = 1.478 - 0.215$

FORMULA:

$$\{Na_{.30}Ca_{.08}Mg_{.04}K_{.06}\}\ <Al_{1.26}Fe(III)_{.26}Fe(II)_{.01}Mg_{.43}Ca_{.09}>\ [Si_{3.79}Al_{.21}O_{10}]\ (OH)_2$$

5. Cation exchange equilibria

5.1 Formal treatment of exchange equilibria

One of the most evident reactions observed when aqueous solutions interact with bentonite is the exchange of alkali and earth-alkali cations between solution and clay minerals. The nature, direction and magnitude of the exchange depend on the initial cation concentrations in both aqueous and solid phases, on the water/rock ratio, on temperature, and on the ionic strength of the solution. A general exchange reaction between two cations A^{+a} and B^{+b} being sorbed on a substrate Z^- may be defined as follows:

$$b\,A^{+a} + a\,BZ_b = a\,B^{+b} + b\,AZ_a \qquad (3)$$

Equilibrium conditions may be defined by an exchange (or selectivity) constant based on the law of mass action:

$$K_{ex} = \frac{[B^{+b}]^a \{AZ_a\}^b}{[A^{+a}]^b \{BZ_b\}^a} \qquad (4)$$

where:

[ ] is the dissolved cation concentration [mol/l]

{ } is the sorbed concentration normalised to the sorbent mass [eq/kg]

The sorbed concentrations can be normalised to the solution volume, which is convenient for modelling purposes. The two concentrations are related through the equation:

$$[AZ_a] = \frac{\{AZ_a\}}{a} \rho_s \frac{1-\epsilon}{\epsilon} \qquad (5)$$

where:

ρ_s is the density of the *solid* (bentonite excluding pores) [kg / l]

ε is the porosity (volume of fluid / total volume) [-]

Equations (3) and (4) can be translated, for the cations considered in this study, into the following system of exchange equilibria:

$$2\,Na^{+} + CaZ_2 = Ca^{+2} + 2\,NaZ \quad (6a)$$

$$Ca^{+2} + MgZ_2 = Mg^{+2} + CaZ_2 \quad (6b)$$

$$Mg^{+2} + 2\,KZ = 2\,K^{+} + MgZ_2 \quad (6c)$$

$$2\,Na^{+} + MgZ_2 = Mg^{+2} + 2\,NaZ \quad (6d)$$

$$Ca^{+2} + 2\,KZ = 2\,K^{+} + CaZ_2 \quad (6e)$$

$$Na^{+} + KZ = K^{+} + NaZ \quad (6f)$$

which are characterised by the exchange constants:

$$K_{ex}(Na-Ca) = \frac{[Ca^{+2}]\,[NaZ]^2}{[Na^{+}]^2\,[CaZ_2]} \quad (7a)$$

$$K_{ex}(Ca-Mg) = \frac{[Mg^{+2}]\,[CaZ_2]}{[Ca^{+2}]\,[MgZ_2]} \quad (7b)$$

$$K_{ex}(Mg-K) = \frac{[K^{+}]^2\,[MgZ_2]}{[Mg^{+2}]\,[KZ]^2} \quad (7c)$$

$$K_{ex}(Na-Mg) = \frac{[Mg^{+2}]\,[NaZ]^2}{[Na^{+}]^2\,[MgZ_2]} \quad (7d)$$

$$K_{ex}(Ca-K) = \frac{[K^{+}]^2\,[CaZ_2]}{[Ca^{+2}]\,[KZ]^2} \quad (7e)$$

$$K_{ex}(Na-K) = \frac{[K^{+}]\,[NaZ]}{[Na^{+}]\,[KZ]} \quad (7f)$$

Exchange constants like those defined above cannot be used in conventional computer codes like MINEQL and PHREEQE. In order to use them for equilibrium calculations, surface complexation constants have to be defined following Wanner's procedure (Wanner, 1986, pp.26-30):

$$K_{sc}(Na) = \frac{(NaZ)}{(Na^{+})\,(Z^{-})} \equiv 10^{20} \quad (8a)$$

$$K_{sc}(Ca) = \frac{(CaZ_2)}{(Ca^{+2})\,(Z^{-})^2} = \frac{K_{sc}(Na)^2}{K_{ex}(Na-Ca)}\,\frac{\lambda^2_{Na^{+}}\,\lambda_{CaZ_2}}{\lambda_{Ca^{+2}}\,\lambda^2_{NaZ}} \quad (8b)$$

$$K_{sc}(Mg) = \frac{(MgZ_2)}{(Mg^{+2})\,(Z^{-})^2} = \frac{K_{sc}(Na)^2}{K_{ex}(Na-Mg)}\,\frac{\lambda^2_{Na^{+}}\,\lambda_{MgZ_2}}{\lambda_{Mg^{+2}}\,\lambda^2_{NaZ}} \quad (8c)$$

$$K_{sc}(K) = \frac{(KZ)}{(K^{+})\,(Z^{-})} = \frac{K_{sc}(Na)}{K_{ex}(Na-K)}\,\frac{\lambda_{Na^{+}}\,\lambda_{KZ}}{\lambda_{K^{+}}\,\lambda_{NaZ}} \quad (8d)$$

where:

( ) is the activity of the species considered
λ is the activity coefficient of the species considered

The activity of the sorption sites (Z^-) is not known from the available analytical data. Consequently, assumptions on the value of (Z^-) must be made. Wanner postulated that all sites contributing to the total exchange capacity are occupied by exchanged cations at any time. This assumption is implicit in the very high value of the surface complexation constant in equation (8a). The choice of this value is arbitrary, but it must be large enough to ensure that the resulting *free site* activity (Z^-) is negligibly small. Also the choice of $K_{sc}(Na)$ as the normalising constant is arbitrary: any of the three remaining surface complexation constants could have been selected, yielding a new set of constants which would lead to identical computational results. Once a surface complexation constant has been assigned a fixed value ($K_{sc}(Na) = 10^{20}$), the other constants ($K_{sc}(Ca)$, $K_{sc}(Mg)$, $K_{sc}(K)$) can be calculated from the exchange constants (equations 7a,7d,7f) and from the activity coefficients of the species involved. The activity coefficients of the sorbed complexes (λ_{NaZ} , λ_{KZ} , λ_{CaZ2} and λ_{MgZ2}) are assumed to be unity, since they are not known, while activity coefficients of dissolved cations are calculated with Davie 's approximation (at 50 ^{o}C):

$$\log \lambda_{A^a} = - 0.5146\, a^2 \frac{\sqrt{I}}{1+\sqrt{I}} - 0.3\, I \qquad (9)$$

where A is a generic cation of valency a and I is the ionic strength [eq / l].

The set of surface complexation constants defined by equations (8a-d) is an implicit representation of the exchange constants listed in equations (7a-f), which takes into account a correction for the ionic strength. Each exchange constant can be represented by an appropriate combination of surface complexation constants, as can be seen by solving equations (8b-d) for K_{ex} (taking the left and right terms of the equations). Consistency between the two sets of constants can be checked by substituting into equations (8 b-d) the appropriate K_{sc} and K_{ex} values from Table 7, and the activity coefficients calculated from equation (9).

5.2 Extrapolation of exchange and surface complexation constants from the BGS experiments

The main objective in this section is to determine, if possible, reliable exchange and surface complexation constants from the BGS data; the aim being to use these later for the modelling of bentonite pore waters. In the procedure adopted, reaction quotients as formulated in equations (7 a-f) and (8 a-d) are first computed for all BGS experiments, then

the averages are determined. The extrapolated constants will be judged acceptable when the following criteria are met:

(1) the various quotients of a specific ion exchange reaction should be similar throughout all BGS experiments of the same type (in one type the bentonite samples reacted with the *simple LOW* and in the other with the *simple HIGH* solution). This criterion is not expected to apply through all experiments, since selectivity constants are usually ionic strength-dependent (Stumm and Morgan, 1981, p.644).

(2) the BGS constants should not deviate from the constants reported in the literature by more than one order of magnitude.

The results of this analysis are presented in Tables 7 and 8. Table 7 reports the quotients and averages for all BGS experiments, which are compared to the constants given by Wanner (1986). The BGS quotients are fairly uniform for all exchange reactions, as expressed by statistical uncertainties equal to or lower than half a logarithmic unit for the averages. The quotients for some cation pairs (Na^{+} - Ca^{+2} , Ca^{+2}- Mg^{+2} , Na^{+}- Mg^{+2}) tend to discriminate after the the ionic strength. As expected, the selectivity for magnesium with respect to sodium is larger in the more dilute solutions. In contrast, the selectivity for calcium with respect to sodium in the dilute *simple LOW* solutions is lower than in the *simple HIGH* solutions, which is contrary to the predicted behaviour (Stumm and Morgan, 1981, ibid.). The remaining cation pairs do not have distinctive selectivities as a function of ionic strength. For these reasons, the data from *simple LOW* and *simple HIGH* experiments have been "mixed", and no separate averages have been determined. Averages have therefore been calculated taking all the available values, with the exclusion of the lowest and highest whenever they appeared to be in evident disagreement with the general trend. Following this principle, it was found that the excluded data cluster on experiments B1 and B5. Since the quotients from these two experiments are consistently anomalous, it is suggested that they might be affected by serious systematic errors, which would justify their exclusion from this evaluation. Bateman et al. (1991) are aware of a "contamination" for experiment B1, but do not mention any problem with experiment B5.

The BGS constants are reasonably close to Wanner's values for the reactions involving all cations but K^{+}, for which discrepancies up to 1.7 log units are stated. This is not so surprising, considering the very low potassium concentrations involved in both Snellman's and BGS experiments, which should make measurements somewhat inaccurate.

The comparison with constants from the literature is based on Bolt's compilation (Bolt, 1982). To enable a comparison with the compiled data, the BGS and Wanner constants had to be recalculated to conform to Bolt's definition of *reduced constant* (Table 8). The values from the literature reported in Table 8 include only constants extracted from low temperature experiments with smectites. They tend to be smaller than the BGS and Wanner constants. However, the differences are small, considering the heterogeneity of materials and conditions in the experiments reported by Bolt.

In summary, it seems that the criteria mentioned above are met reasonably well for the BGS data. Therefore, the derived average surface complexation quotients have been incorporated in the MINEQL-PSI database for modelling cation exchange reactions between bentonite and aqueous solutions.

TABLE 7 - Tabulation of quotients for cation exchange equilibria, as defined in equations (7a-f) and (8a-d). The averaged surface complexation quotients (K_{sc}) are used for later model calculations. Wanner's constants (Wanner, 1986) are given for comparison.

	B1	B2	B3	B4	B5	B6	B7	B8	B9	B10	AVERAGE[1]	WANNER
Reacting solution[4] :	L	L	H	H	H	H	L	L	L	H		
log $K_{sc}(Na)$[2]	20.0	20.0	20.0	20.0	20.0	20.0	20.0	20.0	20.0	20.0	20.0	20.0
log $K_{sc}(Ca)$	40.3*	41.6	42.7	42.7	43.1*	42.5	42.1	42.3	42.0	41.6	42.2 ± 0.5	42.2[3]
log $K_{sc}(Mg)$	39.7*	40.8	41.5	41.4	41.5	41.4	41.8	41.7	41.7	40.9	41.4 ± 0.3	41.7
log $K_{sc}(K)$	20.7*	20.9	20.9	21.0	20.9	20.9	21.0	20.9	21.0	20.9	20.9 ± 0.1	20.4
log $K_{ex}(Na\text{-}Ca)$	- 0.3*	-1.6	-2.7	-2.7	-3.1*	-2.5	-2.1	-2.3	-2.0	-1.6	-2.2 ± 0.4	-2.2[3]
log $K_{ex}(Ca\text{-}Mg)$	0.6	0.7	1.2	1.3	1.6*	1.1	0.3*	0.6	0.3	0.7	0.8 ± 0.3	0.6[3]
log $K_{ex}(Mg\text{-}K)$	-1.7*	-1.3	-0.4	-0.5	-0.3*	-0.4	-0.2	-0.1	-0.3	-0.8	-0.5 ± 0.3	0.9
log $K_{ex}(Na\text{-}Mg)$	+0.3*	-0.8	-1.5	-1.4	-1.5	-1.4	-1.8	-1.7	-1.7	-0.9	-1.4 ± 0.3	-1.7
log $K_{ex}(Ca\text{-}K)$	-1.1*	-0.3	0.9	0.5	1.3*	0.8	0.2	0.6	0.0	-0.1	0.3 ± 0.4	1.4[3]
log $K_{ex}(Na\text{-}K)$	-0.7*	-0.9	-0.9	-1.0	-0.9	-0.9	-1.0	-0.9	-1.0	-0.9	-0.9 ± 0.05	-0.4

NOTES:

[1] Averages have been calculated excluding the anomalous values marked with an asterisk (see text for more explanation).

[2] $K_{sc}(Na)$ values are set to 20 by definition (see text for detailed explanation).

[3] The constants involving *Ca* do not correspond exactly to those given by Wanner (1986) in his Table 5. It seems that an error has occurred in the transformation of the sorbed *Ca* concentration (9.45 meq / 26.7 g bentonite, Table 4 in Wanner, 1986) from equivalent to molar concentration.

[4] **L** : experiment with *simple LOW* solution , **H** : experiments with *simple HIGH* solution.

TABLE 8 - Comparison between exchange constants derived from bentonite-water interaction experiments for radioactive waste disposal (Wanner, 1986; Bateman et al., 1991) and values from the literature (Bolt, 1982). The BGS and Wanner constants have been reduced to the form used in Bolt's compilation: log $K^*_{ex}(A\text{-}B) = (1/ab)$ log $K_{ex}(A\text{-}B)$, where *a,b* are the valencies of cations *A* and *B*, respectively.

log $K^*_{ex}(A\text{-}B)$	LITERATURE	WANNER	BGS
K - Na	0.15 to 0.75	0.4	0.90 ± 0.05
Ca - Na	0.15 to 0.72	1.1	0.95 ± 0.20
Ca - Mg	0.02 to 0.11	0.15	0.20 ± 0.10

6. Analysis of BGS solution data: are fluid compositions controlled by saturated solids ?

6.1 Mineral composition of bentonites: implications for the solution chemistry

The main components of bentonites are clay minerals of the montmorillonite - beidellite series (smectites), which are invariably accompanied by a number of trace minerals. These are either relics of the original volcanic rock from which the bentonite derives, or secondary alteration products. According to Grim and Güven (1978), bentonites may contain free SiO_2 (as quartz, cristobalite or trydimite), zeolites, feldspars, kaolinite, micas, illite, gypsum and calcite in appreciable amounts (up to about 15%). Zircon, magnetite, magnesite, apatite, pyroxenes and many opaque minerals may be present as accessory phases. Only a few studies, however, deal with the detailed mineralogical composition of bentonites. Müller-Vonmoos and Kahr (1983) determined the mineralogy of the MX-80 and MONTIGEL bentonites, which may be used as a backfill in the Swiss HLW repository. Srodon (1976) identified a number of primary and secondary minerals in bentonites from the upper Silesian basin, which allowed him to draw some conclusions on the genesis of the studied rocks. Harr (1976) concentrated on the study of accessory minerals from Swiss and German bentonite occurrences in an attempt to unravel the petrologic history of their volcanic precursors. A list of the minerals identified in these studies (Table 9) shows that carbonates, quartz and probably kaolinite, feldspars, micas and chlorite are ubiquitous in the studied bentonites. Among the opaque minerals, goethite and pyrite were found most frequently in the investigated samples. Surprisingly, Harr (1976) does not mention the presence of hematite, but this mineral may be hidden as exsolution lamellae within ilmenite. Exsolution of hematite from ilmenite is very common, since this primarily magmatic mineral can dissolve only limited amounts of Fe_2O_3 at low temperatures (Deer et al., 1966). Neither is magnetite reported, but this mineral will be present in large amounts in the Swiss repository as the main corrosion product of cast iron (Simpson, 1989).

The occurrence of trace minerals in bentonite cannot be ignored when modelling bentonite-water interactions in the repository environment. Because of the low water/rock ratios, the dissolution of a trace mineral may readily produce saturated solutions. Speciation calculations reveal, for instance, that amounts of calcite less than 0.5 % by volume in the starting material would be sufficient to saturate the pore water (see Tables 17 and 18). Conditions close to calcite saturation were obtained, for example, in the solutions produced by Snellman's experiments, in which a bentonite with only 1.4 weight % calcite reacted with a synthetic groundwater (Wanner, 1986).

Moreover, some trace iron minerals like goethite, pyrite and hematite might be important in controlling the oxidation potential of the solution, which is a major parameter governing the solubility of redox-sensitive nuclides (Schweingruber, 1983). Because the BGS experiments did not yield any information in this respect, it will be necessary to estimate the oxidation potential of bentonite pore fluids with the help of thermodynamic data on these minerals (see chapter 7).

TABLE 9 - List of minerals identified in bentonites from various localities. The amounts of mineral found in the bentonite samples are given as weight percentages (in parentheses), where known. Otherwise, only qualitative indications are given, according to the legend below. Empty cells do not necessarily imply absence of the mineral in the investigated samples: in most cases, the identification was simply not attempted.

Legend:

N : number of bentonite localities studied
(X) : amount not known
(+++) : very common to ubiquitous, in appreciable amounts
(++) : found frequently in appreciable amounts
(+) : found seldom, but locally abundant
(-) : never in appreciable amounts

REFERENCE	Müller-Vonmoos and Kahr (1983)	Bateman et al. (1991)	Harr (1976)	Srodon (1976)
N:	2	1	10	5
MINERAL				
ILMENITE			(+)	
GOETHITE			(+++)	
HEMATITE				
MAGNETITE				
PYRITE	(0 - 0.3%)		(++)	
APATITE			(-)	(X)
GARNET			(++)	
TOURMALINE			(-)	
EPIDOTE			(++)	
CARBONATES	(1 - 4%)	(X)	(+++)	(X)
QUARTZ	(8 -15%)	(X)	(+++)	(X)
FELDSPARS	(2 - 8%)		(-)	(X)
MICAS	(1 - 15%)		(+++)	(X)
CHLORITE		(X)	(+)	(X)
KAOLINITE		(X)		(X)

6.2 Procedure for the definition of bentonite pore waters

In the following sections, the BGS solution data will be carefully examined in order to identify possible saturation equilibria between the pore water and minerals in the bentonite. The objective is to find out whether the BGS final solution compositions can be reproduced using a set of empirical solubility constants, which may or may not be related to minerals known to be present in the bentonite samples. In detail, the procedure adopted here can be summarised in the following steps:

1. Speciation and activities of the BGS *final* solutions are calculated with the MINEQL-PSI code, using the updated *Nagra thermochemical database* (Pearson and Berner, 1991; Pearson et al., 1991).

2. Activities of various species are plotted against each other in logarithmic plots in order to identify correlations reflecting saturation equilibria (Figure 2).

3. On the basis of these correlations, mineral formulae are defined. The corresponding activity quotients are calculated and the average over all the experiments is determined. If the relative mean standard deviation is small, the average is selected as the solubility constant of a model phase with the specified stoichiometry.

4. The reaction between a reference crystalline water and the bentonite MX-80 is simulated with the MINEQL-PSI code, assuming the water/rock ratio expected in a resaturated compacted bentonite ($\varepsilon = 0.4$). In these simulations, saturation of the selected model solids is imposed, and the previously derived cation exchange constants must also apply. The redox potential is calculated by assuming equilibrium between the solution and iron solids selected on the basis of mineralogical criteria (chapter 7). These solids are included in the set of minerals for which saturation is required during the geochemical calculations. The resulting fluid composition then defines a *bentonite pore water.*

The stoichiometries of the model solids have been derived by combining the results of cross activity plots with mineralogical considerations (see following discussion). In some cases, stated activity correlations cannot be related to any solubility constant of minerals known or expected to occur in bentonites. In spite of this limitation, such constants can be used to model bentonite waters if they are regarded as purely empirical tools for predicting the dissolution behaviour of the BGS bentonite.

In the simulation, it is assumed that the bentonite is not supplied with dissolved species from outside, after it has been saturated with groundwater. This assumption is not realistic, since interdiffusion of dissolved chemicals between the repository and a groundwater reservoir is likely to occur after resaturation of the bentonite in the repository. A continuous supply of chemicals from the groundwater reservoir would certainly affect the chemical evolution of the bentonite pore water. Wanner (1986) tried to predict such an evolution by modelling the changes in exchangeable cation populations as an increasing volume of groundwater reacts with a fixed amount of bentonite. The model implies that the exchanged cations will ultimately be in equilibrium with the original groundwater, after more than 100 water exchange cycles (in each cycle, the equilibrated pore solution is replaced with an equivalent volume of unreacted groundwater). Thus, according to Wanner's model, the original groundwater itself would be the final, stable bentonite pore water. This seems very unlikely, as the long-term composition of bentonite waters will be largely determined by kinetically slow dissolution / precipitation reactions, which are not detectable on the time scale of laboratory experiments. Such reactions, however, cannot be modelled on the basis of current knowledge, as previously discussed (see *Introduction).* Therefore, it seems useless to attempt a prediction of the long-term chemistry of bentonite pore waters in the Swiss HLW repository. Such modelling is not possible even in a strongly simplified system containing pure montmorillonite and distilled water. In a repository environment, additional

complexities arise from the mutual interactions among the various repository materials. For instance, the bentonite water would react with the steel canister, causing the precipitation of iron silicates. The thermodynamic properties, and even the identity, of such silicates are still unknown (Grauer, 1988).

In view of the above considerations, and because the parameters of our model (exchange and solubility constants) are extrapolated from short-term experiments, the assumption of a closed system, which cannot exchange chemical species with the surroundings once the bentonite has been resaturated, appears more reasonable. However, one has to keep in mind that the modelled water compositions refer to an early stage in the evolution of the repository, and do not necessarily represent stable equilibrium conditions.

6.3 Incongruent dissolution of montmorillonite

In the recent literature on clay-water interaction, a central and still unresolved question is whether smectites dissolve congruently according to a well-defined thermodynamic equilibrium constant (Kittrick, 1971a,b,c ; Kittrick and Peryea 1988, 1989 ; Tardy and Fritz, 1981; Tardy et al., 1987), or whether they should be regarded as complex, incongruently dissolving phases with no well-defined solubility constant (Churchman and Jackson, 1976; May et al., 1986). In the former case, it was attempted to demonstrate the attainment of equilibrium conditions from both undersaturation and oversaturation by means of activity plots derived from solution data. The results of experiments carried out on American montmorillonites at 25 ^{o}C under acid conditions (Kittrick, 1971a,b,c) suggested that the solution compositions moved towards an empirical montmorillonite equilibrium line on a $p(H_4SiO_4)$ vs. pH-1/3 $p(Al^{+3})$ plot, but were inconclusive in spite of the long equilibration times (3-4 years). In contrast, analogous experiments with other American and Hawaiian montmorillonites at near-neutral pHs (5 to 8) lasting for about 3 years (May et al., 1986) failed to reveal any evidence of an equilibrium line with the slope dictated by the montmorillonite formula. These data suggested that montmorillonite dissolves incongruently, and that the solution composition is controlled by secondary alumosilicate minerals, either present in trace amounts in the initial sample (it is almost impossible to completely purify a smectite) or as newly formed precipitates. Similar findings had been reported earlier for experiments carried out under acid conditions (Churchman and Jackson, 1976).

To test whether a solubility limit for montmorillonite was reached during the BGS experiments, or secondary phases controlled the fluid compositions, a series of cross activity and concentration plots have been prepared (Figures 1 to 8). In Figure 1, the total Al and Si concentrations have been plotted against each other, along with the line describing congruent dissolution of the BGS montmorillonite (derived from the montmorillonite stoichiometry determined earlier), in order to check whether the montmorillonite used in the BGS experiments dissolves congruently or not. Al and Si were preferred to other elements because they are not involved in exchange reactions (they occupy only octahedral or tetrahedral sites). All dissolution paths depart from the origin of the plot, since the starting solutions were virtually free of dissolved Si and Al. Congruent dissolution of montmorillonite would be indicated by dissolution paths following the montmorillonite line.

The first segments of each path refer to analyses carried out on fluids sampled shortly after the reaction temperature of 50 °C had been reached (some hours after preparation of the fluid/bentonite mixtures). They indicate incongruent dissolution for all but 2 experiments. In the experiments with a low-ionic-strength starting fluid (*simple LOW*), the dissolution proceeds at a consistently low Si:Al ratio of about 0.5, which is clearly lower than the stoichiometric ratios of the montmorillonite (2.58) and even of kaolinite (1.0). This means that Al is preferentially leached with respect to Si. Contrasting behaviour is observed in the experiments performed with the high-ionic-strength fluid (*simple HIGH*), which invariably show higher initial Si:Al ratios. In some cases, near-congruent dissolution is observed, while in the other cases the Si:Al ratio in solution is higher than in montmorillonite.

After the initial increase there is, in general, a considerable decrease in the Al concentration. At the same time, the Si concentration tends to increase further to values between 2 and 4 x 10^{-4} [mol/l]. Such a pattern strongly suggests that, after a first stage in which Al is released rapidly into solution, precipitation of an aluminous solid occurs. Sorption of Al by the clay is not likely, because this process is usually fast and because the dominant aluminum species is $Al(OH)_4^-$, which is negatively charged. In summary, Figure 1 shows that montmorillonite dissolves incongruently and that precipitation of a secondary Al-bearing solid probably occurs after an initial increase in the Al concentration. It should be remembered, however, that all but experiments B9 and B10 were carried out using materials containing significant amounts of impurities, which could interfere with the montmorillonite dissolution (superimposed dissolution of silicates and alumosilicates).

6.4 A method for determining solids in equilibrium with a solution

Further insight into the role of secondary phases in controlling the BGS solution compositions is gained through the use of logarithmic activity plots for dissolved species. Activities are combined in such a way that the assumption of saturation with a solid of specified stoichiometry can be checked. In a first step, the activities of *single* species are plotted against each other in logarithmic plots, with the aim of detecting possible linear correlations. If, for instance, the activities of the calcium and bicarbonate ions in the BGS final solutions lead to a well-defined linear trend on a log-log plot, one can either assume that a carbonate phase (not necessarily calcite) is saturated in all solutions, or that different amounts of the carbonate mineral have been dissolved in the various solutions. In other words, linear trends in cross activity plots may be due either to saturation or to kinetic effects. The distinction is made by the *slope* of the linear relation. For a calcite, linear trends caused by kinetic effects would have a positive slope, because both activities would increase in a plot of $\log(Ca^{+2})$ vs. $\log(CO_3^{-2})$. Conversely, if the linear correlation is due to saturation effects, the slope must be negative, with a value of *precisely* -1 as dictated by the stoichiometry of the mineral. This is because the logarithms of the 2 activities must be inversely proportional to each other, according to the relation $\log(Ca^{+2}) = \log K - \log(CO_3^{-2})$, when saturation conditions apply.

Thus, in order to detect saturation with a solid phase, assumptions as to its stoichiometry

must first be made, and a dissolution reaction with corresponding activity quotient has to be defined. If the reaction quotients calculated for the various BGS experiments equal each other, saturation equilibrium with a phase of the postulated stoichiometry can be assumed. However, the solid can be identified as a real phase only if the modelled activity quotients coincide with a well-known solubility constant.

Such analyses can be visualised in appropriate cross activity plots. As an example, consider the dissolution of an alumosilicate with kaolinite composition:

$$Al_2Si_2O_5(OH)_4 + 6\,H^+ = 2\,Al^{+3} + 2\,H_4SiO_4 + H_2O$$

The logarithm of the reaction constant ($\log K$) can be defined as:

$$\log K = 2\log(H_4SiO_4) + 2\log(Al^{+3}) - 6\log(H^+) \qquad (11)$$

Defining $p = -\log_{10}$, equation (11) can be rearranged as follows:

$$[p(H_4SiO_4)+p(Al^{+3})] = [3pH] - 1/2\log K \qquad (12)$$

In a plot with $x = [3pH]$ and $y = [p(H_4SiO_4)+p(Al^{+3})]$, equilibrium with a solid of the stoichiometry defined in equation (11) would imply that the data must lie on a line with slope +1 and intercept - 1/2 log K. Several relations of this kind have been plotted for the BGS experiments according to the list of dissolution reactions given in Table 10 (Figures 2 to 8). The results of activity quotient calculations related to these dissolution reactions are presented in Table 11, from which a set of empirical solubility constants has been extracted. Solubility constants of known minerals with corresponding stoichiometries, to be used for comparison with the calculated average quotients, are compiled in Table 12. This method has been used previously by several authors (Kittrick 1971 a,b,c; Churchman and Jackson, 1976; May et al., 1986) to test the assumption of thermodynamic equilibrium between a solution and selected minerals.

The next sections are devoted to the detailed discussion of such plots. The goal is to determine whether the BGS activity data can be related to solids in saturation equilibrium with the solutions. The ion activities used stem from speciation models of the BGS final solutions, which have been calculated with the MINEQL-PSI code.

FIGURE 1 - Plot showing the dissolution paths defined by the total Si and Al concentrations during the BGS experiments. All paths start at the origin, because the initial solutions (*simple HIGH* or *simple LOW*) were virtually free of dissolved Si and Al. Open symbols refer to samples taken a few hours after the beginning of the experiments or to later intermediate sampling, while solid symbols represent the results of final solution analyses (2-4 weeks leaching time). The 2 thick lines mark the paths for congruent dissolution of the montmorillonite used in the experiments and of kaolinite. Some path lines are arbitrarily curved for clarity. Source data are found in Appendix A.

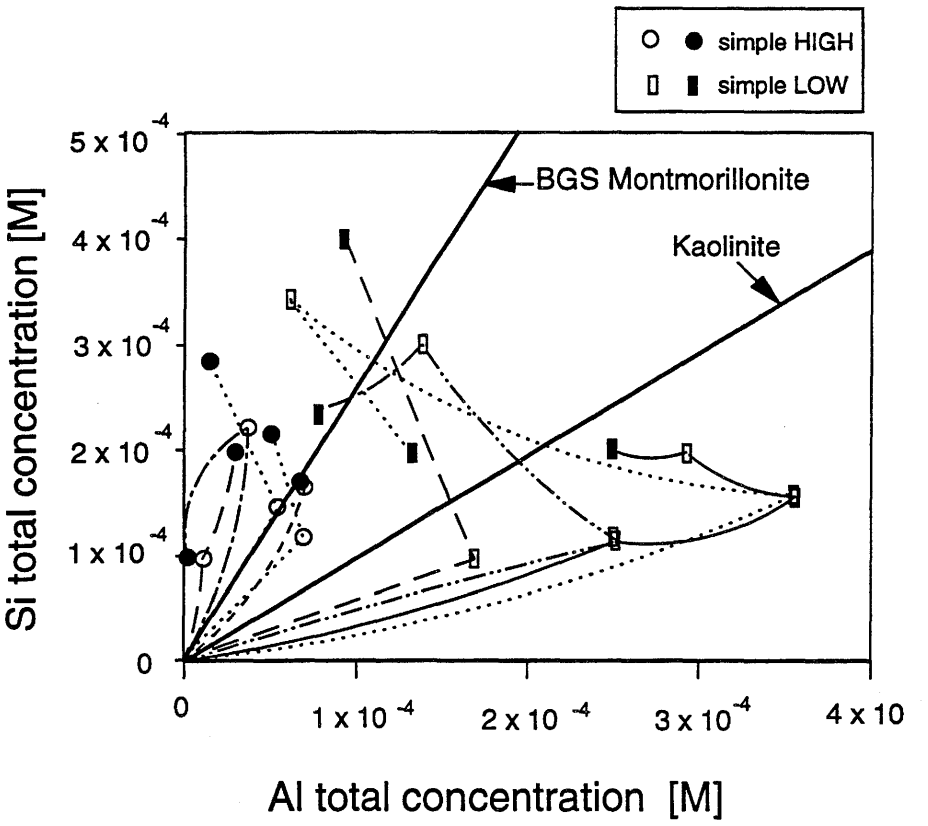

6.5 Simple correlations

Figure 2 shows cross activity diagrams, in which 2 species are plotted against one another. Of the combinations shown, the $p(Al^{+3})$ vs. pH plot (Fig. 2a) displays the best fit to a line. This well-defined correlation is, however, an artifact, since a linear correlation between pH and Al^{+3} activity logarithms occurs necessarily because of the progressive hydrolysis of Al^{+3} with increasing pH. At constant total dissolved aluminum concentration and alkaline pH, a slope of -4 in the plot of Figure 2a is imposed by the equilibrium $Al^{+3} + 4\ H_2O = Al(OH)_4^- + 4\ H^+$ (remember that the total Al concentration is almost equal

to that of $Al(OH)_4^-$ at pH > 8). Because the variation of the total dissolved aluminum in the considered BGS solutions is limited, lying within about a logarithmic unit (1.4×10^{-5} to 2.5×10^{-4} [mol/l]), and pH values are invariably larger than 8, a linear correlation with a slope of -4 ± 1 would result from the hydrolysis of dissolved Al species alone. Therefore, the correlation observed in the $p(Al^{+3})$ vs. pH plot does not necessarily imply the presence of a saturated solid. To obviate this problem, all plots involving Al^{+3} will be accompanied by equivalent plots in which the the Al^{+3} activity has been replaced with the activity of $Al(OH)_4^-$, by far the dominant Al species in the pH region of interest. These plots (Figures 2 b,d,f,h,j) are not flawed, since the activity of $Al(OH)_4^-$ is closely related to the measured total Al concentration.

Figure 2b shows that a satisfying linear correlation exists between $p(Al(OH)_4^-)$ and pH, although the fit is not as good as in Figure 2a. Correlations are also evident in the plots of $p(K^+)$ and $p(Na^+)$ against $p(Al(OH)_4^-)$ (Figures 2h,j). Interestingly, the linear trends in these two plots are even better defined than those in the corresponding $p(Al^{+3})$ plots.

In all other cases, either no correlation is detected, as in the $p(K^+)$ vs. $p(Al^{+3})$, $p(Ca^{+2})$ vs. $p(Al^{+3})$, $p(Mg^{+2})$ vs. $p(H_4SiO_4)$ plots, or the trend is defined by only 2 clusters, as shown by the $p(Mg^{+2})$ vs. $p(CO_3^{-2})$, $p(Ca^{+2})$ vs. $p(CO_3^{-2})$, $p(Mg^{+2})$ vs. pH and $p(Mg^{+2})$ vs. $p(Al^{+3})$ plots.

Not all possible activity combinations are represented in Figure 2. The selected combinations reflect mineralogical criteria. For instance, it seems reasonable to look for combinations corresponding to common carbonates (calcite, magnesite) but not for the highly soluble sodium and potassium carbonates, which cannot reach saturation in the investigated fluids. Further combinations with $p(H_4SiO_4)$ have been also excluded, since this parameter has a very small variation (less than 0.5 log units). This means that plotting $p(H_4SiO_4)$ against other activity logarithms will always lead to unrelated patterns, as exemplified by the $p(Mg^{+2})$ vs. $p(H_4SiO_4)$ plot.

TABLE 10 - Summary of mineral dissolution reactions for which the saturation state in the BGS final solutions has been tested, with the corresponding equilibrium equations.

	REACTIONS	*MINERALS*
1.	$Al_2Si_2O_5(OH)_4 + 6\,H^+ = 2\,Al^{+3} + 2\,H_4SiO_4 + H_2O$ $\log K_1 = 6\,pH - 2\,p(Al^{+3}) - 2\,p(H_4SiO_4)$	KAOLINITE HALLOYSITE DICKITE NACRITE
2.	$Al(OH)_3 + 3\,H^+ = Al^{+3} + 3\,H_2O$ $Al\,O\,OH + 3\,H^+ = Al^{+3} + 2\,H_2O$ $\log K_2 = 3\,pH - p(Al^{+3})$	GIBBSITE amorph.-$Al(OH)_3$ DIASPORE BOEHMITE
3.	$Al_2Si_4O_{10}(OH)_2 + 4\,H_2O + 6\,H^+ = 2\,Al^{+3} + 4\,H_4SiO_4$ $\log K_3 = 6\,pH - 2\,p(Al^{+3}) - 4\,p(H_4SiO_4)$	PYROPHYLLITE
4.	$NaAlSi_2O_6.H_2O + H_2O + 4\,H^+ = Na^+ + Al^{+3} + 2\,H_4SiO_4$ $\log K_4 = 4\,pH - p(Al^{+3}) - 2\,p(H_4SiO_4) - p(Na^+)$	ANALCIME
5.	$CaAl_2Si_4O_{12}.H_2O + 3\,H_2O + 8\,H^+ = Ca^{+2} + 2\,Al^{+3} + 4\,H_4SiO_4$ $\log K_5 = 8\,pH - 2\,p(Al^{+3}) - 4\,p(H_4SiO_4) - p(Ca^{+2})$	WAIRACKITE
6.	$KAlSi_2O_6 + 2\,H_2O + 4\,H^+ = K^+ + Al^{+3} + 2\,H_4SiO_4$ $\log K_6 = 4\,pH - p(Al^{+3}) - 2\,p(H_4SiO_4) - p(K^+)$	LEUCITE
7.	$CaCO_3 = Ca^{+2} + CO_3^{-2}$ $\log K_7 = - p(Ca^{+2}) - p(CO_3^{-2})$	CALCITE
8.	$Mg_3Si_4O_{10}(OH)_2 + 4\,H_2O + 6\,H^+ = 3\,Mg^{+2} + 4\,H_4SiO_4$ $\log K_8 = 6\,pH - 3\,p(Mg^{+2}) - 4\,p(H_4SiO_4)$	TALC
9.	$Mg(OH)_2 + 2\,H^+ = Mg^{+2} + 2\,H_2O$ $\log K_9 = 2\,pH - p(Mg^{+2})$	BRUCITE
10.	$MgAl_2Si_3O_{10}.2H_2O + 8\,H^+ = Mg^{+2} + 2\,Al^{+3} + 3\,H_4SiO_4$ $\log K_{10} = 8\,pH - p(Mg^{+2}) - 2\,p(Al^{+3}) - 3\,p(H_4SiO_4)$	(-)

FIGURE 2 - Cross activity plots between selected species, constructed with activity data obtained from speciation models of the BGS final solutions. The prefix *p* stands for $-log_{10}$. The aim of these representations is to detect possible linear correlations, which would suggest the presence of saturated solids in the BGS solutions. All the plots involving Al have been represented using both the Al^{+3} and $Al(OH)_4^-$ activities. Because linear correlations in plots constructed with $p(Al^{+3})$ may be artifacts (see text for a detailed explanation), only the corresponding plots with $p(Al(OH)_4^-)$ should be used to assess possible correlations.

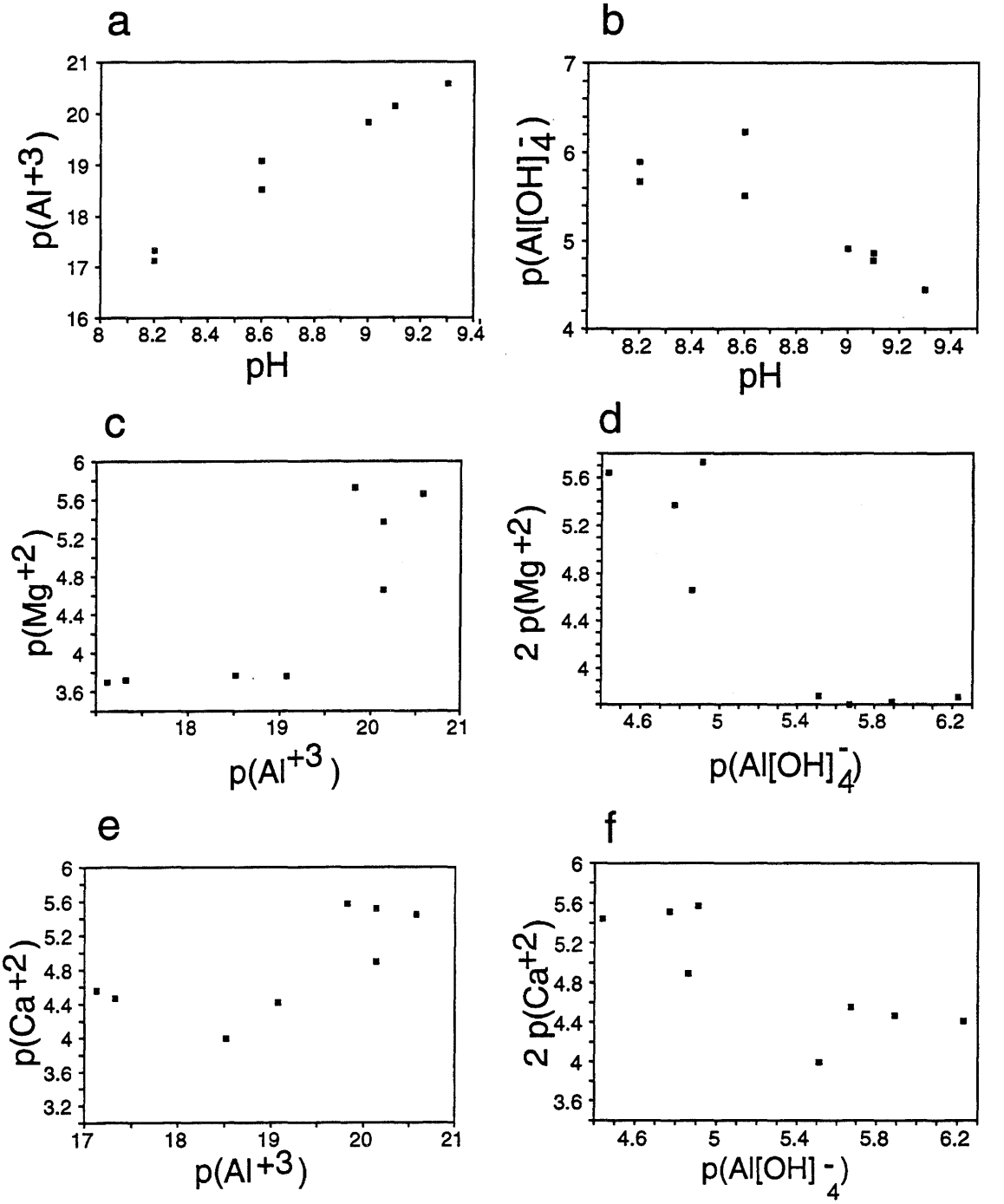

Figure 2 (continued)

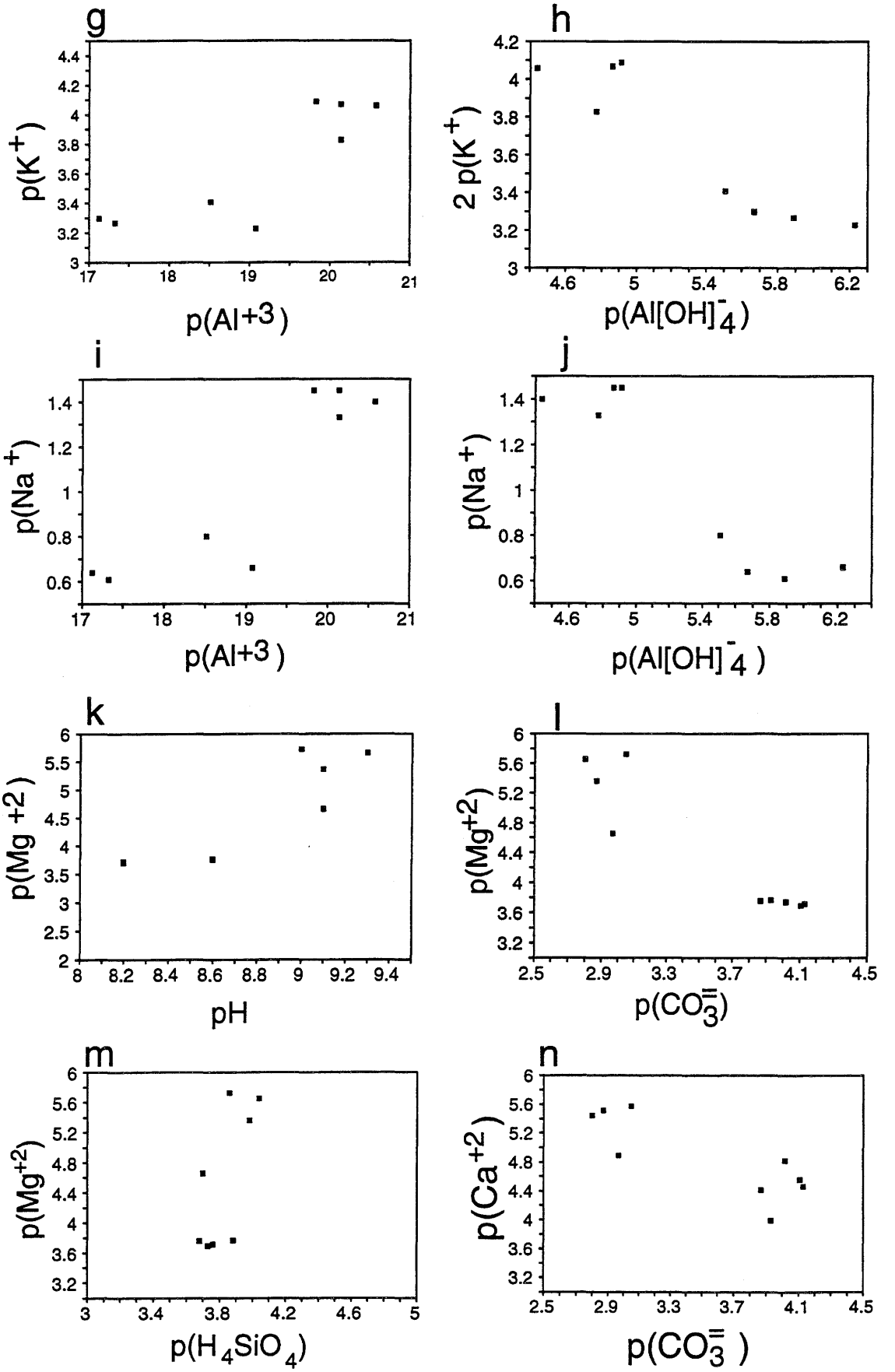

6.6 Al - Si - pH relations

In the previous analysis, the activities of $Al(OH)_4^-$ and H^+ were found to be linearly dependent on a log-log plot. These linear correlations suggest that the BGS solutions may be saturated with an aluminum hydroxide. Figure 3a shows that the calculated activities plot very close to a theoretical gibbsite equilibrium line, while amorphous $Al(OH)_3$ cannot be the controlling phase, as it is clearly undersaturated in all solutions.

Another prominent feature is the approximately constant silicic acid activity (Figures 3e,f). This finding, together with the fact that most calculated H_4SiO_4 activities are below quartz saturation (2.5×10^{-4} at 50 °C), suggests that the Al and Si concentrations in solution may be regulated by the coexistence of an Al-hydroxide phase and an alumosilicate of kaolinite composition, after the following reaction:

$$Al_2Si_2O_5(OH)_4 + 5\,H_2O = 2\,Al(OH)_3 + 2\,H_4SiO_4 \qquad (13)$$

Figure 3c shows that the BGS solution data are roughly consistent with a saturation equilibrium controlled by the mineral *halloysite*, one of several modifications of $Al_2Si_2O_5(OH)_4$, rather than by *kaolinite*. The buffered (H_4SiO_4) activities, on the other hand, lie within the range defined by the coexistence of *diaspore* and *kaolinite* at equilibrium (Figure 3e). The low silicic acid activities may also be explained assuming re-equilibration of the solutions with unfiltered quartz at room temperature (see equilibrium activity for quartz at 25° C in Figure 3f).

These relations show how difficult it may be to *identify* saturated minerals by this method: because of large uncertainties in the selected thermodynamic data, it is often impossible to distinguish which of several minerals could be saturated. The uncertainties of the constants used are sometimes larger than the differences that should be discerned, even for well-studied minerals like these simple alumosilicates (see Table 12). Another intrinsic danger of this extrapolation method is illustrated by Figure 3g: the BGS speciation data plot very close to the equilibrium line of the mineral *pyrophyllite*, an alumosilicate with formula $Al_2Si_4O_{10}(OH)_2$, i.e. with twice more Si than kaolinite per formula unit. In spite of the differing stoichiometry, which should in general be reflected by distinct slopes for the data on Figures 3c and 3g, the BGS activity data lie parallel also to the pyrophyllite equilibrium line. This effect is due to the small variation of the $p(H_4SiO_4)$ values: because the variables on the ordinates in the mentioned two plots differ only by 1 $p(H_4SiO_4)$, the effect of adding this parameter is almost equivalent to the addition of a constant, so that nearly identical slopes are obtained. These problems, however, are not crucial for the modelling work. The important and useful feature of the data is that empirical solubility constants for specific stoichiometries can be extracted with a reasonable degree of accuracy, even if they cannot be associated to real solids.

FIGURE 3 - Cross activity plots for the dissolution reactions of simple alumosilicates and Al-hydroxide (Table 10). The activity data from the BGS final solutions are compared with the lines defined by saturation equilibrium of selected solids. See text for a detailed discussion of these plots.

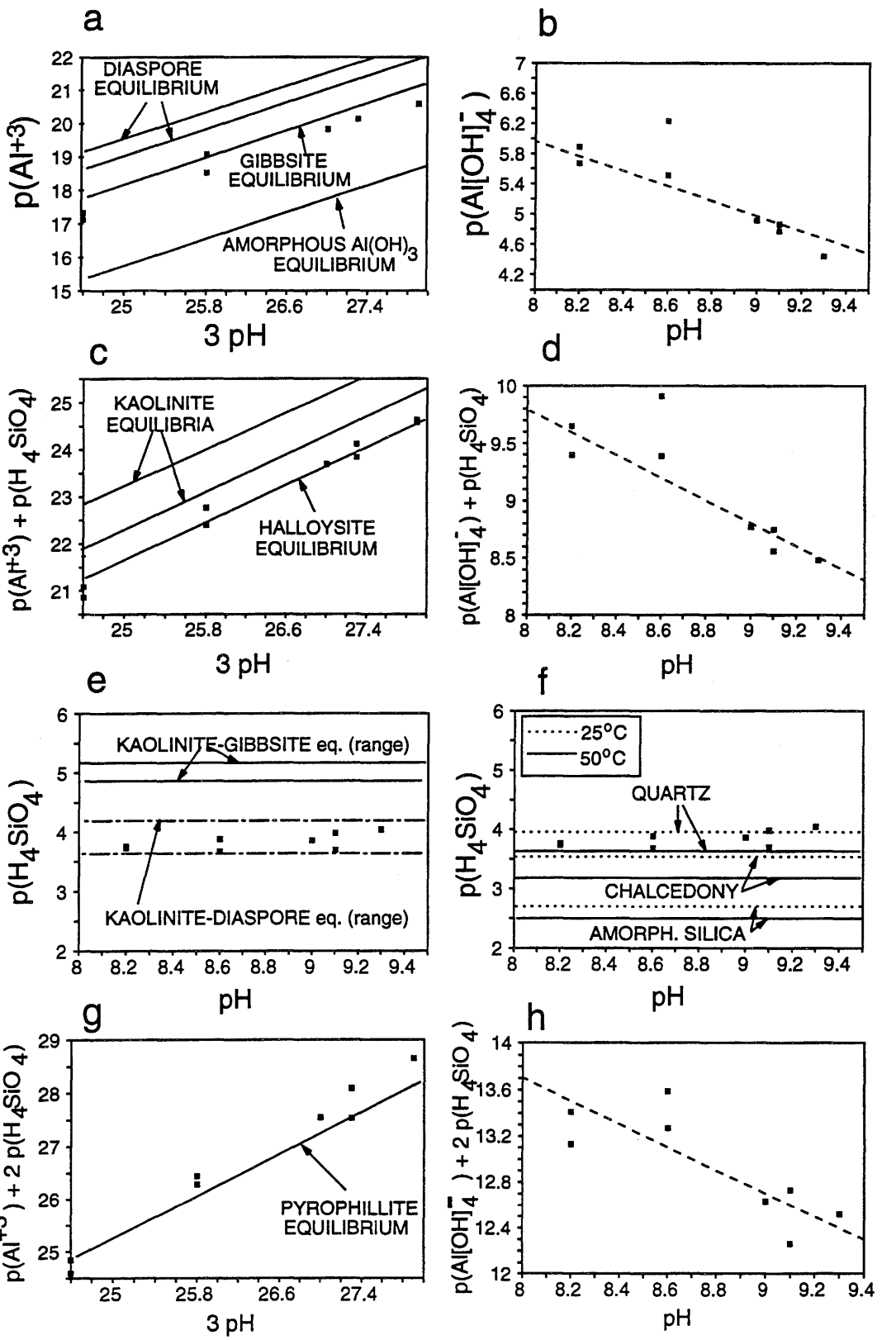

FIGURE 4 - Cross activity plots for testing the assumption that an Al-hydroxide (Fig. 4a) and a solid with kaolinite stoichiometry (Fig. 4b) control the Al and Si dissolved concentrations in bentonite pore waters. The BGS data are plotted along with data from the literature. The bounding lines correspond to the ranges of equilibrium constants compiled in Table 12 defined by: all $Al(OH)_3$ solids between 25 and 50 °C (Fig. 4a), and all $Al_2Si_2O_5(OH)_4$ solids at 50 °C (Fig. 4b).

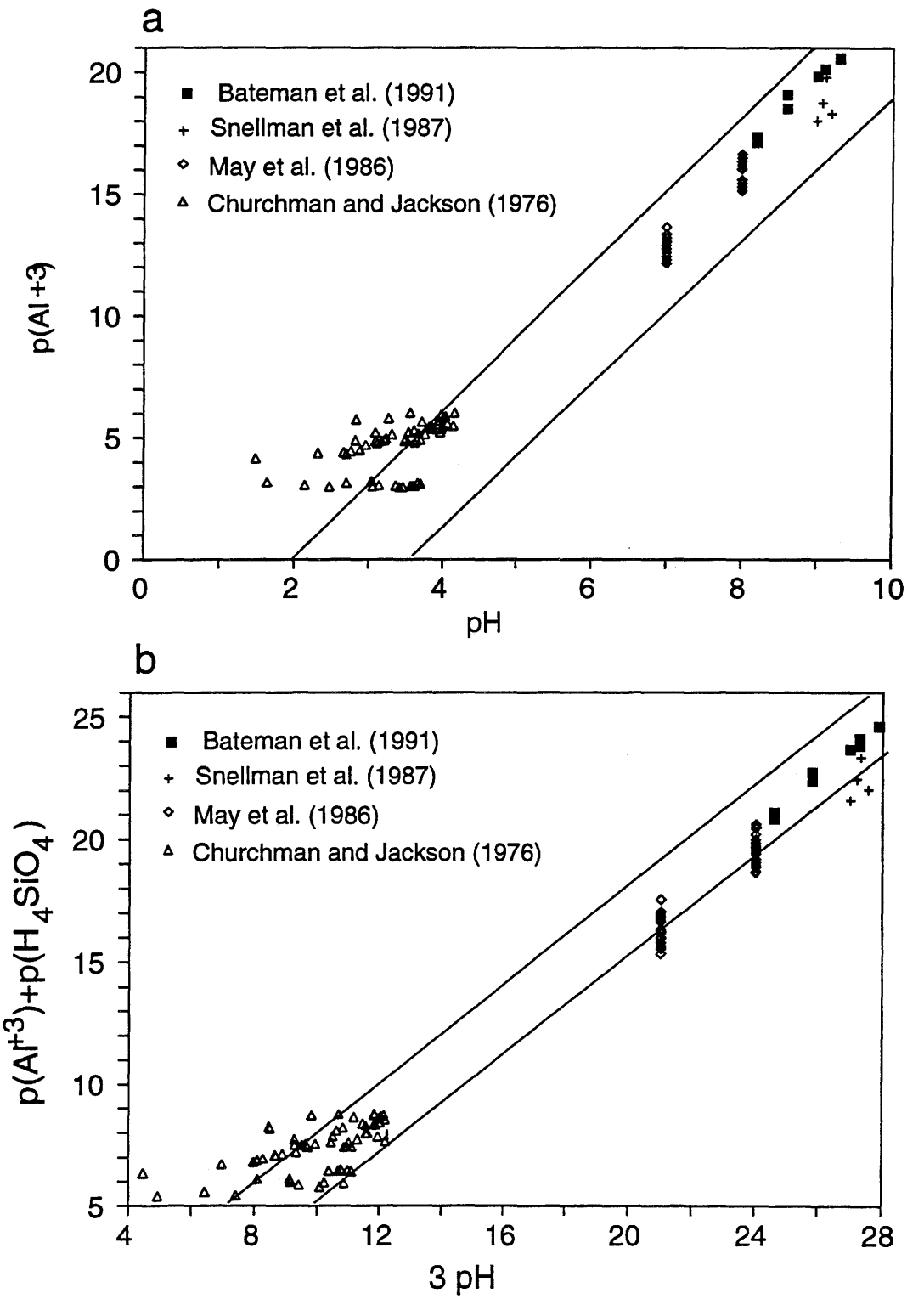

TABLE 11 - Statistical analysis of activity quotients for the reactions listed in Table 10, calculated from the BGS final solution data (Appendix A).

	$\log Q_1$	$\log Q_2$	$\log Q_3$	$\log Q_4$	$\log Q_5$	$\log Q_6$	$\log Q_7$	$\log Q_8$	$\log Q_9$	$\log Q_{10}$
B1	9.6	7.9	3.3	9.1	17.6	6.7	-6.7	30.7	14.4	20.9
B2	6.9	7.2	-0.5	7.4	12.8	4.8	-7.9	25.8	13.5	16.8
B3	7.0	7.3	-0.5	7.3	11.4	4.7	-8.6	23.0	12.7	15.9
B4	7.5	7.5	0.0	7.6	11.9	4.9	-8.7	23.2	12.7	16.5
B5	4.3	6.2	-3.8	5.9	8.1	3.3	-8.8	22.9	13.1	13.3
B6	6.1	6.7	-1.3	7.3	11.5	4.7	-8.3	25.6	13.4	15.8
B7	6.6	7.2	-1.1	7.0	11.3	4.4	-8.7	21.4	12.3	15.0
B8	6.4	7.2	-1.6	7.0	11.1	4.5	-8.4	22.6	12.8	15.2
B9	6.6	7.3	-1.5	7.1	11.6	4.5	-8.3	22.7	12.9	15.5
B10	6.8	7.3	-1.0	7.3	12.2	4.7	-7.9	24.8	13.4	16.4
AVERAGE (B1 and B5 excluded)	6.7	7.2	-0.9	7.3	11.7	4.7	-8.4	24.0	13.1	15.9
STANDARD DEVIATION	± 0.4	± 0.2	± 0.5	± 0.2	± 0.5	± 0.2	± 0.3	± 1.3	± 0.3	± 0.6
MINERAL FORMULA	$Al_2Si_2O_5(OH)_4$	$Al(OH)_3$	$Al_2Si_4O_{10}(OH)_2$	$NaAlSi_2O_6$.	$CaAl_2Si_4O_{12}$	$KAlSi_2O_6$	$CaCO_3$	$Mg_3Si_4O_{10}(OH)_2$	$Mg(OH)_2$	$MgAl_2Si_3O_{10}$

TABLE 12 - Compilation of solubility constants for alumosilicates and other minerals with compositions and equilibrium equations as given in Table 10. The constants are used for comparison with the averaged reaction quotients of Table 11, in order to identify minerals which may control the composition of the BGS solutions. The constants at 50 °C, except where noted, were calculated with Van't Hoff 's approximation: log (K_{T2} /K_{T1}) = 0.43 (ΔH^{o}_{R} / R) ($T1^{-1}$ - $T2^{-1}$), where T1 is the reference temperature, T2 the temperature for which the reaction constant has to be calculated, ΔH^{o}_{R} the standard reaction enthalpy, and R the gas constant. References are as follows: [1] PHREEQE database, kindly supplied by B. Grambow, Hahn Meitner Inst., 1988 ; [2] PSI-MINEQL database ; [3] Hemingway, Robie and Kittrick (1978).

MINERAL	FORMULA	log K (25°C)	ΔH_R^o [kcal/mol]	log K (50°C)	REFERENCE
KAOLINITE	$Al_2Si_2O_5(OH)_4$	5.73	-35.28	3.73	[1]
		7.44	-36.42	5.37	[2]
		5.51	-34.83	3.56	[3]
HALLOYSITE	$Al_2Si_2O_5(OH)_4$	8.99	-39.73	6.74	[1]
GIBBSITE (crystalline)	$Al(OH)_3$	8.05	-22.8	6.76	[1]
		8.11	-22.8	6.82	[2]
		8.06	-22.8	6.78	[3]
GIBBSITE (microcrystalline)	$Al(OH)_3$	9.35	-24.5	7.96	[2]
AMORPHOUS	$Al(OH)_3$	10.8	-26.5	9.30	[2]
DIASPORE	Al O OH	6.87	-24.63	5.47	[1]
		7.31	-24.39	5.94	[3]
BOEHMITE	Al O OH	8.58	-28.13	6.99	[1]
		7.95	-26.19	6.48	[3]
PYROPHYLLITE	$Al_2Si_4O_{10}(OH)_2$	1.25	-31.07	-0.51	[1]
		-1.02	-27.46	-2.56	[3]
ANALCIME	$NaAl\ Si_2O_6.H_20$	6.72	-22.84	5.42	[1]
WAIRACKITE	$CaAl_2Si_4O_{12}.2H_2O$	18.87	-63.15	15.29	[1]
LAUMONTITE	$CaAl_2Si_4O_{12}.4H_2O$	14.46	-50.45	11.60	[1]
LEUCITE	$KAlSi_2O_6$	6.42	-22.08	5.17	[1]
CALCITE	$CaCO_3$	-8.48	-2.59	-8.76[1]	[1]
		-8.48	-2.30	-8.61	[2]
TALC	$Mg_3Si_4O_{10}(OH)_2$	23.06	-35.01	21.07	[1]
BRUCITE	$Mg(OH)_2$	16.79	-25.84	15.32	[1]
		16.84	-27.10	15.30	[2]

[1]calculated with the interpolation formula given in [1]

The observed initial increase and subsequent drop in the Al concentration, with concomitant increase in the silica concentration (Figure 1), can be explained in terms of the equilibrium stated by equation (13). The kaolinite present in the bentonite samples would initially dissolve, releasing both Al and Si, until the solution becomes critically *oversaturated* with $Al(OH)_3$. At this time the excess of Al in solution would be removed by precipitation of $Al(OH)_3$, while some kaolinite would keep dissolving to maintain equilibrium. The precipitation of aluminum hydroxide would then cease when *both* solids are in equilibrium with the solution.

In Figure 4, the BGS data are plotted along with literature data on enlarged activity plots for the $Al(OH)_3$ and $Al_2Si_2O_5(OH)_4$ equilibria. Most data lie on a broad linear trend *between* limiting equilibrium lines extracted from the thermodynamic constants compiled in Table 12. Only part of the data gained from experiments conducted under acidic conditions (Churchman and Jackson, 1976) fall outside. These relations suggest that the control of the solution composition by secondary Al phases in bentonites is a common phenomenon, not necessarily limited to the bentonite used in the BGS experiments. It is noteworthy, however, that only the BGS data define good linear trends on the mentioned plots, if the various datasets are considered separately.

Further supporting evidence is provided by the experimental work of Hem et al. (1973), who tested equilibrium conditions for synthetic solutions containing variable amounts of dissolved Al and Si in a wide pH range (4-10) at 25 °C. Many tests were performed with solutions initially oversaturated with respect to the known Al-hydroxides and alumosilicates, in order to test whether equilibrium conditions could also be reached through *precipitation* (this path is more difficult than equilibration through *dissolution* of minerals, since precipitation is often kinetically hindered at low temperatures). The results of the study indicate that a poorly crystalline precipitate of kaolinite composition formed in both acidic and alkaline solutions, provided the initial silica concentration exceeded 10^{-4} mol/l, whereas an aluminum hydroxide precipitated at lower dissolved silica concentrations (microcrystalline gibbsite in the acidic, bayerite in the alkaline solutions). The solutions equilibrated with these solids after a few months aging. These results corroborate the interpretation of the Al-Si-H activity patterns given in this report for the BGS experiments. The shorter interaction times (2-4 weeks) in the BGS experiments should nevertheless have been sufficient to guarantee attainment of equilibrium, because they were carried out at a considerably higher temperature than the experiments of Hem at al. (50 °C vs. 25 °C), and reaction kinetics should therefore have been considerably faster.

6.7 Other activity correlations

Plots testing equilibrium with alumosilicates and other phases containing the cations Na^+, Ca^{+2}, Mg^{+2}, K^+ and bicarbonate anions can be found in Figures 5 to 9. The selected formulae are, in some cases, related to minerals which are known to be stable in low-temperature environments (analcime, calcite, magnesite and brucite). In other cases, the formulae do not correspond to minerals expected to form under weathering conditions (e.g.

leucite, talc). The choice of some stoichiometries was guided in this case only by the analysis of the activity data, not by mineralogical criteria. Finally, the formula of the Mg alumosilicate does not correspond to any known mineral, but was defined in such a way as to be compatible with the structure of zeolites, a mineral group stable at low temperatures and characterised by a large chemical variability.

Figure 5a shows the equilibrium line for the common zeolite analcime. In this plot the activity combinations extracted from the algebraic equilibrium relation for the analcime dissolution (Table 10) imply a slope of +1 for the equilibrium line, and the intercept at the origin would yield the negative logarithm of the solubility constant. The BGS data define a linear trend parallel to the analcime equilibrium line. However, this trend is clearly displaced from the analcime line, meaning that the BGS solutions are all oversaturated with this mineral. The well-defined linear trend in Figure 5a is not necessarily indicative of saturation equilibrium, because of the previously discussed intrinsic dependency of $p(Al^{+3})$ on pH. In the corresponding plot with $p(Al(OH)_4^-)$, the data do not fit a line. Nevertheless, they are distributed in 2 clusters centered on a line with slope -1, as expected when the following reaction is at equilibrium (Figure 5b):

$$NaAlSi_2O_6.H_2O + 5\,H_2O = Na^+ + 2\,H_4SiO_4 + Al(OH)_4^-$$

Therefore, saturation conditions with a hypothetical solid with the stoichiometry of analcime can be assumed in this case. Analogous arguments lead to the selection of a phase with the composition of leucite (Figure 6) and of an Mg silicate with stoichiometry $Mg_2Al_2Si_3O_{10}.nH_2O$ (Figure 7). Although the plot involving $p(Al(OH)_4^-)$ does not define a linear relation (Figure 7d), again the activity data cluster on a line with the required slope. This hypothetical Mg-silicate has to be preferred to a real phase like talc, which can be excluded on the basis of a clear disagreement between the slope required by stoichiometric dissolution and the slope defined by the data. It is recalled again that the good correlation in Figure 7c relies primarily on the previously discussed dependency of $p(Al^{+3})$ on pH. Since the abscissa ($x = 8pH-p(Mg^{+2})$) represents a quantity in which the pH is multiplied by a factor 8 with respect to $p(Mg^{+2})$, the magnesium ion activity has a low weight in the correlation. The same argument applies to Figure 8a, where equilibrium tests for calcium alumosilicates of composition $CaAl_2Si_4O_{12}.nH_2O$ are presented. The observed linear trend, though not as well-defined as for the Mg-alumosilicate, would suggest that the solutions are nearly saturated with the mineral laumontite. However, the scatter of the activity data on the corresponding $p(Al(OH)_4^-)$ plot (Figure 8b) is too large to justify the selection of a solid with laumontite stoichiometry. It appears more reasonable to choose calcite as the solid controlling Ca^{+2} concentrations in solution, as most of the calcium ion and bicarbonate ion activities fall within or near the theoretical equilibrium lines for this mineral in Figure 8c. Since the temperature dependency of the calcite solubility product is known quite accurately, the degree of confidence in the equilibrium lines for 50°C is much higher than for the other minerals. The equilibrium test for the mineral magnesite, on the other hand, yields mostly oversaturated solutions (Figure 8d), so that also this mineral can be excluded as a solid controlling Mg^{+2} solution concentrations.

FIGURE 5 - Cross activity plots for the dissolution reaction of an Na-silicate with the stoichiometry of analcime. The activity data from the BGS final solutions are compared with the line defined by analcime equilibrium (Fig. 5a). The broken line in Figure 5b has a slope dictated by the same dissolution reaction as in 5a written with $Al(OH)_4^-$ instead of Al^{+3}, and was fitted to the BGS data. See text for a detailed discussion.

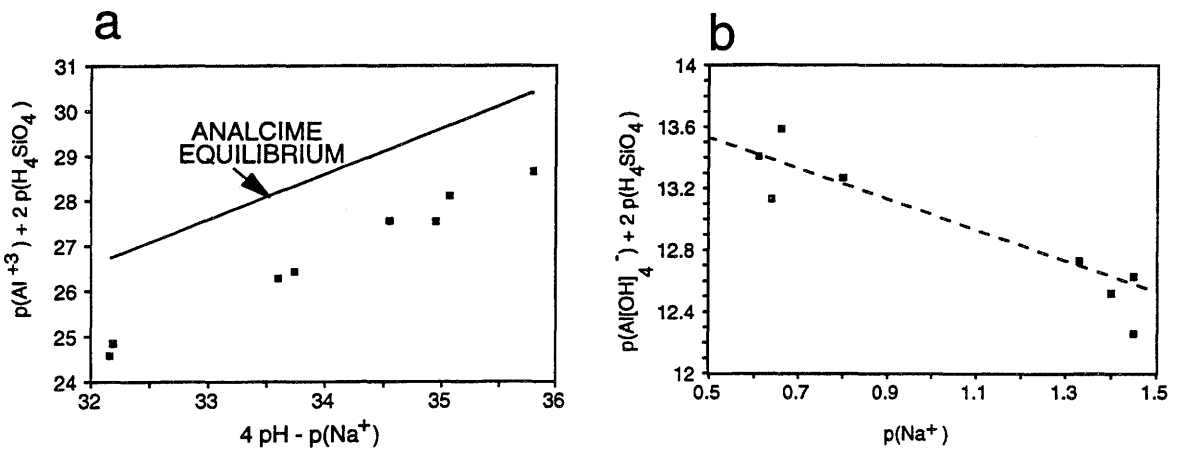

FIGURE 6 - Cross activity plots for the dissolution reaction of a K-silicate with the stoichiometry of leucite. The activity data from the BGS final solutions are compared with the line defined by leucite equilibrium (Fig. 6a). The broken line in Figure 6b has a slope dictated by the same dissolution reaction as in 6a written with $Al(OH)_4^-$ rather than with Al^{+3}, and was fitted to the BGS data. See text for a detailed discussion.

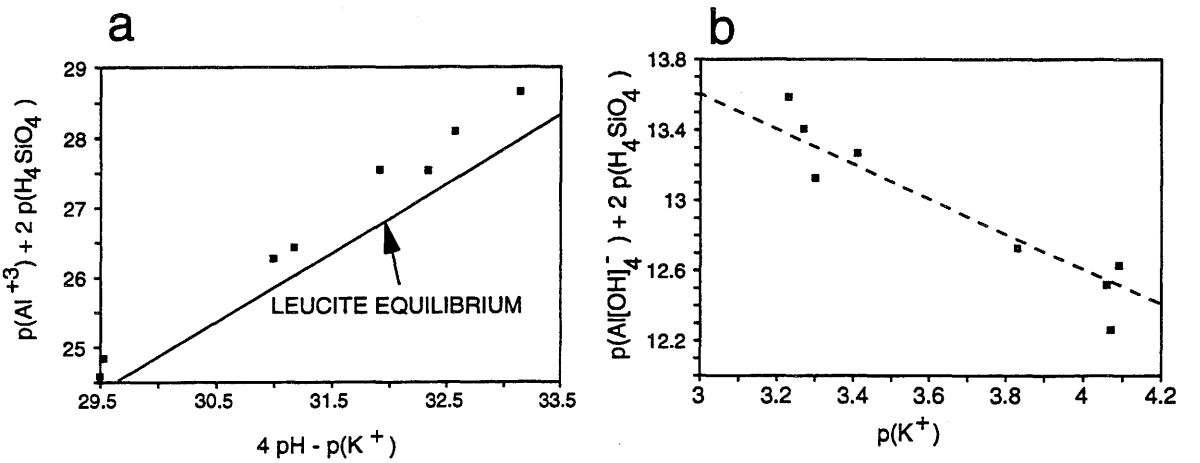

FIGURE 7 - Cross activity plots for the dissolution of various magnesian solids. The activity data from the BGS final solutions are compared with the lines defined by saturation equilibrium of known minerals with the selected stoichiometries (Figures 7a,b,c). The broken line in Figure 7d has a slope dictated by the same dissolution reaction as in 7c written with $Al(OH)_4^-$ instead of Al^{+3}, and was fitted to the BGS data. See text for a detailed discussion.

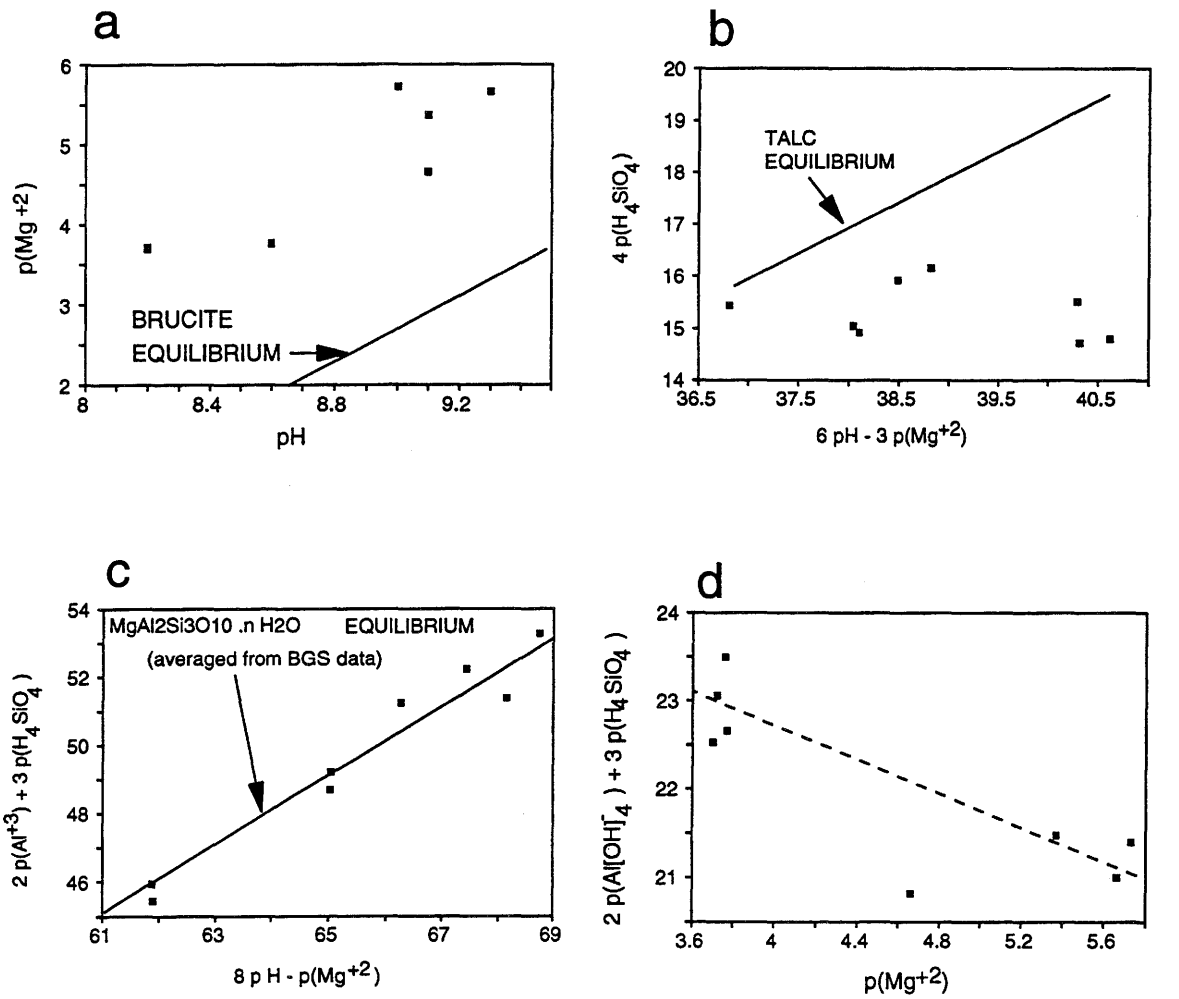

FIGURE 8 - Cross activity plots for the dissolution of various calcium solids and magnesite. The activity data from the BGS final solutions are compared with the lines defined by equilibrium of known minerals with the selected stoichiometries (Figures 8a,c,d). The broken line in Figure 8b has a slope dictated by the same dissolution reaction as in 8a written with $Al(OH)_4^-$ instead of Al^{+3}, and was fitted to the BGS data. See text for a detailed discussion.

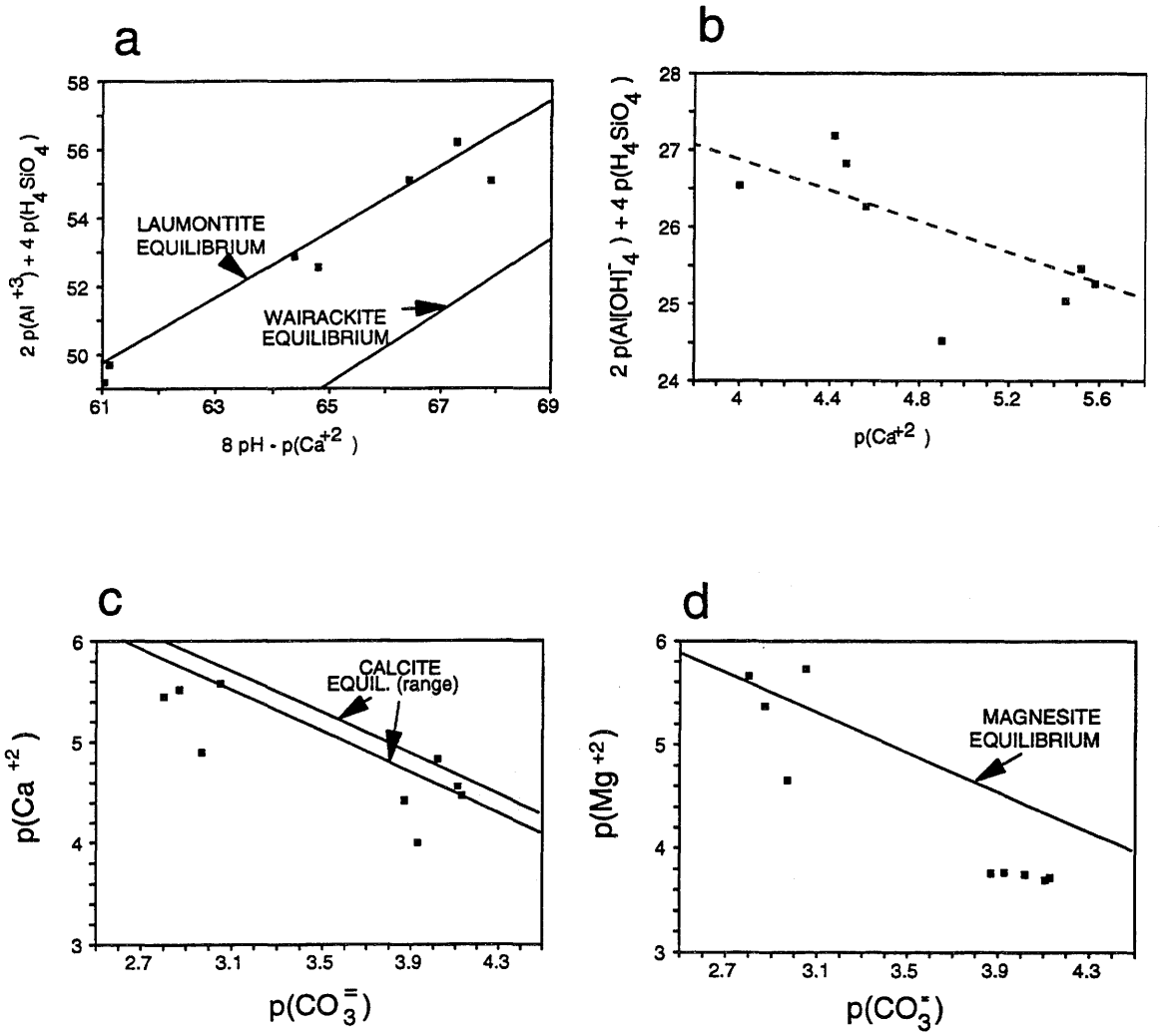

7. Redox control in bentonite pore waters

7.1 Significance of the oxidation potential for repository safety

The oxidation potential of solutions which might come into contact with the waste packages in a repository is one of the most safety-relevant chemical parameters, since it has a strong influence on the solubilities of multivalent radionuclides. In general, solubility limits for U and Np are predicted to be orders of magnitude lower under strongly reducing conditions than in a mildly oxidising environment. The opposite behaviour is observed for Pu (Schweingruber, 1983; Wanner, 1985). In either case, solubilities may change by an order of magnitude for Eh variations of a few tens mV.

In view of these findings, it is desirable to have precise information on the redox conditions prevailing in the saturated near-field environment. In the Swiss HLW repository, the presence of a massive steel canister will initially provide strongly reducing conditions, as metallic iron corrodes to magnetite (McKinley, 1985). The iron may be totally consumed or become inaccessible to further aqueous attack, for instance through encapsulation in an impervious layer of corrosion products. In such a situation, it is not clear which solid(s), besides magnetite, will buffer the Eh of the bentonite pore fluid.

Since Eh measurements, which are notoriously problematic and often unreliable, were not made during the BGS experiments, the alternative method of thermodynamic equilibrium modelling was followed. Thus, a range for the oxidation potential in the repository near-field was estimated with the help of appropriate redox equilibria, as will be discussed in the following section.

7.2 Modelling the oxidation potential in bentonite pore waters

Trace minerals in bentonites contain various elements (Fe, C, S), which can conceivably participate in redox reactions and may thus determine the oxidation potential of the pore water in the near-field. Reactions involving the transfer of 1 or 2 electrons are usually kinetically fast, whereas reaction sequences in which an element gains or loses several electrons may proceed very slowly, or require biological mediation. For instance, it is well-known that sulphate cannot be reduced to sulphide at a measurable rate without the aid of microbial catalysis below 100 °C (Grauer, 1991; Krauskopf, 1979). The formation of native sulphur deposits in evaporitic environments adjacent to oil fields can be unequivocally ascribed to the microbial reduction of sulphate in the evaporites (gypsum, anhydrite) by the carbon in the oil, which is oxidised to carbon dioxide (Krauskopf, op. cit., p.226).

In the model calculations for the definition of bentonite pore waters (chapter 8), sulphate reduction and carbon oxidation/reduction will be neglected in consideration of the low

probability of a persistent bacterial activity in the repository (McKinley, 1985). Only the following electron transfers are allowed:

$$Fe^{+2} \leftrightarrows Fe^{+3} + e^-$$

$$S^{-2} \leftrightarrows S^{-1} \rightarrow S^{+6} + 8\,e^-$$

Thus, the oxidation potential is assumed to be controlled by the iron and sulphur systems, with the limitation that sulphate reduction is prohibited. In practical terms, this means that all reactions involving *both* sulphate and sulphide have been turned off in the MINEQL runs whenever a test calculation showed that sulphate ions must be reduced to achieve overall equilibrium. Conversely, if the simulations required sulphide oxidation to reach equilibrium, sulphate/sulphide reactions were allowed to proceed.

It is nevertheless instructive to construct a full Eh-pH diagram for the Fe-S-O system at equilibrium, i.e. involving also reversible sulphide-sulphate reactions. Such a diagram, calculated for the conditions expected in the repository near-field, will be used to check whether or not the BGS solutions are in equilibrium with specific mineral assemblages (see later). A list of solids potentially involved in redox reactions with the bentonite pore water is presented Table 13, where the equilibrium relations needed to construct the Eh-pH diagrams of Figure 9 are compiled. Besides magnetite, which will be available in large amounts as the main product of anaerobic steel corrosion, hematite, goethite, pyrite and siderite are considered. This list is far from being complete, as many other conceivable iron and sulphur compounds exist, but is dictated by the frequent occurrence of these minerals in bentonites, as summarised in Table 9. Siderite is not frequent, but has been included because of the ubiquitous presence of soluble carbonates in bentonites, which may lead to its precipitation in reducing environments. An inspection of the pe-pH equations in Table 13, however, reveals that siderite is not stable under the conditions prevailing in the repository near-field (pH= 8.0 to 9.5, $pCO_2 \sim 10^{-2}$ bar, $[SO_4^{-2}] \sim 10^{-3}$ to 10^{-2} M). For that reason, this mineral does not appear in the Eh-pH diagrams.

The Eh-pH plots in Figure 9 depict stability relations at 50 °C among the mentioned iron minerals, and were calculated using the constants of the actualised MINEQL_PSI database (Pearson and Berner, 1991; Pearson et al., 1991). The equilibrium lines have been calculated in such a way that triple points must fall in the range of pH values commonly observed in bentonite pore waters (i.e. around 8.5). This constraint implies a total dissolved sulphur activity of $\sim 10^{-7}$, as can be checked by solving the magnetite-hematite, pyrite-magnetite, and pyrite-hematite equations, listed in Table 13, with the pH fixed at 8.5 and reasonable activities for the sulphur species (10^{-2} to 10^{-3}). For the reactions involving carbonate, a fixed carbon dioxide partial pressure of $10^{-1.7}$ bar has been assumed, which corresponds to the highest value observed in the Swiss crystalline waters (Pearson and Scholtis, 1992).

In the upper plot of Figure 9, hematite, the most stable ferric solid according to the database used, is assumed to control the oxidation potential along with pyrite and magnetite. This diagram shows that the BGS solutions cannot be in equilibrium with *all three* minerals, because at the triple point the total dissolved sulphur is fixed at a concentration several orders of magnitude smaller than that actually measured ($\sim 10^{-7}$ vs. $\sim 10^{-3}$ M). The equilibrium relations calculated assuming a higher total sulphur concentration would shift the triple point to much more alkaline pHs (about 13.5 for a total sulphur activity of 10^{-3}). Therefore, the oxidation potential of the BGS solutions may be governed (metastably) by

only 2 of these 3 minerals. A control by the binary equilibrium hematite-pyrite in the near-field environment is not likely, since large amounts of magnetite, the final canister corrosion product, will be available, providing a virtually unlimited reservoir of reactive ferric and ferrous iron. A control through the binary equilibrium magnetite-hematite is then the most reasonable choice. Since the pe-pH equation for this couple is neither dependent on the carbon dioxide partial pressure nor on sulphur species activities (Table 13), this buffer would constrain the Eh within narrow limits for the pH range of bentonite pore waters (pH ~ 8 to 10).

Hematite, although already observed, is far less common than goethite in bentonites. The latter mineral is a typical weathering product which persists metastably at low temperatures. For these reasons, it appears sensible to consider also the possibility that the metastable equilibrium goethite-magnetite may determine the oxidation potential in bentonite pore waters (Figure 9, bottom). Unfortunately, the solubility constant for goethite is not well-defined, and widely differing values appear in the literature (Pearson and Berner, 1991; Pearson et al., 1991). The reason seems to lie in the variable grain size of natural goethites. Finely subdivided goethite has a surface area large enough to increase the free energy, and thus the solubility, of this mineral. Conversely, coarse goethites have a lower solubility. For equally sized mineral particles larger than 0.76 μm, goethite turns out to be even more stable than hematite (Langmuir and Whittermore, 1971). In order to remain on the conservative side, the goethite-magnetite equilibrium yielding the highest oxidation potentials has been considered for the definition of an Eh-pH range for bentonite pore waters in the near-field.

The resulting Eh-pH window is shown in Figure 10. The lines labeled *M-H* and *M-G* correspond to the magnetite-hematite and to the conservative magnetite-goethite equilibria, respectively, while the vertical lines are defined by the range of pH values obtained from the bentonite waters modelled in chapter 8. The four vertices of this field will serve as reference pH-Eh coordinates for the calculation of radionuclide solubility limits in the near-field.

TABLE 13 - Compilation of the reactions and equilibrium equations used to construct the pH-Eh diagrams in Figures 9a-b. The underlying thermodynamic data stem from the MINEQL_PSI database (Pearson and Berner, 1991). All equations have been calculated for 50°C.

BOUNDARY	REACTION (OXIDATION)	EQUATION	NOTES
MAGNETITE-HEMATITE	$2\ Fe_3O_4 + H_2O = 3\ Fe_2O_3 + 2\ H^+ + 2\ e^-$	pe = 2.77 - pH	
$(SO_4^{-2}) = (HS^-)$	$SO_4^{-2} + 9\ H^+ + 8\ e^- = HS^- + 4\ H_2O$	pe = 3.83 - 1.13 pH	
PYRITE - HEMATITE	$2\ FeS_2 + 19\ H_2O = Fe_2O_3 + 4\ SO_4^{-2} + 38\ H^+ + 30\ e^-$	pe = 5.98 -1.27 pH - 0.134 $p(SO_4^{-2})$	(1)
HEMATITE-PYRITE	$Fe_2O_3 + 2\ H^+ + 4\ HS^- = 2\ FeS_2 + 3\ H_2O + 2\ e^-$	pe = pH - 28.43 + 2 $p(HS^-)$	(2)
PYRITE-MAGNETITE	$3\ FeS_2 + 28\ H_2O = Fe_3O_4 + 6\ SO_4^{-2} + 56\ H^+ + 44\ e^-$	pe = 6.06 - 1.273 pH - 0.136 $p(SO_4^{-2})$	(1)
MAGNETITE-PYRITE	$Fe_3O_4 + 2\ H^+ + 6\ HS^- = 4\ H_2O + FeS_2 + 4\ e^-$	pe = 0.50 pH + 1.5 $p(HS^-)$ -20.63	(2)
SIDERITE-HEMATITE	$2\ FeCO_3 + H_2O = 2\ CO_2(g) + Fe_2O_3 + 2\ H^+ + 2\ e^-$	pe = 2.50 - pH + $\log(pCO_2)$	(3)
SIDERITE-MAGNETITE	$3\ FeCO_3 + H_2O = Fe_3O_4 + 3\ CO_2(g) + 2\ H^+ + 2\ e^-$	pe = 2.38 - pH + 3 $\log(pCO_2)$	(4)
PYRITE-SIDERITE	$FeS_2 + 9\ H_2O + CO_2(g) = FeCO_3 + 2\ SO_4^{-2} + 38\ H^+ + 30\ e^-$	pe = 6.23 -1.29 pH - 0.143 $p(SO_4^{-2})$ - 0.07 $\log(pCO_2)$	(3)
SIDERITE-PYRITE	$FeCO_3 + 2\ HS^- = FeS_2 + CO_2(g) + H_2O + e^-$	pe = -25.94 + $\log(pCO_2)$ + 2 $p(HS^-)$	(4)
GOETHITE-PYRITE	$FeOOH + H^+ + 2\ HS^- = FeS_2 + 2\ H_2O + e^-$	pe = -30.89 + pH + 2 $p(HS^-)$	(3)
PYRITE-GOETHITE	$FeS_2 + 10\ H_2O = FeOOH + 2\ SO_4^{-2} + 19\ H^+ + 15\ e^-$	pe = 6.15 -1.27 pH - 2 $p(SO_4^{-2})$	(3)
MAGNETITE-GOETHITE	$Fe_3O_4 + 2\ H_2O = 3\ FeOOH + H^+ + e^-$	pe = 10.14 - pH	
SIDERITE-GOETHITE	$FeCO_3 + H_2O = FeOOH + CO_2(g) + H^+ + e^-$	pe = 4.96 - pH + $\log(pCO_2)$	(3)
H_2O STABILITY	$2\ H^+ + 2\ e^- = H_2(g)$	pe = 0.864 -pH	(5)

KEY FOR NOTES:

(1) STABLE FOR $[SO_4^{-2}] >> [HS^-]$

(2) STABLE FOR $[SO_4^{-2}] << [HS^-]$

(3) METASTABLE

(4) UNSTABLE IN WATER

(5) CALCULATED FOR $p(H_2) = 100$ bar

FIGURE 9 - Eh-pH diagram for the Fe-S-O system at 50 °C, constructed with thermodynamic data from the MINEQL-PSI database (Pearson and Berner, 1991; Pearson et al., 1991). The upper diagram shows relations among the most stable phases. In the lower diagram, goethite is assumed to persist metastably over the more stable hematite.

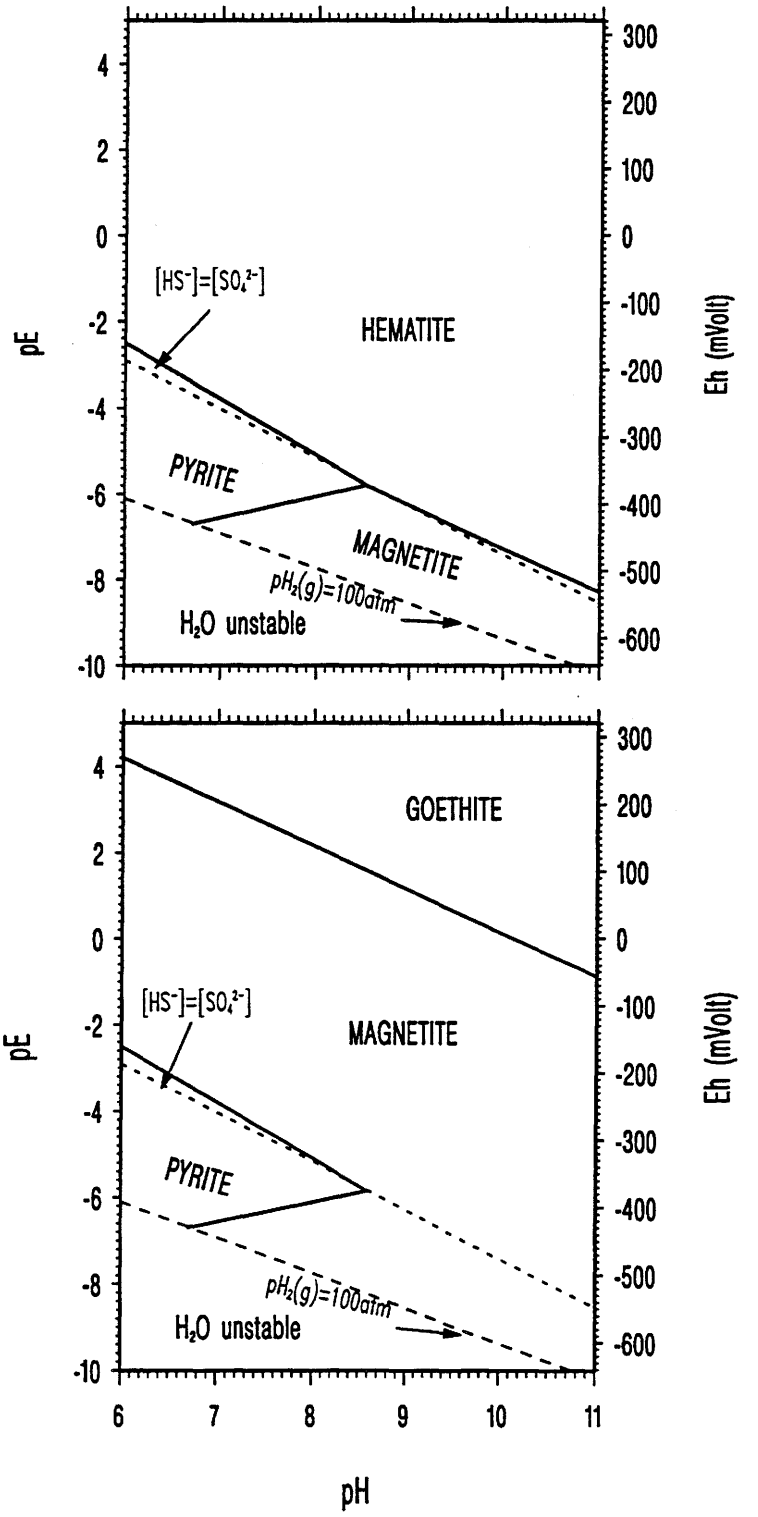

FIGURE 10 - Eh-pH window for the calculation of radionuclide solubilities. The pH range is defined by the bentonite waters modelled using either the Boettstein water (BT1300) or a more dilute crystalline reference water (CRW) as reacting solution. The Eh is bounded by the magnetite-goethite (M-G) and magnetite-hematite (M-H) equilibria.

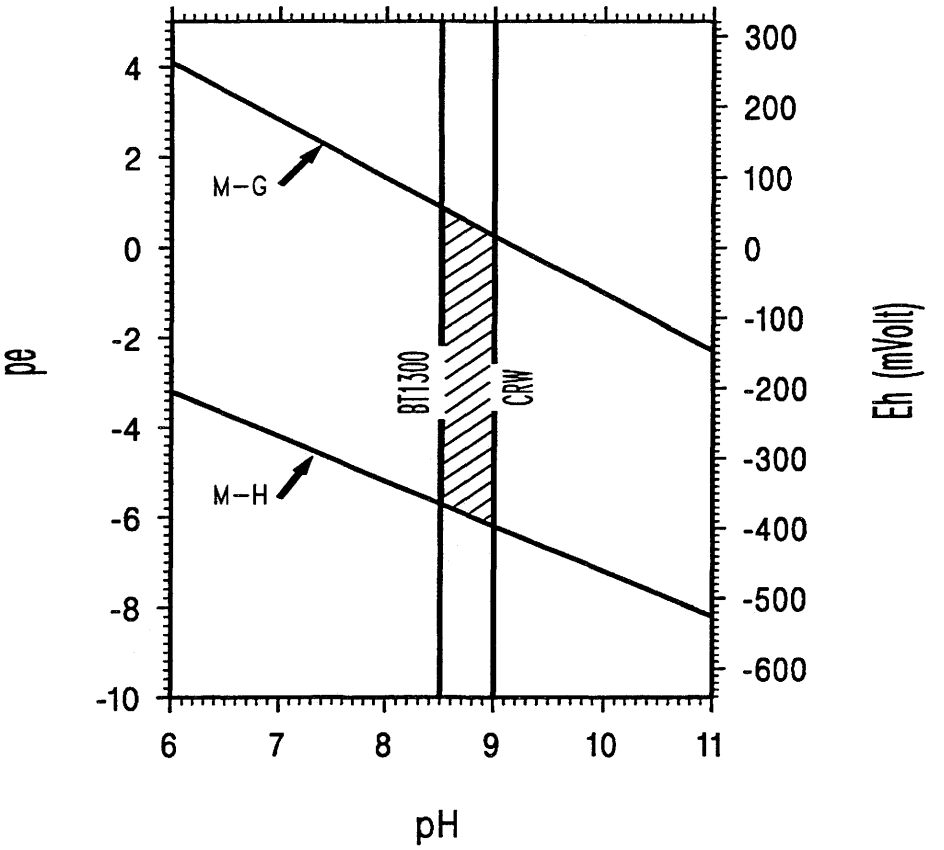

8. Modelling bentonite pore waters

8.1 Why a model ?

A pertinent question is why is it important to *model* bentonite pore waters, instead of using directly representative concentrations from the BGS experiments. Several arguments led to the choice of the former option. In the first place, the conditions under which the BGS experiments were carried out differ somewhat from those expected in the repository. Moreover, a bentonite with different exchanged ion population and mineralogy could be used as backfill material in the repository. Finally, the saturated compacted bentonite in the repository will have a considerably lower water/rock ratio, and some chemical boundary conditions characterising the repository environment were not satisfied during the BGS experiments. For instance, the reacting fluids were prepared under atmospheric conditions, leading to a carbon dioxide partial pressure of $10^{-3.5}$ atm, whereas most investigated Swiss crystalline waters are in equilibrium with a much higher partial pressure ($pCO_2 \sim 10^{-2.0}$ atm) (Pearson and Scholtis, 1992). In addition, the oxidation potential was not controlled during the BGS experiments.

Since all the parameters mentioned above (initial single ion capacities, pCO_2, *Eh*, bentonite porosity) can largely affect the chemistry of the bentonite pore water, and consequently radionuclide solubilities, it was preferred to define bentonite pore waters through model calculations, rather than selecting representative compositions directly from the BGS data.

8.2 Definition of input waters

Bentonite pore waters have been defined by simulating exchange and precipitation / dissolution reactions between bentonite and selected groundwaters at 50 ^{o}C, with the help of the geochemical code MINEQL (see section 6.2). Reactant fluids were selected from representative analyses of waters sampled during the *NAGRA* drilling campaigns in the crystalline basement of Northern Switzerland. Four water compositions have been considered (Table 14).

The water BT1300 had been already used as reference crystalline water for Project "GEWÄHR" (Schweingruber, 1984). Its composition was derived from a highly mineralised water sampled at a depth of ~1300 m from the Boettstein borehole, at an early phase of the *NAGRA* drilling program. Subsequent analyses from other drilling sites yielded considerably lower dissolved mineral contents, even for deeper water samples. Thus, BT1300 is an exceptional crystalline water, which is used in this study as a contrast to the more common, less mineralised waters. CRW is an early attempt to define a crystalline reference water (Scholtis, 1990). The CRW and BT1300 waters were used for the modelling of bentonite waters, since the finalised crystalline reference waters were still unavailable when the radionuclide solubility calculations for the KRISTALLIN I safety analysis started.

Meanwhile, 2 finalised crystalline reference waters, with compositions very similar to CRW, have been defined (Pearson and Scholtis, 1992): one for the Eastern Crystalline (ECRW) and the other for the Western Crystalline district (WCRW). These waters have also been used to calculate bentonite pore water compositions, in order to identify possible significant deviations from the bentonite water composition determined using CRW water as reactant fluid.

A comparison of the crystalline water compositions listed in Table 14 with the original data reveals small differences in the concentrations of some elements. These discrepancies are due to temperature adjustments. For instance, the CRW water was defined at 25 °C , with chalcedony, calcite and fluorite as saturated solids (Scholtis, 1990). Because the cation exchange and solubility constants used to model the bentonite pore waters have been extrapolated from experiments carried out at 50 °C, the input waters had to be remodelled at this temperature, with the same minerals in equilibrium. Thus, the concentrations depending on these saturation equilibria have shifted according to the temperature dependency of the solubility constants. For the CRW water, the redefinition leads to the following modifications of the original composition:

[Ca]	from	5.60×10^{-4}	to	3.17×10^{-4}	M
[C(inorg.)]	from	5.10×10^{-3}	to	4.23×10^{-3}	M
[F]	from	4.50×10^{-4}	to	7.02×10^{-4}	M
[Si]	from	2.80×10^{-4}	to	5.77×10^{-4}	M
pH	from	7.80	to	7.86	

Such changes are due to the increased solubilities of chalcedony and fluorite, and to the decrease in calcite solubility, with temperature. For the remaining waters, the changes in concentration are smaller, since temperature differences are only 5 to 10 °C.

8.3 Definition of bentonite

The present model assumes that the composition of aqueous solutions interacting with bentonite at low temperatures for short times can be predicted applying the set of empirical equilibrium relations extrapolated from the BGS experiments.

Four surface complexation constants represent cation exchange reactions between the solution and the interlayer sites of the smectites, and a set of solubility constants describe the control exerted by reactive trace solids on the bentonite pore solution (Table 15). The real existence of some of these minerals is questionable, but this is not essential considering the empirical nature of the model. For instance, the occurrence of a distinct phase with stoichiometry $MgAl_2Si_3O_{10}$ in the bentonite used for the BGS experiments seems very unlikely. However, such virtual phases are convenient *descriptors* of the dissolution behaviour of montmorillonite and are thus valuable modelling tools in the absence of a mechanistic understanding of the processes involved. On the other hand, some correlations presented in the previous chapter yield convincing evidence that minor amounts of *real* solid phases with simple stoichiometry (kaolinite, Al-hydroxide, and calcite formulae) regulate the Al and Si concentrations in the BGS solutions through precipitation or

TABLE 14 - Composition of crystalline waters used as reactants for the modelling of bentonite pore waters. Small differences with respect to the original compositions are due to the recalculation of saturation equilibria at 50°C. The composition of BT1300 was reported, without temperature adjustements, as given in the source reference. Our MINEQL calculations, performed with an up-to-date thermodynamic database (Pearson and Berner, 1991; Pearson et al., 1991), indicate that the BT1300 water is saturated with quartz and rhodochrosite, which is not mentioned in the original work.

	BT1300	CRW	ECRW	WCRW
REFERENCE	Schweingruber (1984)	Scholtis (1990)	Pearson and Scholtis (1992)	Pearson and Scholtis (1992)
T [°C]	55	50	50	50
pH	6.78	7.86	7.63	7.61
pe	-1.66	-0.20	-0.52	-2.72
I [eq / l]	0.24	0.02	0.01	0.02
log pCO_2 [atm]	-1.73	-2.35	-2.06	-2.02
TOTAL CONCENTRATIONS IN [mol / l] :				
[Ca]	2.17×10^{-2}	3.17×10^{-4}	3.54×10^{-4}	4.26×10^{-4}
[Mg]	1.07×10^{-4}	1.20×10^{-5}	4.53×10^{-5}	1.24×10^{-5}
[Sr]	2.40×10^{-4}	--	4.00×10^{-6}	5.26×10^{-6}
[K]	1.15×10^{-3}	3.00×10^{-4}	1.07×10^{-4}	2.18×10^{-4}
[Na]	1.76×10^{-1}	1.60×10^{-2}	7.70×10^{-3}	1.41×10^{-2}
[Fe (tot)]	8.06×10^{-6}	--	1.79×10^{-7}	1.26×10^{-7}
[Mn]	5.64×10^{-5}	--	9.10×10^{-8}	6.75×10^{-7}
[Ba]	--	1.00×10^{-7}	5.84×10^{-7}	3.93×10^{-7}
[Si]	2.83×10^{-4}	5.77×10^{-4}	5.53×10^{-4}	5.53×10^{-4}
[B]	--	--	1.46×10^{-5}	5.51×10^{-5}
[Al]	--	--	2.62×10^{-7}	2.59×10^{-7}
[Li]	--	--	9.22×10^{-5}	1.59×10^{-4}
[N (V)]	--	--	1.45×10^{-5}	2.00×10^{-6}
[N (III)]	--	--	2.77×10^{-7}	7.78×10^{-6}
[C (inorg.)]	2.10×10^{-3}	4.23×10^{-3}	4.69×10^{-3}	5.10×10^{-3}
[S (VI)]	1.62×10^{-2}	4.50×10^{-3}	1.41×10^{-3}	3.09×10^{-3}
[Cl]	1.87×10^{-1}	3.00×10^{-3}	7.33×10^{-4}	3.62×10^{-3}
[F]	1.90×10^{-4}	7.02×10^{-4}	5.54×10^{-4}	5.73×10^{-4}
[P]	--	1.60×10^{-6}	6.46×10^{-7}	1.29×10^{-6}
SATURATION INDICES :				
(0 = saturated, -- = undersaturated, + = oversaturated, ? = not determinable)				
QUARTZ	0	+	+	+
CHALCEDONY	--	0	0	0
CALCITE	0	0	0	0
FLUORITE	+	0	0	0
BARITE	?	--	0	0
RHODOCHROSITE	0	?	--	--

dissolution. It is possible that the presence of colloids may have affected the analysed solution concentrations, since the pore size of the filters used was quite large (0.2 μm). However, if they had contributed significantly to the measured Al and Si concentrations, linear correlations with a slope reflecting the postulated stoichiometries, like that in Figure 3b, would be unlikely (a scattered distribution would be expected). In addition, the presence of minerals like *calcite* and *kaolinite* in the BGS bentonite has been unequivocally confirmed by X-ray diffraction analyses.

TABLE 15 - Thermodynamic constants used to model the reaction of bentonite with aqueous solutions. The list represents a selection from the averaged constants of tables 7 and 11. The reactions and formal equations corresponding to the solubility constants listed below are reported in Table 10.

CATION EXCHANGE :		
$Na^+ + Z^- = NaZ$	$\log K_{sc}(Na)$	20.0 (by definition)
$Ca^{+2} + 2\ Z^- = CaZ_2$	$\log K_{sc}(Ca)$	42.1 ± 0.5
$Mg^{+2} + 2\ Z^- = MgZ_2$	$\log K_{sc}(Mg)$	41.4 ± 0.3
$K^+ + Z^- = KZ$	$\log K_{sc}(K)$	20.9 ± 0.1
SOLUBILITY CONSTANTS :		
$Al_2Si_2O_5(OH)_4$	$\log K_1$	6.7 ± 0.4
$Al(OH)_3$	$\log K_2$	7.2 ± 0.2
$NaAlSi_2O_6$	$\log K_4$	7.3 ± 0.2
$KAlSi_2O_6$	$\log K_6$	4.7 ± 0.2
$CaCO_3$	$\log K_7$	- 8.4 ± 0.3
$MgAl_2Si_3O_{10}$	$\log K_{10}$	15.9 ± 0.6

A bentonite-water system must also be defined through a water/rock ratio, since the concentrations in the aqueous phase strongly depend on this parameter. The water/rock ratio in mixtures dominated by the solid fraction can be conveniently described by a quantity analogous to the porosity (ε). In low-porosity systems, where the relative volume of fluid is small, tiny amounts of dissolved minerals may be sufficient to saturate the pore solution. For instance, the modelling results presented later show that only 0.04 volume percent calcite must dissolve in order to saturate the solution. If, say, the bentonite contains 1% by volume of calcite, only a small fraction of the calcite inventory would dissolve. Thus, only small mass transfers will take place between solids and solution, and cation exchange

equilibria will be re-established without affecting the single ion capacities in a dramatic way. The same equilibria, applied to the same bentonite-water system with a much larger water/rock ratio, would yield quite different water compositions. In such systems, the available amounts of dissolving trace minerals may not be sufficient to saturate the solution.

Geochemical codes like MINEQL allow a mineral to reach saturation from an *unlimited reservoir*. This means that the simulation may allow the dissolved amount of a mineral to exceed the amount available in bentonite, or the volume of precipitated minerals to be larger than the pore volume. Although such unreasonable results may be identified by looking at the number of moles of mineral dissolved or precipitated per liter solution (this information is provided by the MINEQL output), it is more convenient to define a new and more understandable parameter, which we call *equivalent volume percentage (V%)*. This is defined as follows:

$$V\% = 0.1 \frac{W_M C_M \epsilon}{\rho_M (1 - \epsilon)} \qquad (10)$$

where :

$V\%$ is the *equivalent volume percentage* of precipitated or dissolved solid M [-]
W_M is the molar weight of M [g / mol]
C_M is the precipitated or dissolved concentration of M [mol/ l]
ϵ is the porosity [-]
ρ_M is the mineral density [g/ cm^3]

The *equivalent volume percentage* indicates how large is the increase or decrease in volume of the considered mineral (due to precipitation or dissolution) relative to the total volume of solids initially present in the bentonite. It is an important control parameter, since it allows a quick check of whether the modifications of the mineral inventory predicted by the model fall within reasonable limits.

The amount of interlayer sites available for cation exchange is specified in MINEQL as the concentration of a newly defined master species Z^-. Because they are modelled as dissolved complexes of the ligand Z^-, sorbed cation concentrations must be normalised to the solution volume for the calculations, and are therefore expressed in mol/l. If the water/rock ratio is modified, keeping the bentonite mass constant, the normalised concentrations must also vary, because the fluid volume changes. Thus, the total site concentration, $[Z^-]_{tot}$, must also be a function of porosity. The expression for converting the single ion capacity of a cation A to a concentration normalised to the solution volume has already been reported in equation (5). The total concentration of sorption sites, $[Z^-]_{tot}$, can be derived with the same formula by replacing the single ion capacity $\{AZ_a\}$ with the total exchange capacity of the sorbent (CEC) expressed in eq/kg. This concentration, which must be specified in the MINEQL input, is an implicit expression of the porosity of the system in the geochemical computations.

In the Swiss HLW repository, the compacted bentonite blocks will have a porosity of 0.38 (*NAGRA*, 1985), which is considerably lower than the porosity of the BGS mixtures

TABLE 16 - Sorbed cation and total exchange site concentrations for the MX-80 and BGS bentonites (starting materials). The transformation from [eq / g] to [mol / l] relies on equation (5). The total initial dissolved Na, K, Ca and Mg concentrations to be specified in the MINEQL input file are obtained by *summing*, for each cation, sorbed and dissolved concentrations.

Symbol definitions:

{ } stands for the sorbed concentrations expressed in [eq / g]

[ ] stands for the sorbed concentration expressed in [mol / l]

ε is the porosity of the system (fluid volume divided by total volume)

	MX - 80	BGS
ε	0.38	0.67
$\{Z^-\}_{tot}$	7.30×10^{-4}	1.36×10^{-3}
$\{NaZ\}$	6.24×10^{-4}	7.46×10^{-4}
$\{KZ\}$	2.00×10^{-6}	1.30×10^{-5}
$\{CaZ_2\}$	7.40×10^{-5}	4.04×10^{-4}
$\{MgZ_2\}$	3.00×10^{-5}	1.99×10^{-4}
$[Z^-]_{tot}$	3.29×10^{0}	1.85×10^{0}
$[NaZ]$	2.81×10^{0}	1.01×10^{0}
$[KZ]$	9.00×10^{-3}	1.77×10^{-2}
$[CaZ_2]$	1.67×10^{-1}	2.75×10^{-1}
$[MgZ_2]$	6.75×10^{-2}	1.35×10^{-1}

(0.55-0.76). In addition, the bentonite used by Bateman et al. (1991) does not have the same exchanged cation populations as the two reference bentonites for the Swiss repository (MX-80 and MONTIGEL) studied by Müller-Vonmoos and Kahr (1983). The model calculations presented below assume reaction with the MX-80 bentonite and a porosity of 0.38. MX-80 is a sodium bentonite, and was preferred to the MONTIGEL calcium bentonite because it has cation populations similar to those of the BGS samples. Modelling bentonite pore waters by simulating the reaction with a Ca-bentonite would lead to results which are incompatible with the observed mineralogy. For instance, the model would predict dissolution of large amounts of $NaAlSi_2O_6$,which supplies the sodium ions needed to satisfy the exchange equilibria. Large amounts of sodium minerals, however, have never been observed in the investigated bentonites. With Na-bentonite as reacting material, on the other hand, the sodium silicate *precipitates* (instead of dissolving), implying that this mineral need not be present in the bentonite before it interacts with water.

Table 16 reports the sorbed cation concentrations, both in [eq / g] and [mol / l], for the MX-80 and BGS bentonites. Note that the "dissolved" site concentration $[Z^-]_{tot}$ is higher for the MX-80 than for the BGS bentonite, although the latter has a considerably higher CEC. This is due to the considerably lower porosity, and consequently smaller fluid volumes, assumed for the MX-80 bentonite in the calculations.

8.4 Calculation of bentonite pore waters

The results of the speciation calculations performed to define two representative bentonite pore waters are shown in Tables 17 and 18. The compositions of the input waters and the exchanged cation concentrations of the *unreacted* bentonite are also listed to facilitate the appraisal of the results. The crystalline waters BT1300 and CRW have been selected as starting fluids for the simulated reaction with MX-80 bentonite, and the complete set of solubility and surface complexation constants specified in Table 15 has been applied.

The calculations have been carried out using alternatively two redox-controlling assemblages. In the runs labeled BT1300_6a and CRW_2A, the oxidation potential is controlled by the ternary equilibrium pyrite-magnetite-hematite[1], which buffers the Eh to fairly reducing conditions (~ -370 to -400 mV). The model pore waters BT1300_8A and CRW_3A have been determined assuming Eh control by the metastable equilibrium magnetite-goethite. In all these computations, the sulphate-sulphide equilibria were excluded, as preliminary runs indicated that sulphate ions would be reduced.

One of the most evident results is that elemental concentrations in the modelled pore

[1] In section 7.2 it was argued that the BGS solutions could have not been in equilibrium with the assemblage pyrite-magnetite-hematite. It may therefore seem contradictory to assume equilibrium with the same ternary assemblage for the calculation of bentonite pore waters. However, the term "equilibrium" has a different meaning in either case. Whereas the algebraic equations listed in Table 13 specify conditions of *full equilibrium*, including reactions among sulphide and sulphate species, in the MINEQL calculations the equilibrium relations among the three mentioned minerals involve electron transfers only between Fe^{+2} and Fe^{+3}, or between S^{-2} and S^{-1} (in pyrite). The mineral pyrite can thus participate in redox reactions with iron or sulphide, but cannot exchange electrons with sulphate species. Pyrite, magnetite and hematite are therefore in mutual equilibrium, while pyrite is only in *partial equilibrium* with the solution.

waters do not depend on the applied redox model. The concentrations are almost identical, whichever of the two assemblages buffers the Eh. This behaviour can be related to the very low amounts of magnetite, pyrite, goethite and hematite which dissolve or precipitate in order to reach equilibrium conditions. These minerals cannot affect the results of speciation calculations because their mass transfers are negligible.

The ionic strength of the modelled waters is strongly related to the ionic strength of the input waters. Using the highly mineralised Boettstein water as a reactant (I = 0.24) yields a bentonite water with virtually unaltered ionic strength. When the weakly mineralised CRW water is used, the ionic strength of the resulting pore water is about a factor 4 larger than in the starting solution, which is within the same order of magnitude. This behaviour can be explained by the lack of model solids which, by dissolving or precipitating, could largely modify the anion concentration in solution: no sulphate or chloride solid is involved in the modelled reactions, and the amount of bicarbonate ions released by calcite is too small to have a significant effect on the ionic strength. Therefore, *unless significant amounts of sulphates or other soluble salts are present in the bentonite*, the dissolved mineral content of the interacting water will determine the ionic strength of the resulting pore water.

The carbon dioxide equilibrium partial pressure differs from the values in the input waters because the calculations are for *closed systems* (no fixed pCO_2 condition was assumed). In all cases, the partial pressure in the resulting water is significantly less than in the reacting fluid, as a consequence of the increasing pH, which reduces the carbonic acid concentration.

One of the most striking effects predicted by the model calculations is the considerable desorption of sodium, which is replaced by calcium, magnesium and potassium (about 25% of the initially exchanged sodium is released into solution). These changes are driven by the precipitation and dissolution of model solids. The desorbed sodium is fixed in the $NaAlSi_2O_6$ precipitate, while the adsorbed cations are provided by dissolution of calcite, $KAlSi_2O_6$ and $MgAl_2Si_3O_{10}$.

The modelled bentonite pore waters have lower dissolved potassium, silica and calcium concentrations than the initial waters, while sodium, magnesium and total carbonate are gained. The decrease in calcium concentration is related to calcite equilibrium: since the pH and the bicarbonate ion activity increase as calcite dissolves, the Ca^{+2} concentration must fall to maintain saturation with calcite.

The dissolved silica concentration decreases because: a) the equilibrium between $Al_2Si_2O_5(OH)_4$ and $Al(OH)_3$ buffers the silicic acid activity to a value below quartz saturation (the BT1300 water is saturated with quartz, and the CRW water with chalcedony), and b) silicic acid dissociation is moderate at the calculated pHs (8.5 - 9.2). Such low silica concentrations in the repository would in principle have consequences for the glass degradation kinetics, since the glass corrosion rate increases linearly with decreasing silicic acid activity (Curti, 1991). However, such low silica concentrations are not likely to persist near the glass surface, where silica from the glass will be continuously released. The glass corrosion rate (~ 10^{-1} to 10^{-4} g SiO_2 $m^{-2}day^{-1}$) will probably exceed the rate of precipitation of most silicates and a higher Si concentration will thus be established near the glass. Although it is impossible to predict precipitation rates accurately for most minerals, estimates based on the conservative assumption that precipitation rates are equal to dissolution rates lead to typical precipitation rates in the range of 10^{-3} - 10^{-6} g SiO_2 . $m^{-2}.day^{-1}$, if the data compiled by Stumm and Wieland (1990) are used. These data are

TABLE 17 - Bentonite pore waters resulting from the reaction of bentonite MX-80 with the crystalline water BT1300 (Boettstein) at 50°C. The composition of the BT1300 water is reported again in order to facilitate the interpretation of the results. BT1300_6A is the bentonite water calculated assuming equilibrium with hematite-magnetite-pyrite. BT1300_8A assumes equilbrium with goethite-magnetite.

	BT1300_1 (input water)	BT1300_6A (hem-mag-pyr)		BT1300_8A (goe-mag)	
T [°C]	55	50		50	
pH	6.78	8.49		8.49	
pe [V]	- 1.66	- 5.72		+ 1.65	
Eh [mV]	- 107	- 367		+ 106	
I [M]	0. 24	0. 25		0. 24	
log pCO_2 [bar]	- 1.73	- 2.53		- 2.53	
DISSOLVED [M] :					
[Na]	1.76×10^{-1}	2.40×10^{-1}		2.40×10^{-1}	
[K]	1.15×10^{-3}	5.73×10^{-4}		5.73×10^{-4}	
[Mg]	1.07×10^{-4}	4.81×10^{-4}		4.81×10^{-4}	
[Ca]	2.17×10^{-2}	5.48×10^{-5}		5.48×10^{-5}	
[Sr]	2.40×10^{-4}	2.40×10^{-4}		2.40×10^{-4}	
[Al]	(not determined)	3.57×10^{-5}		3.57×10^{-5}	
[Si]	2.83×10^{-4}	1.88×10^{-4}		1.88×10^{-4}	
[Cl]	1.87×10^{-1}	1.87×10^{-1}		1.87×10^{-1}	
[F]	1.90×10^{-4}	1.90×10^{-4}		1.90×10^{-4}	
[C] inorg.	2.10×10^{-3}	1.84×10^{-2}		1.84×10^{-2}	
[S (VI)]	1.62×10^{-2}	1.62×10^{-2}		1.62×10^{-2}	
[S (-II)]	(not determined)	3.76×10^{-7}		below 10^{-9}	
[Fe (III)]	(not determined)	below 10^{-9}		below 10^{-9}	
[Fe (II)]	8.06×10^{-6}	below 10^{-9}		below 10^{-9}	
[1] **SORBED [M] :**					
[NaZ]	2.81×10^{0}	2.09×10^{0}		2.09×10^{0}	
[KZ]	9.00×10^{-3}	3.98×10^{-2}		3.98×10^{-2}	
[MgZ2]	6.75×10^{-2}	3.76×10^{-1}		3.76×10^{-1}	
[CaZ2]	1.67×10^{-1}	2.04×10^{-1}		2.04×10^{-1}	
			V%		**V%**
[2] **SOLIDS [M] :**					
$Al_2Si_2O_5(OH)_4$	--	$- 1.67 \times 10^{-1}$	(1.0)	$- 1.67 \times 10^{-1}$	(1.0)
$Al(OH)_3$	--	$+ 3.21 \times 10^{-1}$	(0.6)	$+ 3.21 \times 10^{-1}$	(0.6)
$NaAlSi_2O_6$	--	$+ 6.60 \times 10^{-1}$	(3.7)	$+ 6.60 \times 10^{-1}$	(3.7)
$MgAl_2Si_3O_{10}$	--	$- 3.09 \times 10^{-1}$	(3.1)	$- 3.09 \times 10^{-1}$	(3.1)
$KAlSi_2O_6$	--	$- 3.02 \times 10^{-2}$	(0.2)	$- 3.02 \times 10^{-2}$	(0.2)
$CaCO_3$	--	$- 1.63 \times 10^{-2}$	(0.4)	$- 1.63 \times 10^{-2}$	(0.4)
Fe_2O_3	--	$- 7.68 \times 10^{-6}$	(0.0)	--	
FeO(OH)	--	--		$- 1.61 \times 10^{-5}$	(0.0)
Fe_3O_4	--	$+ 7.87 \times 10^{-6}$	(0.0)	$+ 8.06 \times 10^{-6}$	(0.0)
FeS_2	--	$- 1.88 \times 10^{-7}$	(0.0)	--	

[1] sorbed concentrations specified under BT1300_1 refer to the starting material (MX-80).

[2] positive values indicate precipitation, negative values dissolution. Numbers in parentheses (V%) are the corresponding equivalent volume percentages.

TABLE 18 - Bentonite pore waters resulting from the reaction of bentonite MX-80 with the reference crystalline water CRW at 50°C. The composition of the CRW water is reported again to facilitate the interpretation of the results. CRW_2A is the bentonite water calculated assuming equilibrium with hematite-magnetite-pyrite. CRW_3A assumes equilbrium with goethite-magnetite.

	CRW_1A (input water)	CRW_2A (hem-mag-pyr)		CRW_3A (goe-mag)	
T [°C]	50	50		50	
pH	7.86	8.97		8.99	
pE [V]	-0.20	-6.18		+1.19	
Eh [mV]	-13	-396		+76	
I [M]	0.02	0.08		0.07	
log pCO_2 [bar]	- 2.35	- 2.55		- 2.55	
DISSOLVED [M]:					
[Na]	1.60×10^{-2}	7.84×10^{-2}		7.84×10^{-2}	
[K]	3.00×10^{-4}	1.66×10^{-4}		1.64×10^{-4}	
[Mg]	1.20×10^{-5}	6.65×10^{-5}		6.57×10^{-5}	
[Ca]	3.17×10^{-4}	1.07×10^{-5}		1.05×10^{-5}	
[Ba]	1.00×10^{-7}	1.00×10^{-7}		1.00×10^{-7}	
[Al]	(not determined)	1.04×10^{-4}		1.03×10^{-4}	
[Si]	5.77×10^{-4}	2.61×10^{-4}		2.60×10^{-4}	
[Cl]	3.00×10^{-3}	3.00×10^{-3}		3.00×10^{-3}	
[F]	7.02×10^{-4}	7.02×10^{-4}		7.02×10^{-4}	
[P]	1.60×10^{-6}	1.60×10^{-6}		1.60×10^{-6}	
[C] inorg.	4.23×10^{-3}	5.16×10^{-2}		5.10×10^{-2}	
[S (VI)]	4.50×10^{-3}	4.50×10^{-3}		4.50×10^{-3}	
[S (-II)]	(not determined)	1.09×10^{-6}		below 10^{-9}	
[Fe (III)]	(not determined)	below 10^{-9}		below 10^{-9}	
[Fe (II)]	(not determined)	below 10^{-9}		below 10^{-9}	
[1] **SORBED [M]:**					
[NaZ]	2.81×10^{0}	2.08×10^{0}		2.08×10^{0}	
[KZ]	9.00×10^{-3}	3.96×10^{-2}		3.96×10^{-2}	
[MgZ2]	6.75×10^{-2}	3.71×10^{-1}		3.72×10^{-2}	
[CaZ2]	1.67×10^{-1}	2.14×10^{-1}		2.14×10^{-1}	
			V%		**V%**
[2] **SOLIDS [M]:**					
$Al_2Si_2O_5(OH)_4$	--	-1.85×10^{-1}	(1.1)	-1.84×10^{-1}	(1.1)
$Al(OH)_3$	--	$+3.36 \times 10^{-1}$	(0.7)	$+3.36 \times 10^{-1}$	(0.7)
$NaAlSi_2O_6$	--	$+6.71 \times 10^{-1}$	(3.8)	$+6.71 \times 10^{-1}$	(3.8)
$MgAl_2Si_3O_{10}$	--	-3.04×10^{-1}	(3.0)	-3.04×10^{-1}	(3.0)
$KAlSi_2O_6$	--	-3.04×10^{-2}	(0.2)	-3.04×10^{-2}	(0.2)
$CaCO_3$	--	-4.74×10^{-2}	(0.1)	-4.74×10^{-2}	(0.1)
Fe_2O_3	--	$+1.09 \times 10^{-2}$	(0.0)	--	
FeO(OH)	--	--		-1.30×10^{-11}	(0.0)
Fe_3O_4	--	-5.44×10^{-7}	(0.0)	-4.84×10^{-15}	(0.0)
FeS_2	--	-5.44×10^{-7}	(0.0)	--	

[1] sorbed concentrations specified under CRW_1A refer to the starting material (MX-80).

[2] positive values indicate precipitation, negative values dissolution. Numbers in parentheses (V%) are the corresponding volume percentages.

based on short-term dissolution rate measurements conducted under acidic conditions, and can therefore serve only as first estimates. Specifically, the mentioned glass dissolution rates refer to a temperature of about 50 °C, while the mineral precipitation rates were derived from experiments at 25 °C.

The concentrations of some dissolved elements listed in Tables 17 and 18, such as [Cl], [F], [P], [Sr], are not altered by the simulated reaction with bentonite, since these elements are not included in any model solid or exchange reaction. They have not been modelled for two reasons: either these are trace elements, which do not significantly affect the speciation of major elements, or they do not show systematic relations in cross activity plots (no saturated solid can be inferred). The amounts of dissolved or precipitated model solids required to reach overall equilibrium are listed under the heading "SOLIDS". These quantities are given as molar concentrations normalised to the fluid volume. The values in parentheses are the *equivalent volume percentages (V%)*, and serve to check whether a sufficient reservoir of a dissolving mineral is present in the bentonite. An inspection of the tables reveals that most minerals have *V%* values equal to or less than 1%, which means that the presence of minor amounts of the model solids in bentonite would be sufficient to saturate the solutions. On the other hand, the model predicts the precipitation of significant amounts of $NaAlSi_2O_6$ (*V%* = 3.7 - 3.8) which fix the large amount of desorbed sodium. Such amounts of precipitate should be identifiable with the aid of a microscope in the solid reaction products. The model also predicts the dissolution of a considerable amounts of $MgAl_2Si_3O_{10}$ (V% = 3.0 - 3.1). Since the MX-80 bentonite does not contain Mg silicates in such high concentrations, the consumption of this model solid must be interpreted as representing dissolution of the montmorillonite framework, i.e. the released Mg must originate from the octahedral sites in montmorillonite. This hypothesis is corroborated by the model results: in each case, the amount of Mg dissolved is about 10 times the amount of K released by the potassium silicate, which is similar to the element ratio in the montmorillonite formula. (Mg/K ~ 8, see Table 6).

If all V% values of a simulation are summed up (with a negative sign if the mineral dissolves and a positive sign for precipitation), a model value for the relative increase or decrease of the solid volume after the interaction with water is obtained. Note that since the calculated V% values depend on the density of each mineral, this sum is only an estimation: it is not clear which density should be assigned to the model phases not representing identified minerals. For the calculations in this report, a density of 2.2 [g/cm^3] , a typical value for zeolites, has been chosen for the Mg, K and Na silicates; the densities of kaolinite and gibbsite have been used for the model solids with corresponding stoichiometries. The results of the bentonite pore water simulations should be rejected if this sum is unreasonably high, since considerable volumetric changes of the solid assemblage *due to precipitation /dissolution reactions* are not observed when bentonite reacts with groundwater. In the simulations presented in Tables 17 and 18, the total volume of solids decreases by 0.3% (reaction with BT1300) or 0.02% (reaction with CRW), which is reasonable.

The results of the computations performed using the finalised *NAGRA* crystalline reference waters as reacting fluids are shown in Table 19. The dissolved concentrations ensuing from the interaction with the Western crystalline water (WCRW) are almost identical to those resulting from reaction with the provisional crystalline water (CRW). The composition of the bentonite water generated by reaction with the Eastern crystalline water (ECRW) is somewhat different (note especially the higher Al and the lower Ca

concentrations) , but the differences lie within the same order of magnitude. Therefore, the bentonite pore water derived using the provisional CRW input water can be considered to be representative.

8.5 Calculations with a reduced set of saturated solids

The list of equilibria reported in Table 15 may give the impression that the system is overdefined. For instance, each of the alkali and earth-alkali ion activities is governed by two equilibria: one describing cation exchange and the other determining the solubility of a model solid. This might suggest that one is superfluous, but this is not the case, as will be shown later. If the system were overdefined, then the bentonite water compositions calculated *excluding* the equilibria with solids containing exchangeable cations would be identical to the compositions modelled using *all* equilibrium constants specified in Table 15.

To check for this, the simulations summarised in Tables 17 and 18 have been repeated without most of the model solids containing exchangeable cations (i.e. $NaAlSi_2O_6$, $KAlSi_2O_6$ and $MgAl_2Si_3O_{10}$). Calcite was retained, since it is demonstrably present in the MX-80 bentonite and is very reactive. The objective of these calculations was to see whether bentonite pore waters modelled assuming control of the Na, K, and Mg dissolved concentrations solely by the exchange constants, have the same compositions of those obtained using the full set of model solids. In other words, these new computations yield an answer to the following question: are the excluded solids superfluous, or are they necessary in order to obtain water compositions comparable to the BGS solutions?

The results of the calculations with the reduced set of saturated minerals are presented in Table 20. They should be compared with Table 19, where a summary of results for the bentonite waters modelled with the complete mineral set is listed in the same format. The comparison shows clearly that ignoring the Na, K and Mg model solids has important consequences for the resulting water compositions. The Mg and, in some cases, the Ca concentrations are considerably lower, while the Al and Si concentrations are higher by up to an order of magnitude than in the calculations with the full set of solids. Moreover, the pH is increased by a whole unit. The high pH may be understood by setting up a proton balance for 2 corresponding simulations, i.e. one with the complete mineral set and the other with the reduced set, using the same reacting water (Table 21). In the *full set* calculations, the interplay of mineral dissolution and precipitation leads to a considerable net production of protons, which neutralises a large fraction of the bicarbonate ions released from calcite. Thus, the pH increase is *limited* by the formation of hydrogen carbonate. In the *reduced set* calculations, the amounts of minerals dissolved and precipitated are much smaller, and the mass balance indicates *consumption* of a minor amount of protons. Thus, if equilibrium with the Na, K and Mg silicates is not required, there is no production of acidity to counteract the pH increase induced by calcite dissolution and the final pH is higher. As a consequence of the higher pH, the bicarbonate ion activity is larger and the calcium concentration becomes very small to comply with the requirement for calcite saturation. In addition, the extensive dissociation of silicic acid at pH ~ 10 leads to an increased Si solubility.

The results of these calculations show that the model solids play an important role in defining the bentonite pore water composition. If the Ca, Mg and K dissolved

concentrations were merely controlled by exchange equilibria, different, more alkaline water compositions would be produced by interaction of the BGS bentonite with crystalline groundwaters, which clearly disagrees with the observations.

8.6 Non-uniqueness of the model solids

The selection of stoichiometries for the model solids was mainly guided by mineralogical criteria. Specifically, the K, Na and Mg phases were defined in such a way as to be consistent with the structure of silicates, since these are the most common alteration minerals resulting from the interaction of clays with aqueous solutions. Therefore, some of the selected formulae reflect those of low-temperature silicates, like analcime and kaolinite.

For modelling purposes, however, the choice is not limited to the selected stoichiometries. It is possible to obtain the same bentonite pore water compositions defined in this study by extrapolating, from the BGS activity data, a new set of solubility constants for alternative model solid stoichiometries. As an example, consider silica. This component appears in four of the solids listed in Table 15. However, just two of these solids, $Al_2Si_2O_5(OH)_4$ and $Al(OH)_3$, are sufficient to *fix* the silicic acid activity at a constant value. Therefore it is not necessary to include silicon in other phases: simple hydroxide phases (KOH, NaOH, $Mg(OH)_2$) may be defined to replace the K, Na and Mg silicates, and formal solubility products for these hydroxides may be derived from the BGS activity data by the same averaging procedure adopted earlier.

This has been done, yielding the following constants for the dissociation reactions: $\log K_{KOH} = -8.1$, $\log K_{NaOH} = -5.5$ and $\log K_{Mg(OH)2} = -13.3$. The BT1300_6a water was then recalculated replacing the constants for the K, Na and Mg silicates with the hydroxide solubility products listed above. The new simulation yielded, as expected, the same pore water composition as with the silicate constants. The only remarkable differences are the much smaller amounts of $Al_2Si_2O_5(OH)_4$ and $Al(OH)_3$ dissolved or precipitated (about 3-4 orders of magnitude less).

8.7 Testing the model against specific BGS waters

The exchange and solubility constants used in the model calculations of bentonite pore waters have been extrapolated from the BGS solution data by *averaging* over the whole set of experiments. It is therefore useful to test the model against *individual* BGS final solutions, in order to assess how much the modelled water compositions deviate from the analytical data. The BGS waters chosen for the comparison were B6/2 (representing the highly mineralised water produced by reaction of the bentonite with the *simple HIGH* fluid) and B8/3 (produced by reaction with more dilute *simple LOW* solution). In order to reproduce the compositions of the 2 selected waters, the exchange and solubility constants specified in Table 15 have been applied in MINEQL simulations to the solutions used as starting fluids for the experiments (*simple HIGH* or *simple LOW*). The concentrations of elements not included in model phases but present in the BGS solutions have been added to

TABLE 19 - Bentonite pore waters resulting from the reaction of bentonite MX-80 with 4 reference crystalline waters at 50°C. These waters have been modelled using the *full set of solubility constants* listed in Table 15. The compositions labeled BT1300_6A and CRW_2A correspond exactly to those given in Tables 17 and 18. They are reported here in the same format as in Table 20 to facilitate the comparison with the waters modelled with a reduced set of solubility constants. The waters labeled ECRW_4 and WCRW_4 are the bentonite pore waters obtained using the finalised crystalline reference waters (Pearson and Scholtis, 1992) as reacting fluids, and should be compared with CRW_2A, which is the bentonite water resulting from the simulated reaction between MX-80 bentonite and a provisional crystalline reference water (Scholtis, 1990). An inspection of the results reveals that the bentonite pore waters obtained with the finalised crystalline reference waters are very similar to the bentonite water modelled using the provisional crystalline reference water CRW. Hence, the use of CRW_2A for the calculation of radionuclide solubilities is justified.

	BT1300_6A	CRW_2A	ECRW_4	WCRW_4
T [°C]	50	50	50	50
pH	8.49	8.97	9.02	8.97
pE [V]	-5.72	-6.18	-6.21	-6.19
I [M]	0.25	0.08	0.07	0.08
log pCO_2 [bar]	- 2.53	- 2.55	-2.56	- 2.55
DISSOLVED [M] :				
[Na]	2.40×10^{-1}	7.84×10^{-2}	7.33×10^{-2}	7.68×10^{-2}
[K]	5.73×10^{-4}	1.66×10^{-4}	1.52×10^{-4}	1.62×10^{-4}
[Mg]	4.81×10^{-4}	6.65×10^{-5}	5.75×10^{-5}	5.89×10^{-5}
[Ca]	5.48×10^{-5}	1.07×10^{-5}	5.42×10^{-6}	1.09×10^{-5}
[Al]	3.57×10^{-5}	1.04×10^{-4}	1.52×10^{-4}	1.03×10^{-4}
[Si]	1.88×10^{-4}	2.61×10^{-4}	2.69×10^{-4}	2.63×10^{-4}
[C] inorg.	1.84×10^{-2}	5.16×10^{-2}	5.44×10^{-2}	5.26×10^{-2}
[1] **SOLIDS [M] :**				
$Al_2Si_2O_5(OH)_4$	-1.67×10^{-1}	-1.85×10^{-1}	-1.86×10^{-1}	-1.85×10^{-1}
$Al(OH)_3$	$+3.21 \times 10^{-1}$	$+3.36 \times 10^{-1}$	$+3.37 \times 10^{-1}$	$+3.36 \times 10^{-1}$
$NaAlSi_2O_6$	$+6.60 \times 10^{-1}$	$+6.71 \times 10^{-1}$	$+6.71 \times 10^{-1}$	$+6.71 \times 10^{-1}$
$MgAl_2Si_3O_{10}$	-3.09×10^{-1}	-3.04×10^{-1}	-3.03×10^{-1}	-3.04×10^{-1}
$KAlSi_2O_6$	-3.02×10^{-2}	-3.04×10^{-2}	-3.06×10^{-2}	-3.05×10^{-2}
$CaCO_3$	-1.63×10^{-2}	-4.74×10^{-2}	-4.98×10^{-2}	-4.75×10^{-2}

[1] positive values indicate precipitation, negative values dissolution.

TABLE 20 - Bentonite pore waters resulting from the reaction of bentonite MX-80 with 4 reference crystalline waters at 50°C. These waters have been modelled using a *reduced set of solubility constants*. ECRW_6 and WCRW_6 are the bentonite pore waters obtained using the finalised crystalline reference waters (Pearson and Scholtis, 1992) as reacting fluids in the simulations, and should be compared with CRW_4, which is the bentonite water resulting from the simulated reaction between MX-80 bentonite and a provisional crystalline reference water (Scholtis, 1990). A comparison with the results of Table 19, where the full set of solids as specified in Table 15 is required to be in equilibrium with the solution, shows that the exclusion of the Na, K and Mg silicates leads to markedly different water compositions.

	BT1300_10	CRW_4	ECRW_6	WCRW_6
T [°C]	50	50	50	50
pH	9.47	10.01	10.05	10.00
pE [V]	-6.70	-7.20	-7.24	-7.20
I [M]	0.24	0.08	0.07	0.08
log pCO_2 [bar]	- 4.02	- 4.30	-4.30	- 4.30
DISSOLVED [M]:				
[Na]	2.37×10^{-1}	8.16×10^{-2}	7.75×10^{-2}	8.04×10^{-2}
[K]	1.08×10^{-4}	2.74×10^{-5}	2.47×10^{-5}	2.65×10^{-5}
[Mg]	5.46×10^{-5}	8.75×10^{-6}	7.91×10^{-6}	8.46×10^{-6}
[Ca]	2.97×10^{-5}	5.47×10^{-6}	5.16×10^{-6}	1.21×10^{-5}
[Al]	3.40×10^{-4}	1.12×10^{-3}	1.20×10^{-3}	1.08×10^{-3}
[Si]	5.25×10^{-4}	1.49×10^{-3}	1.59×10^{-3}	1.44×10^{-3}
[C] inorg.	1.01×10^{-2}	3.66×10^{-2}	3.92×10^{-2}	3.78×10^{-2}
[1] **SOLIDS [M]:**				
$Al_2Si_2O_5(OH)_4$	-1.22×10^{-4}	-4.55×10^{-4}	-5.16×10^{-4}	-4.42×10^{-4}
$Al(OH)_3$	-9.50×10^{-5}	-2.12×10^{-4}	-1.65×10^{-4}	-2.01×10^{-4}
$NaAlSi_2O_6$	--	--	--	--
$Mg_2Al_2Si_3O_{10}$	-	-	-	--
$KAlSi_2O_6$	--	--	--	--
$CaCO_3$	-8.03×10^{-3}	-3.24×10^{-2}	-3.45×10^{-2}	-3.27×10^{-2}

[1] positive values indicate precipitation, negative values dissolution.

the MINEQL input exactly as measured in the B6/2 and B8/3 analyses. Although their *total* concentrations remain unaffected in the simulations, these elements can have an influence on the speciation due to the possible formation of complexes with elements involved in precipitation/dissolution reactions.

The resulting water compositions are compared with the analytical concentrations in Table 22 (only the elements involved in the model equilibrium constants are listed, since the concentrations of other elements remain unaffected). An inspection of the results shows, as expected, discrepancies between modelled and measured concentrations. These differences, however, are always within the same order of magnitude. The ratios of modelled to measured concentrations lie within a factor of 3, which is satisfactory for such speciation calculations.

These calculations cannot serve as a proof of the model, since the model is applied here to the same data used to extrapolate its parameters (the selectivity and solubility constants). However, such comparisons are useful for indicating how good the averages used to define the model parameters are. They therefore reflect the statistical uncertainty of the model constants.

TABLE 21 - Proton and carbonate mass balance in 2 MINEQL simulations for bentonite pore waters computed using either the full set of equilibrium constants as specified in Table 15, or a reduced set in which the K, Na and Mg silicates have been excluded (all data are taken from the MINEQL output).

	FULL SET		REDUCED SET	
	$[H^+]$	$[CO_3^{-2}]$	$[H^+]$	$[CO_3^{-2}]$
[1] **SOLIDS [mM] :**				
$Al_2Si_2O_5(OH)_4$	+ 369.2	--	+ 0.9	--
$Al(OH)_3$	- 1008.6	--	+ 0.6	--
$NaAlSi_2O_6$	--	--	[2] n.e.	n.e.
$MgAl_2Si_3O_{10}$	+ 607.8	-	n.e.	n.e.
$KAlSi_2O_6$	--	--	n.e.	n.e.
$CaCO_3$	--	- 47.4	--	- 32.4
BALANCE	- 31.6	- 47.4	+ 1.5	- 32.4
EXCESS $[CO_3^{-2}]$	15.8		33.9	

[1] positive values indicate fixation of protons or bicarbonate ions in solids, negative values indicate addition of protons or bicarbonate ions to solution.

[2] n.e. : the mineral was not required to be in equilibrium with the solution.

TABLE 22 - Comparison of modelled and measured dissolved concentrations for the BGS bentonite waters B6/2 and B8/3, the first representing interaction with the high ionic strength synthetic water *simple HIGH*, the other arising from the interaction with the low ionic strength *simple LOW* water. The differences between measured and modelled concentrations are a consequence of the averaging procedure over all BGS experiments adopted to extrapolate the model constants listed in Table 15.

	B 6/2 MODEL	B 6/2 MEASURED	B 8/3 MODEL	B 8/3 MEASURED
T [^{o}C]	50	50	50	50
pH	8.5	8.6	9.3	9.1
I [eq/l]	0.21	0.32*	0.05	0.07*
DISSOLVED [M] :				
[Na]	2.14×10^{-1}	3.16×10^{-1}	3.80×10^{-2}	6.51×10^{-2}
[K]	5.12×10^{-4}	8.43×10^{-4}	8.37×10^{-5}	1.89×10^{-4}
[Mg]	3.05×10^{-4}	8.43×10^{-4}	1.39×10^{-5}	2.18×10^{-5}
[Ca]	1.77×10^{-4}	1.77×10^{-4}	1.16×10^{-5}	2.01×10^{-5}
[Al]	3.85×10^{-5}	1.41×10^{-5}	1.91×10^{-4}	1.33×10^{-4}
[Si]	1.90×10^{-4}	2.89×10^{-4}	3.56×10^{-4}	1.97×10^{-4}
[C] inorg.	3.40×10^{-3}	1.04×10^{-2}	1.89×10^{-2}	2.65×10^{-2}

* these "measured" ionic strengths were actually determined from a speciation model of the B6/2 and B8/3 solutions (MINEQL calculations).

9. Summary and conclusions

1) In recent years there has been a debate on the applicability of classical thermodynamic equilibrium models for predicting the composition of waters interacting with complex clays. Some authors assert that equilibrium constant models cannot be applied to montmorillonite - water systems, while others claim that it is possible to define solubility constants for this mineral. In the absence of a generally accepted chemical model, an empirical approach has been developed in this study, which relies on the evaluation of bentonite-water experiments recently performed by the *British Geological Survey* (BGS experiments).

2) Selectivity constants describing cation exchange between clay minerals and solutions for Na-K, Na-Ca and Ca-Mg have been extrapolated. These constants are in good agreement with those derived by Wanner (1986) from independent water-bentonite interaction experiments, and are comparable with other literature values.

3) The analysis of the Al and Si total concentrations from the BGS data indicates that montmorillonite dissolves incongruently. In most cases, there is an initial preferential leaching of Al followed by a sudden decrease in the Al dissolved concentration, while the Si concentration continuously increases. This pattern suggests precipitation of a silica-free Al compound (i.e. an Al-hydroxide).

4) Cross activity plots involving the species H^+ , $Al(OH)_4^-$ and H_4SiO_4 indicate that the BGS solutions can be interpreted to be at or close to equilibrium with 2 solids which could have the stoichiometry of kaolinite ($Al_2Si_2O_5(OH)_4$) and aluminum hydroxide ($Al(OH)_3$). These two solids apparently buffer the silicic acid activity to values slightly below quartz saturation. The relations between calcium and bicarbonate ion activities are roughly consistent with calcite equilibrium.

5) Other correlations involving the Mg^{+2} , K^+ and Na^+ activities can be formulated as solubility constants of alumosilicates with stoichiometries which cannot be related to any identified bentonite phase. These constants should therefore be considered as purely empirical tools through which the compositional characteristics of bentonite pore waters can be reproduced in speciation calculations.

6) It is assumed that the oxidation potential of bentonite pore waters under repository conditions is controlled by the iron and partially by the sulphur systems. The Fe^{+2}/Fe^{+3} system was selected as a redox buffer because it involves the kinetically favourable transfer of a single electron and because iron is the most abundant redox-sensitive element in the repository. Petrographic observations from the available literature show that pyrite, goethite and hematite are the most frequent iron minerals in bentonites. Therefore, it was assumed that these minerals and the steel corrosion product magnetite determine the oxidation potential in the repository environment. At mildly alkaline pHs, equilibrium among pyrite, hematite, magnetite and the solution constrains the Eh values in the range from ~ -400 to -300 mV. As a conservative alternative, the metastable equilibrium goethite-magnetite,

which buffers the Eh to more oxidising conditions (Eh ~ +50 to +100 mV), has been selected.

7) Bentonite pore waters for repository conditions have been defined by simulating the interaction between the MX-80 bentonite and 2 *provisional* crystalline waters (the highly mineralised Boettstein water, and the "normal" CRW water). In each case both redox models have been applied alternatively, yielding a total of 4 water compositions. Equilibrium between the input water and the bentonite has been calculated by imposing the empirical exchange and solubility constants derived from the BGS data. The results of simulations with the finalised crystalline reference waters, which were available only at a late stage of the present study, deviate only slightly from those obtained using CRW as input water.

8) The bentonite pore waters generated by our model have ionic strengths similar to those of the reacting waters. This behaviour is readily explained by the absence of model solids containing soluble anions. In the model, the amounts of bicarbonate ions released through the dissolution of calcite are not sufficient to affect considerably the ionic strength. However, if a poorly mineralised water reacts with a bentonite containing significant amounts of soluble salts, high ionic strength bentonite waters could be produced. Such a behaviour cannot be simulated by our model. Thus, the mineralogy of the bentonite under investigation should always be carefully studied before the model is applied.

9) The modelled bentonite waters do not represent long-term equilibrium conditions. They have compositions which could be found at a very early stage in the chemical evolution of the saturated near-field. The model does not consider the influence of the elements released from the dissolving glass (B, Si, Na, Mg), nor the interaction with the steel canister. It is based on results of experiments carried out over a very short time span (a few weeks), and its predictive power is thus limited.

10) Radionuclide solubilities are expected to be insensitive to variations in major element concentrations (Na, Al, Si, Mg, K) since complexes are formed almost exclusively with OH^-, Cl^- and CO_3^{-2}. The master variables controlling radionuclide solubilities are consequently (besides Eh) the pH, the chloride and the carbonate concentrations (Berner, pers. comm.). While the carbonate and chloride concentrations can be predicted with a reasonable degree of confidence, large uncertainties affect both pH and Eh (~2 pH units, ~ 500 mV respectively). Therefore, future investigations should focus on the determination of reliable values for these 2 parameters.

11) The waters determined in chapter 8 are similar in composition to those reported in the literature (Snellmann et al., 1987; Fritz and Kam, 1985). Thus, although the model is not strictly applicable to the prediction of long-term water-bentonite interaction, the compositions given here could be safely used to determine reference conditions for the near-field performance assessment.

12) It is recommended that further bentonite-water interaction experiments be carried out in order to test the range of validity of the model developed in this study. Such experiments should be performed for various water/rock ratios and with compositions of the starting fluids differing from those of the solutions used in the BGS experiments. Yet the temperature should be the same (50 °C), because the kinetics of dissolution / precipitation reactions, and even the composition and crystallinity of the precipitating solids, are expected to be strongly temperature-sensitive.

Acknowledgements

The preparation of this report was greatly aided by the continuous assistance of many colleagues at *Paul Scherrer Institute*, *NAGRA* and other institutions. I am particularly indebted to Dr. F.J. Pearson, Jr., who contributed new ideas and meticulous reviewing of the manuscripts, and to Dr. I.G. McKinley for valuable discussions and for his efficient coordination work. Special thanks are due to Prof. I. Grenthe, Dr. U. Berner, Prof. R. Grauer, Dr. A. Thoenen and Dr. H. Wanner for their constructive and stimulating criticism, and to Mrs. L. McKinley for language improvements. *NAGRA* is gratefully acknowledged for financial support of this work.

References

Bateman K., Entwisle D.C., Kamp S., and Savage, D. (1991): *Bentonite-groundwater interactions: results of compression rig experiments.* NIB 91-53, *NAGRA*, Baden, Switzerland, 58 p.

Bolt G.H. (1982): *Soil Chemistry.* 2nd edition, Developments in Soil Sciences 5, Elsevier, Amsterdam.

Curti E. (1991): *Modelling the dissolution of borosilicate glasses for radioactive waste disposal with the PHREEQE/GLASSOL code: Theory and practice.* NTB 91-08, *NAGRA*, Wettingen, Switzerland; and *PSI* Report 86, Paul Scherrer Institute, Villigen and Würenlingen, Switzerland, 62 p.

Churchman G.J., and Jackson, M.L. (1976): *Reaction of montmorillonite with acid aqueous solutions: solute activity control by a secondary phase.* Geochim. Cosmochim. Acta, Vol. 40, pp. 1251-1259.

Deer W.A., Howie R.A., and Zussman J. (1966): *An Introduction to the Rock Forming Minerals.* Longman, London, 528 p.

Fritz B., and Kam M. (1985): *Chemical Interactions between the Bentonite and the Natural Solutions from the Granite near a Repository for Spent Nuclear Fuel.* SKB TR 85-10, Svensk Kärnbränslehantering AB, Stockholm.

Grauer, R. (1986): *Bentonit als Verfüllmaterial im Endlager für hochaktiven Abfall: Chemische Aspekte. EIR* Report 576, Würenlingen, Switzerland, 179 p.

Grauer, R. (1988): *Zum chemischen Verhalten von Montmorillonit in einer Endlagerverfüllung. PSI* Report 11, Paul Scherrer Institute, Villigen and Würenlingen, Switzerland, 76 p.

Grauer, R. (1991): *The Reducibility of Sulphuric Acid and Sulphate in Aqueous Solution. PSI* Report 109, Paul Scherrer Institute, Villigen and Würenlingen, Switzerland, 33 p.

Grim R.E. and Güven N. (1978): *Bentonites - Geology, Mineralogy, Properties and Uses.* Developments in Sedimentology 24, Elsevier, Amsterdam.

Harr K. (1976): *Mineralogisch-petrographische Untersuchungen an Bentoniten in der Süddeutschem Molasse.* ph.D. Thesis, Eberhard-Karl-Universität, Tübingen, Germany.

Hem J.D., Roberson C.E., Lind C.J., and Polzer W.L. (1973): *Chemical Interactions of Aluminum with Aqueous Silica at 25 ^{O}C.* Geological Survey Water-supply paper 1827-E, United States Geological Survey, Washington, 57 p.

Hemingway B.S., Robie R.A., and Kittrick J.A. (1978): *Revised values for the Gibbs free energy of formation of [Al (OH) $^{-}_{4,aq}$], diaspore, boehmite and bayerite at 298.15 K and 1 bar, the thermodynamic properties of kaolinite to 800 K and 1 bar, and the heats of solution of several gibbsite samples.* Geochim. Cosmochim. Acta, Vol. 42, pp. 1533-1543.

Kittrick J.A. (1971 a): *Stability of Montmorillonites: I Belle Fourche and Clay Spur Montmorillonites.* Soil Sci. Soc. Amer. Proc., Vol. 35, pp. 140-145.

Kittrick J.A. (1971 b): *Soil Solution Composition and Stability of Clay Minerals..* Soil Sci. Soc. Amer. Proc., Vol. 35, pp. 450-454.

Kittrick J.A. (1971 c): *Montmorillonite Equilibria and the Weathering Environment.* Soil Sci. Soc. Amer. Proc., Vol. 35, pp. 815-822.

Kittrick J.A., and Peryea F.J. (1988): *Experimental Validation of the Monophase Structure Model for Montmorillonite Solubility.* Soil Sci. Soc. Am. J.., Vol. 52, pp. 1199-1201.

Kittrick J.A., and Peryea F.J. (1989): *The Monophase Model for Magnesium-saturated Montmorillonite* . Soil Sci. Soc. Am. J.., Vol. 53, pp. 292-295.

Krauskopf K.B. (1979): *Introduction to Geochemistry.* McGraw & Hill, New York, 2nd Edition, 617 p.

Langmuir D., and Whittermore D.O. (1971): In: *Nonequilibrium Systems in Natural Water Chemistry.* Advances in Chemistry Series 106, Americal Chemical Society, Washington D.C.

May H.M., Kinniburgh D.G., Helmke P.A., and Jackson M.L. (1986): *Aqueous dissolution, solubilities and thermodynamic stabilities of common alumosilicate clay minerals: Kaolinite and smectites.* Geochim. Cosmochim. Acta, Vol. 50, pp. 1667-1677.

McKinley I.G. (1985): *The Geochemistry of the Near-field. EIR* Bericht 563, Würenlingen, Switzerland, 94 p.

Müller-Vonmoos M., and Kahr G. (1983): *Mineralogische Untersuchungen von Wyoming Bentonit MX-80 und Montigel.* NTB 83-12, *NAGRA*, Baden, Switzerland.

NAGRA **(1985)**: *Nuclear Waste Management in Switzerland: Feasibility Studies and Safety Analysis.* NGB 85-09, *NAGRA*, Baden, Switzerland

NAGRA **(in prep.)**: *KRISTALLIN I: Safety Analysis Overview.* NTB 93-22, *NAGRA*, Wettingen, Switzerland.

Pearson F.J, Jr., and Berner U. (1991): *Nagra Thermochemical Data Base - I. Core Data.* NTB 91-17, *NAGRA*, Wettingen, Switzerland.

Pearson F.J, Jr., Berner U., and Hummel W. (1991): *Nagra Thermochemical Data Base - II. Supplemental Data 05/92.* NTB 91-18, *NAGRA*, Wettingen, Switzerland.

Pearson F.J., Jr., and Scholtis, A. (1992): *Reference Waters for the Crystalline Basement of Northern Switzerland.* NIB 92-59, *NAGRA*, Wettingen.

Scholtis, A. (1990): AN 90-22, *NAGRA*, Baden, Switzerland.

Schweingruber M. (1983): *Actinide Solubility in Deep Groundwaters - Estimates for Upper Limits Based on Chemical Equilibrium Calculations. EIR* Report 507, Würenlingen, Switzerland, 63 p.

Schweingruber M. (1984): *Deep Crystalline Reference Water for Project "Gewaehr". EIR* Internal Report TM 45-84-21, Würenlingen, Switzerland.

Simpson J.P. (1989): *Experiments on container materials for Swiss high-level waste disposal project - part IV.* NTB 89-19, *NAGRA*, Baden, Switzerland.

Snellman M., Uotila H., and Rantanen, J. (1987): *Laboratory and Modelling Studies of Sodium Bentonite Groundwater Interaction.* In: Scientific Basis for Nuclear Waste Management X, J.K. Bates and W.B. Seefeldt, eds., Mat. Res. Soc. Symp. Proc. Vol. 84, pp. 781-790.

Srodon J. (1976): *Mixed-Layer Smectite/Illites in the Bentonites and Tonsteins of the Upper Silesian Coal Basin.* Polska Akademia Nauk, Komisja Nauk Mineralogicznych, Prace Mineralogiczne 49, Warszawa.

Stumm W., and Morgan J.J. (1981): *Aquatic Chemistry,* 2nd edition, John Wiley and Sons, New York, 780 p.

Stumm W., and Wieland E. (1990): *Dissolution of oxide and silicate minerals: rates depend on surface speciations.* In: *Aquatic Chemical Kinetics,* W. Stumm, ed., Wiley, pp. 367-400.

Tardy Y., and Fritz B. (1981). *An Ideal Solid Solution Model for Calculating Solubility of Clay Minerals.* Clay Minerals, Vol. 16, pp. 361-373.

Tardy Y., Duplay J., and Fritz B. (1987). *Stability fields of smectites and illites as a function of temperature and chemical composition.* SKB TR 87-20, Svensk Kärnbränslehantering AB, Stockholm.

Wanner H. (1985): *Modelling Radionuclide Speciation and Solubility Limits in the Near-field of a Deep Repository.* In: Sci. Basis for Nucl. Waste Manag. IX, L.O. Werme ed., Mat. Res. Soc. Symp. Proc. Vol. 50, pp. 509-516.

Wanner H. (1986): *Modelling Interaction of Deep Groundwaters with Bentonite and Radionuclide Speciation. EIR* Bericht 589, Swiss Federal Institute for Reactor Research (EIR), Würenlingen, Switzerland, 103 p.

Appendix A

Analyses of BGS solutions,
reproduced from Bateman et al. (1991)

Run B1 Anaerobic conditons
'Na-bentonite' with 'Simple LOW' water
Temperature 50°C

Sample	B 1/1	B 1/2
Time taken	Initial	2 weeks
pH	9.1	9.0
Ca	8.68×10^{-5}	1.18×10^{-3}
Mg	6.24×10^{-5}	1.19×10^{-3}
Na	4.93×10^{-2}	4.18×10^{-2}
K	1.83×10^{-4}	1.52×10^{-4}
Si	2.95×10^{-4}	2.08×10^{-3}
Ba	8.05×10^{-7}	1.17×10^{-6}
Sr	3.77×10^{-7}	1.87×10^{-6}
Total Fe	2.47×10^{-5}	2.27×10^{-4}
Al	8.74×10^{-5}	5.31×10^{-4}
Li	$<4.3\times10^{-6}$	3.49×10^{-6}
HCO_3	1.77×10^{-2}	2.36×10^{-2}
Cl	1.88×10^{-2}	1.98×10^{-2}
SO_4	2.34×10^{-3}	2.23×10^{-3}
NO_3	9.08×10^{-5}	5.66×10^{-5}
NO_2	2.79×10^{-4}	1.38×10^{-4}
HPO_4	1.25×10^{-4}	3.53×10^{-4}
F	5.68×10^{-5}	1.83×10^{-5}
Cation Total	50.1	49.0
Anion Total	41.9	48.3
Balance(%)	8.93	0.13

All concentrations are quoted as moles/litre
Cation and anion totals are quoted as meq/litre

Run B2 Aerobic conditons
'Na-bentonite' with 'Simple LOW' water
Temperature 50°C

Sample	B 2/1	B 2/2
Time taken	Initial	2 weeks
pH	9.1	9.1
Ca	2.59×10^{-4}	7.05×10^{-5}
Mg	1.34×10^{-4}	9.42×10^{-5}
Na	5.74×10^{-2}	4.71×10^{-2}
K	1.49×10^{-4}	1.05×10^{-4}
Si	9.68×10^{-5}	4.00×10^{-4}
Ba	$<3.6\times10^{-8}$	1.15×10^{-7}
Sr	2.39×10^{-6}	1.28×10^{-7}
Total Fe	$<8.97\times10^{-7}$	1.81×10^{-5}
Al	1.69×10^{-4}	9.15×10^{-5}
Li	$<3.6\times10^{-6}$	1.00×10^{-6}
HCO_3	2.13×10^{-2}	2.06×10^{-2}
Cl	2.47×10^{-2}	2.39×10^{-2}
SO_4	5.95×10^{-3}	2.39×10^{-3}
NO_3	2.89×10^{-4}	1.12×10^{-4}
NO_2	2.53×10^{-4}	1.52×10^{-4}
HPO_4	2.19×10^{-4}	2.05×10^{-4}
F	6.59×10^{-5}	4.02×10^{-5}
Cation Total	58.8	47.9
Anion Total	59.0	50.0
Balance (%)	-0.11	-2.14

All concentrations are quoted as moles/litre
Cation and anion totals are quoted as meq/litre

Run B3 Aerobic conditons
'Na-bentonite' with 'Simple HIGH' water
Temperature 50°C

Sample	B 3/1	B 3/2
Time taken	Initial	2 weeks
pH	8.1	8.2
Ca	5.96×10^{-3}	1.53×10^{-4}
Mg	7.01×10^{-3}	8.51×10^{-4}
Na	2.38×10^{-1}	3.56×10^{-1}
K	5.55×10^{-4}	7.70×10^{-4}
Si	9.61×10^{-5}	2.02×10^{-4}
Ba	2.39×10^{-6}	9.79×10^{-7}
Sr	1.35×10^{-4}	1.12×10^{-6}
Total Fe	$<3.6\times10^{-7}$	$<1.8\times10^{-7}$
Al	1.09×10^{-5}	3.05×10^{-5}
Li	4.28×10^{-6}	6.03×10^{-6}
HCO_3	7.46×10^{-3}	1.12×10^{-2}
Cl	3.15×10^{-1}	2.55×10^{-1}
SO_4	4.87×10^{-3}	2.77×10^{-3}
NO_3	6.01×10^{-4}	1.71×10^{-4}
NO_2	$<2.2\times10^{-5}$	7.83×10^{-4}
HPO_4	2.67×10^{-4}	9.67×10^{-5}
F	3.38×10^{-5}	3.01×10^{-5}
Cation Total	265.2	358.7
Anion Total	333.5	273.1
Balance(%)	-11.4	13.6

All concentrations are quoted as moles/litre
Cation and anion totals are quoted as meq/litre

Run B4 Anaerobic conditons
'Na-bentonite' with 'Simple HIGH' water
Temperature 50°C

Sample	B 4/1	B 4/2
Time taken	Initial	2 weeks
pH	8.6	8.2
Ca	1.21×10^{-4}	1.27×10^{-4}
Mg	6.71×10^{-4}	9.05×10^{-4}
Na	3.01×10^{-1}	3.60×10^{-1}
K	8.71×10^{-4}	7.21×10^{-4}
Si	1.24×10^{-4}	2.15×10^{-4}
Ba	4.45×10^{-7}	9.51×10^{-7}
Sr	1.97×10^{-7}	2.13×10^{-7}
Total Fe	$<3.6\times10^{-7}$	$<1.8\times10^{-7}$
Al	6.70×10^{-5}	5.07×10^{-5}
Li	3.20×10^{-6}	5.60×10^{-6}
HCO_3	9.55×10^{-3}	1.15×10^{-2}
Cl	3.67×10^{-1}	2.58×10^{-1}
SO_4	4.95×10^{-3}	3.07×10^{-3}
NO_3	7.42×10^{-6}	5.92×10^{-5}
NO_2	$<2.2\times10^{-5}$	9.03×10^{-4}
HPO_4	1.50×10^{-4}	1.33×10^{-4}
F	3.74×10^{-5}	2.76×10^{-5}
Cation Total	303.4	363.1
Anion Total	387.0	277.4
Balance(%)	-12.1	13.4

All concentrations are quoted as moles/litre
Cation and anion totals are quoted as meq/litre

Run B5 Aerobic conditons
'Na-bentonite' with 'Simple HIGH' water
Temperature 50°C

Sample	B 5/1	B 5/2
Time taken	Initial	2 weeks
pH	8.3	8.4
Ca	2.35×10^{-4}	6.94×10^{-5}
Mg	8.43×10^{-4}	8.26×10^{-4}
Na	3.80×10^{-1}	3.70×10^{-1}
K	8.76×10^{-4}	8.89×10^{-4}
Si	2.21×10^{-4}	9.83×10^{-5}
Ba	8.11×10^{-7}	1.13×10^{-6}
Sr	6.12×10^{-7}	2.05×10^{-7}
Total Fe	$<9.6\times10^{-7}$	3.94×10^{-7}
Al	3.68×10^{-5}	2.52×10^{-6}
Li	$<3.9\times10^{-6}$	5.62×10^{-6}
HCO_3	8.58×10^{-3}	1.10×10^{-2}
Cl	2.80×10^{-1}	3.13×10^{-1}
SO_4	2.74×10^{-3}	3.02×10^{-3}
NO_3	3.55×10^{-4}	9.16×10^{-5}
NO_2	8.07×10^{-4}	3.60×10^{-4}
HPO_4	1.70×10^{-4}	$<2.1\times10^{-5}$
F	3.97×10^{-5}	3.11×10^{-5}
Cation Total	383.6	372.7
Anion Total	295.4	330.7
Balance(%)	13.0	5.97

All concentrations are quoted as moles/litre
Cation and anion totals are quoted as meq/litre

Run B6 Anaerobic conditons
'Na-bentonite' with 'Simple HIGH' water
Temperature 50°C

Sample	B 6/1	B 6/2
Time taken	Initial	2 weeks
pH	8.4	8.6
Ca	2.07×10^{-4}	1.77×10^{-4}
Mg	8.47×10^{-4}	7.96×10^{-4}
Na	3.67×10^{-1}	3.16×10^{-1}
K	8.13×10^{-4}	8.43×10^{-4}
Si	1.46×10^{-4}	2.89×10^{-4}
Ba	7.79×10^{-7}	1.48×10^{-6}
Sr	7.39×10^{-7}	3.31×10^{-7}
Total Fe	$<5.2\times10^{-7}$	2.90×10^{-6}
Al	5.43×10^{-5}	1.41×10^{-5}
Li	3.52×10^{-6}	6.48×10^{-6}
HCO_3	7.98×10^{-3}	1.04×10^{-2}
Cl	2.87×10^{-1}	3.01×10^{-1}
SO_4	2.52×10^{-3}	3.09×10^{-3}
NO_3	3.18×10^{-4}	1.00×10^{-4}
NO_2	7.62×10^{-4}	3.21×10^{-4}
HPO_4	9.56×10^{-5}	$<2.1\times10^{-5}$
F	3.74×10^{-5}	2.84×10^{-5}
Cation Total	367.0	319.2
Anion Total	301.4	318.8
Balance(%)	10.2	0.10

All concentrations are quoted as moles/litre
Cation and anion totals are quoted as meq/litre

Run B7 Aerobic conditons
'Na-bentonite' with 'Simple LOW' water
Temperature 50°C

Sample	B 7/1	B 7/2	B 7/3
Time taken	Initial	2 weeks	4 weeks
pH	9.4	8.9	9.0
Ca	1.33×10^{-5}	1.20×10^{-5}	1.36×10^{-5}
Mg	2.78×10^{-5}	2.69×10^{-5}	7.69×10^{-6}
Na	8.18×10^{-2}	7.65×10^{-2}	4.59×10^{-2}
K	2.22×10^{-4}	2.13×10^{-4}	9.96×10^{-5}
Si	1.14×10^{-4}	3.01×10^{-4}	2.34×10^{-4}
Ba	$<1.5\times10^{-7}$	$<1.5\times10^{-7}$	$<1.5\times10^{-7}$
Sr	1.14×10^{-8}	1.14×10^{-8}	6.85×10^{-8}
Total Fe	$<1.8\times10^{-7}$	3.04×10^{-7}	4.92×10^{-6}
Al	2.51×10^{-4}	1.39×10^{-4}	7.73×10^{-5}
Li	$<1.44\times10^{-6}$	$<1.44\times10^{-6}$	2.31×10^{-6}
HCO_3	3.24×10^{-2}	2.81×10^{-2}	2.03×10^{-2}
Cl	2.94×10^{-2}	2.48×10^{-2}	2.01×10^{-2}
SO_4	1.59×10^{-3}	3.40×10^{-3}	2.56×10^{-3}
NO_3	4.39×10^{-4}	7.85×10^{-5}	4.21×10^{-5}
NO_2	8.76×10^{-4}	3.03×10^{-4}	3.50×10^{-4}
HPO_4	$<5.2\times10^{-5}$	4.93×10^{-5}	$<2.1\times10^{-5}$
F	6.26×10^{-5}	5.63×10^{-5}	4.32×10^{-5}
Cation Total	82.8	77.2	46.3
Anion Total	66.5	60.3	45.9
Balance(%)	11.0	12.3	0.47

All concentrations are quoted as moles/litre
Cation and anion totals are quoted as meq/litre

Run B8 Anaerobic conditons
'Na-bentonite' with 'Simple LOW' water
Temperature 50°C

Sample	B 8/1	B 8/2	B 8/3
Time taken	Initial	2 weeks	4 weeks
pH	9.2	8.9	9.1
Ca	2.17×10^{-5}	1.50×10^{-5}	2.01×10^{-5}
Mg	4.52×10^{-5}	4.47×10^{-5}	2.18×10^{-5}
Na	8.19×10^{-2}	7.77×10^{-2}	6.51×10^{-2}
K	2.09×10^{-4}	2.46×10^{-4}	1.89×10^{-4}
Si	1.55×10^{-4}	3.43×10^{-4}	1.97×10^{-4}
Ba	$<1.5\times10^{-7}$	$<1.5\times10^{-7}$	$<1.5\times10^{-7}$
Sr	3.42×10^{-8}	2.28×10^{-8}	5.71×10^{-8}
Total Fe	$<1.8\times10^{-7}$	1.11×10^{-6}	$<1.8\times10^{-7}$
Al	3.56×10^{-4}	6.08×10^{-5}	1.33×10^{-4}
Li	$<1.4\times10^{-6}$	$<1.4\times10^{-6}$	$<1.4\times10^{-6}$
HCO_3	2.96×10^{-2}	3.32×10^{-2}	2.65×10^{-2}
Cl	2.50×10^{-2}	3.13×10^{-2}	2.49×10^{-2}
SO_4	8.42×10^{-4}	4.87×10^{-3}	3.88×10^{-3}
NO_3	3.60×10^{-4}	1.14×10^{-4}	8.40×10^{-5}
NO_2	9.65×10^{-4}	4.81×10^{-4}	3.54×10^{-4}
HPO_4	$<5.2\times10^{-5}$	$<2.1\times10^{-5}$	4.78×10^{-5}
F	6.21×10^{-5}	6.74×10^{-5}	5.32×10^{-5}
Cation Total	83.3	78.3	65.8
Anion Total	57.6	74.9	59.8
Balance(%)	18.2	2.20	4.82

All concentrations are quoted as moles/litre
Cation and anion totals are quoted as meq/litre

Run B9 Anaerobic conditons

'Na-montmorillonite' with 'Simple LOW' water

Temperature 50°C

Sample	B 9/1	B 9/2	B 9/3
Time taken	Initial	2 weeks	4 weeks
pH	9.3	9.2	9.3
Ca	4.42×10^{-5}	1.93×10^{-5}	2.55×10^{-5}
Mg	9.90×10^{-5}	2.41×10^{-5}	1.12×10^{-5}
Na	5.37×10^{-2}	5.92×10^{-2}	5.52×10^{-2}
K	9.09×10^{-5}	1.07×10^{-4}	1.08×10^{-4}
Si	1.58×10^{-4}	1.97×10^{-4}	2.01×10^{-4}
Ba	$<1.5\times10^{-7}$	$<1.5\times10^{-7}$	$<1.5\times10^{-7}$
Sr	2.62×10^{-7}	9.13×10^{-8}	7.99×10^{-8}
Total Fe	$<1.8\times10^{-7}$	$<1.8\times10^{-7}$	$<1.8\times10^{-7}$
Al	3.55×10^{-4}	2.93×10^{-4}	2.49×10^{-4}
Li	$<1.4\times10^{-6}$	$<1.4\times10^{-6}$	1.44×10^{-6}
HCO_3	1.91×10^{-2}	2.54×10^{-2}	2.26×10^{-2}
Cl	2.23×10^{-2}	2.33×10^{-2}	2.03×10^{-2}
SO_4	2.82×10^{-3}	2.63×10^{-3}	2.57×10^{-3}
NO_3	1.36×10^{-4}	$<3.2\times10^{-5}$	5.16×10^{-5}
NO_2	3.77×10^{-4}	3.83×10^{-4}	2.96×10^{-4}
HPO_4	8.09×10^{-5}	2.22×10^{-5}	5.75×10^{-5}
F	6.74×10^{-5}	6.21×10^{-5}	5.39×10^{-5}
Cation Total	55.1	60.3	56.1
Anion Total	47.8	54.4	48.7
Balance(%)	7.13	5.10	7.10

All concentrations are quoted as moles/litre

Cation and anion totals are quoted as meq/litre

Run B10 Anaerobic conditons

'Na-montmorillonite' with 'Simple HIGH' water

Temperature 50°C

Sample	B 10/1	B 10/2	B 10/3
Time taken	Initial	2 weeks	4 weeks
pH	8.7	8.8	8.6
Ca	$<1.2\times10^{-6}$	1.16×10^{-4}	4.33×10^{-4}
Mg	2.95×10^{-4}	3.50×10^{-4}	7.31×10^{-4}
Na	3.16×10^{-1}	3.22×10^{-1}	2.23×10^{-1}
K	6.80×10^{-4}	5.98×10^{-4}	5.44×10^{-4}
Si	$<7.1\times10^{-7}$	1.66×10^{-4}	1.75×10^{-4}
Ba	3.42×10^{-7}	7.87×10^{-7}	7.79×10^{-7}
Sr	$<5.7\times10^{-8}$	2.05×10^{-7}	2.41×10^{-7}
Total Fe	3.76×10^{-7}	1.97×10^{-7}	$<9.2\times10^{-7}$
Al	$<7.4\times10^{-7}$	7.01×10^{-5}	6.15×10^{-5}
Li	1.73×10^{-6}	4.61×10^{-6}	$<7.2\times10^{-7}$
HCO_3	6.70×10^{-3}	7.05×10^{-3}	7.78×10^{-3}
Cl	2.84×10^{-1}	2.49×10^{-1}	2.29×10^{-1}
SO_4	3.72×10^{-3}	2.97×10^{-3}	3.29×10^{-3}
NO_3	$<2.5\times10^{-5}$	$<6.3\times10^{-5}$	$<1.3\times10^{-4}$
NO_2	4.17×10^{-4}	3.99×10^{-4}	3.02×10^{-4}
HPO_4	$<5.2\times10^{-5}$	$<5.2\times10^{-5}$	$<1.0\times10^{-4}$
F	3.89×10^{-5}	3.71×10^{-5}	3.62×10^{-5}
Cation Total	317.5	324.1	225.7
Anion Total	298.9	262.4	244.4
Balance(%)	3.02	10.5	-3.99

All concentrations are quoted as moles/litre

Cation and anion totals are quoted as meq/litre

Appendix B

Moisture contents of clay mixes
Charge balance data
Exchangeable cation data

reproduced from Bateman et al. (1991)

Table 4 Moisture content of clay-fluid mixes.

	A	B	C	D	E
Expt Number	Pre-test weight (g)	Oven dried weight (g)	Moisture Content % Initial	Post test	Initial moisture weight (g)
B1	300.0	104.1	188.2	147.1	195.9
B2	304.5	107.6	182.8	123.4	196.7
B3	248.9	113.9	99.2	83.7	113.0
B4	290.3	145.0	100.2	73.9	145.3
B5	300.3	140.1	114.3	83.9	160.2
B6	259.0	122.0	112.4	74.9	137.0
B7	251.4	120.6	108.5	76.0	130.8
B8	254.5	118.0	115.7	74.3	136.5
B9	253.2	111.5	127.2	72.2	141.8
B10	271.3	119.7	126.6	63.6	151.6

Table 5 Charge balance data for the experiments

Sample code	Cation Total (meq/l)	Anion Total (meq/l)	Balance (%)
'Simple LOW'	12.7	13.1	-1.8
'Simple HIGH'	210.8	201.6	2.3
B 1/1	50.1	41.9	8.9
B 1/2	49.0	48.8	0.1
B 2/1	58.8	59.0	-0.1
B 2/2	47.9	50.0	-2.1
B 3/1	265.2	333.5	-11.4
B 3/2	358.7	273.1	13.6
B 4/1	303.4	387.0	-12.1
B 4/2	363.1	277.4	13.4
B 5/1	383.6	295.4	13.0
B 5/2	372.7	330.7	6.0
B 6/1	370.0	301.4	10.2
B 6/2	319.2	318.6	0.1
B 7/1	82.8	66.5	11.0
B 7/2	77.2	60.3	12.3
B 7/3	46.3	45.9	0.5
B 8/1	83.3	57.6	18.2
B 8/2	78.3	74.9	2.2
B 8/3	65.8	59.8	4.8
B 9/1	55.1	47.8	7.1
B 9/2	60.3	54.4	5.1
B 9/3	56.1	48.7	7.1
B 10/1	317.5	298.9	3.0
B 10/2	324.1	262.4	10.5
B 10/3	225.7	244.5	-4.0

Table 8 Summary of exchangeable cation data

Sample code	Material type	Atmospheric conditions	Fluid	Exchangeable cation (meq/100g) Ca	Mg	Na	K	H
	Na-bentonite	-	-	44.4	20.1	76.4	1.5	<0.1
	Na-montmorillonite	-	-	40.4	19.9	74.6	1.3	<0.1
B1	Na-bentonite	Anaerobic	'Simple LOW'	44.4	14.9	75.5	1.5	<0.1
B2	Na-bentonite	Aerobic	'Simple LOW'	47.6	15.3	73.8	1.5	<0.1
B3	Na-bentonite	Aerobic	'Simple HIGH'	46.9	15.9	84.1	1.5	<0.1
B4	Na-bentonite	Anaerobic	'Simple HIGH'	50.1	16.6	82.3	1.5	<0.1
B5	Na-bentonite	Aerobic	'Simple HIGH'	44.9	14.7	78.2	1.4	<0.1
B6	Na-bentonite	Anaerobic	'Simple HIGH'	47.1	16.7	76.8	1.5	<0.1
B7	Na-bentonite	Aerobic	'Simple LOW'	43.9	14.9	71.1	1.6	<0.1
B8	Na-bentonite	Anaerobic	'Simple LOW'	43.9	14.7	68.5	1.6	<0.1
B9	Na-montmorillonite	Anaerobic	'Simple LOW'	48.6	14.3	75.5	1.6	<0.1
B10	Na-montmorillonite	Aerobic	'Simple HIGH'	47.4	16.3	80.8	1.4	<0.1

Table 9

X-Ray Fluorescence Major Element Analysis - Starting materials.

Clay type	'Na-bentonite'	'Na-montmorillonite'
SiO_2	55.47	56.58
Al_2O_3	18.65	18.77
Fe_2O_3t	5.28	5.35
MgO	4.89	4.77
CaO	2.83	2.35
Na_2O	2.67	2.89
K_2O	0.97	0.79
P_2O_5	0.05	0.04
LOI	8.88	8.35
Total	99.98	100.16